Solidification Behaviour and Mechanical Properties of Cast Mg-alloys and Al-based Particulate Metal Matrix Composites Under Intensive Shearing

by

Spyridon Tzamtzis

A thesis submitted for the degree of

Doctor of Philosophy (PhD)

at the Brunel University

Brunel Centre for Advanced Solidification Technology

(BCAST)

March 2011

To my family and Ioulia…

Abstract

Magnesium alloys, as the lightest of all structural metallic materials, and aluminium-based particulate metal matrix composites (PMMCs), offering unified combination of metallic and ceramic properties, have attracted increased interest from the automotive, aerospace, electronic and recreation industries. Current processing technologies for PMMCs do not achieve a uniform distribution of fine-sized reinforcements and produce agglomerated particles in the ductile matrix, which are detrimental to the ductility. At the same time, molten magnesium alloys contain impurities and oxides and when cast conventionally, the final components usually exhibit a coarse and non-uniform microstructure with various casting defects. The key idea in this thesis has been to adopt a novel intensive melt conditioning process, allowing the application of sufficient shear stress that would disperse solid particles present in the melt and offer unique solidification behaviour, improved fluidity and die-filling during casting.

The Melt Conditioned High Pressure Die Casting (MC-HPDC) process, where intensive shearing is directly imposed on the alloy melt, which is then cast by the conventional HPDC process, has been used to produce PMMC and magnesium alloy castings. The MC-HPDC process for PMMCs leads to a uniform dispersion of the reinforcement in the matrix, confirmed by quantitative statistical analysis, and increased mechanical performance as indicated by an increase in the hardness and the tensile properties of the composites. We describe a solidification path for aluminium containing magnesium alloys, where intensive shearing prior to casting leads to effective dispersion of solid oxide particles, which then effectively act as nucleation sites for magnesium grains, resulting in significant grain refinement. The MC-HPDC processed magnesium castings have a significantly refined microstructure, with reduced porosity levels and casting defects. Evaluation of the mechanical properties of the castings reveals the beneficial effect of intensive shearing. After careful optimization, the MC-HPDC process shows promising potential for the direct recycling of high purity magnesium die casting scrap, producing casting with mechanical properties comparable to those of primary magnesium alloys.

Related Publications

Peer Reviewed Journals

- Tzamtzis S, Zhang H, Hari-Babu N, Fan Z (2010). 'Physical recycling of high-grade AM-series magnesium die-casting scrap by the MC-HPDC process'. *Materials Science and Engineering A*, 528 pp. 2664-2669.
- Tzamtzis S, Zhang H, Hari-Babu N, Fan Z (2010). 'Microstructural refinement of AZ91D alloy by intensive shearing'. *Materials Science and Engineering A*, 527 pp. 2929-2934.
- Tzamtzis S, Barekar NS, Hari-Babu N, Patel J, Dhindaw BK, Fan Z (2009). 'Processing of advanced Al/SiC particulate Metal Matrix Composites under intensive shearing - a novel Rheo process'. *Composites: Part A*, 40 pp. 144-151.
- Barekar NS, Tzamtzis S, Hari-Babu N, Fan Z, Dhindaw BK (2009). 'Processing of ultra-fine size particulate metal matrix composites by advanced shear technology'. *Metallurgical and Materials Transactions A*, 40A pp. 691-701.
- Barekar NS, Tzamtzis S, Dhindaw BK, Patel J, Hari Babu N, Fan Z (2009). 'Processing of Aluminum-graphite particulate metal matrix composites by advanced shear technology'. *Journal of Materials Engineering and Performance*, 18(9) pp. 1230-1240.

Conference proceedings

- Zuo Y, Liu G, Zhang H, Tzamtzis S, Hari-Babu N, Scamans GM, Fan Z (2009), 'Microstructure and Mechanical Properties of M-Alloys produced by the MC-HPDC Process'. In: *Proceedings of Magnesium 8th International Conference*, October 2009, pp. 246-351.
- Tzamtzis S, Zhang H, Liu G, Wang Y, Hari-Babu N, Fan Z (2009): 'Melt Conditioned High Pressure Die Casting (MC-HPDC) of Mg-alloys'. In: *Magnesium Technology 2009*, TMS, San Francisco, CA, February 2009, pp. 91-96.
- Tzamtzis S, Barekar N, Hari-Babu N, Fan Z (2008), 'Introducing a novel Rheo process to produce advanced Al/SiC particulate Metal Matrix Composites under intensive shearing'. In: *Proceedings of ResCon 2008*, Brunel University, June 2008.
- Hari-Babu N, Tzamtzis S, Barekar N, Patel JB, Fan Z (2008). 'Fabrication of Metal Matrix Composites under intensive shearing'. *Solid State Phenomena*, 141-143 pp. 373-378.

Acknowledgements

I would like to express my most sincere gratitude to Professor Zhongyun Fan for providing me with the opportunity to join BCAST and carry out the research that resulted in this thesis. I have found his dedication to science and determination most inspiring.

I am deeply grateful to Dr Hari Babu Nadendla for his supervision and guidance throughout my three years at BCAST. He has been continuously supportive and encouraging, most importantly during the last few difficult months that I was trying to finishing this work. His scientific advice and mentoring have contributed the most towards the completion of my thesis.

Special thanks go to all members of BCAST that made me feel genuinely welcome when I first joined the group. In particular, I have received great scientific and technical guidance from Dr S. Ji, Dr J. Patel, Dr G Liu, Dr M Xia and Dr H. Zhang. Mr S. Cook, Mr P. Lloyd and Mr C. Nunez have provided very useful technical support and were always available to assist with my experimental work. I would also like to mention fellow PhD students, now already taking their first steps in academia, Dr N. Barekar and Dr H. Kotadia. Together we shared endless discussions and managed to get the positive out of the difficulties we faced during our research.

There is a saying that quotes “show me your friends and I’ll tell you who you are” and I wholeheartedly agree with this. I have had valuable support and encouragement from my friends, Dr Z. Doulgerakis and Mr A. Tyrothoulakis who helped me make the most of my life in London. My utmost gratitude goes to my partner in life and best friend, Miss I. Anastasiadou, who stood by me in moments of crisis in my research. It would have been almost impossible to finish this thesis without her support and encouragement.

Last but not least, I would like to thank my family who have invested in me, both emotionally and financially and never stopped believing in me. My parents, Argyris and Georgia, have sacrificed the most to see me succeed, and my brother, Andreas, has always been supportive. I cannot express my full appreciation to them here in words and the least I can do is dedicate my thesis to them.

Contents

Abbreviations

ASTM	American Society for Testing Materials
BCAST	Brunel Centre for Advanced Solidification Technologies
CMCs	Ceramic Matrix Composites
EDX	Energy Dispersive X-ray Spectrometer
ESCs	Externally Solidified Crystals
HCP	Hexagonal Close Packed
HIP	Hot Isostatic Pressing
HPDC	High Pressure Die Casting
HRTEM	High Resolution Transmission Electron Microscopy
MC-HPDC	Melt Conditioned High Pressure Die Casting
MCAST	Melt Conditioned by Advanced Shear Technology
MMCs	Metal Matrix Composites
OM	Optical Microscopy
PM	Powder Metallurgy
PMCs	Polymer Matrix Composites
PMMCs	Particulate Metal Matrix Composites
SEM	Scanning Electron Microscopy
TP1®	Aluminium Association Test Procedure - 1
UTS	Ultimate Tensile Strength
ZAF	Atomic Number Absorption Fluorescence

Nomenclature

Greek symbols

α_0	Atomic radius
α_p	Particle radius
β	Skewness of a statistical distribution
Γ	Equilibrium surface energy
$\dot{\gamma}$	Shear rate
Γ_c	Fracture surface energy
γ_{lv}	Surface energy of a liquid
γ_{sl}	Solid – liquid interfacial energy
γ_{sv}	Surface energy of a solid
ΔT_{fg}	Undercooling required for free growth
ΔS_v	Volumetric entropy of fusion
ε_1	Dielectric constant of phase 1
ε_2	Dielectric constant of phase 2
ε_c	Dielectric constant of a composite
η	Viscosity
θ	Contact angle
λ_p	Particle thermal conductivity
λ_l	Liquid thermal conductivity
ρ_p	Particle density
ρ_R	Reinforcement density
ρ_l	Liquid density
ρ_M	Matrix density
σ_0	Single crystal yield strength
σ_c	Ultimate tensile strength of the composite
σ_m	Ultimate tensile strength of the matrix
σ_n	Normalised ultimate tensile strength
σ_q	Standard deviation of N_q distribution
σ_y	Yield strength
τ	Shear stress
φ	Volume fraction of particles in an agglomerate
Ω	Atomic volume

Roman symbols

a	Magnesium crystal unit cell lattice parameter
a_e	Major ellipse axis
A_{gi}	Relative area fraction
A_p	Area occupied by particle
b_e	Minor ellipse axis
c	Magnesium crystal unit cell lattice parameter
C_f	Volumetric concentration of particles
C_l	Liquid specific heat
C_p	Particle specific heat
D	Diffusion coefficient
d_c	Equivalent circle diameter
d_g	Grain diameter
d_i	Impeller diameter
d_p	Particle diameter
d_{pi}	Potent inoculate particle diameter
D_s	Screw outer diameter
D_v	Vessel inner diameter
F_α	Fragmentation number
F_b	Average binding force
F_p	Maximum force acting on a particle cluster
g	Gravitational acceleration
G_s	Gap between screw flight and barrel surface
k_B	Boltzmann constant
k_y	Strengthening coefficient
L	Latent heat of fusion
$\bar{l}$	Mean intercept length
l_f	Flaw size
L_T	Length of test line
m	Exponent
m_M	Mass of the matrix
m_R	Mass of the reinforcement
M_L	Lacey Index
n	Constant approximately equal to 5
n_b	Average number of bonds per particle
N_i	Number of grain boundary intersections on each test line

N_p	Number of particles
N_q	Number of particles in a quadrat
N_q^{mean}	Mean number of particles per quadrat
N_{qi}	Number of particles in i^{th} quadrat
N_s	Rotational speed of screws
p	Proportion of a component in a mixture
P_c	Property of a composite material
P_f	Property of the reinforcement
P_m	Property of the matrix
q	Proportion of a component in a mixture
q_t	Number of quadrats studied
S^2	Variance of a mixture
S_0^2	Variance of segregated mixture
S_R^2	Variance of randomised mixture
T	Temperature
T_c	Agglomerate strength
U_c	Critical velocity for entrapment
V_0	Settling velocity
V_1	Volume fraction of phase 1
V_2	Volume fraction of phase 2
V_c	Velocity of fall
V_m	Volume fraction of the matrix
V_f	Volume fraction of the reinforcement
V_{tf}	Terminal falling velocity
w_i	Impeller width
X	Volume fraction of the reinforcement

List of Figures

List of Tables

CHAPTER 1

INTRODUCTION

1.1 Background

The worldwide transport and recreation industries are in a constant quest for improved performance, efficiency and cost reduction of the final products. At the same time, there exist demanding safety regulations and environmental legislations for overall fuel efficiency and reduced CO_2 emissions, which have triggered an increased interest in lightweight materials. Magnesium alloys, as the lightest of all structural metallic materials, and aluminium-based particulate metal matrix composites (PMMCs), offering a unified combination of metallic properties and ceramic properties, have emerged as ideal candidates for a wide spectrum of applications.

1.1.1 Metal Matrix Composites

The mechanical properties that metal matrix composites (MMCs) can offer, combined with their relatively low cost, have attracted interest for application in the transport and sport industries [Clyne and Withers 1993, Miracle 2005]. In particular, discontinuously reinforced PMMCs have been shown to offer improvements in strength, structural efficiency, reliability and control of physical properties such as density and coefficient of thermal expansion thereby providing a competitive alternative to un-reinforced metals [Ray 1993, Lloyd 1994, Rohatgi 2001]. Furthermore, with PMMCs problems associated with the continuously reinforced MMCs, such as fibre damage, microstructural non-uniformity, fibre-to-fibre contact and extensive interfacial reactions can be avoided [Ibrahim et al. 1991]. PMMCs can have isotropic properties, offering an increase in strength and stiffness compared to un-reinforced materials. Nevertheless, the less than optimum ductility that PMMCs usually offer and their brittle fracture behaviour have hindered their widespread applications.

A processing challenge with PMMCs is to homogeneously distribute the

reinforcement in the matrix, which would improve the properties and the quality of the composite [Naher et al. 2005]. However, currently available processing methods often produce composites with clustered particles within the matrix resulting in PMMCs with low ductility [Segurado et al. 2003, Deng and Chawla 2006]. The agglomeration of the reinforcement particles leads to an inhomogeneous response and lower macroscopic mechanical properties. Cracks have been found to nucleate on particle clusters at stresses lower than the yield strength of the matrix, causing the PMMC to fail at low stress levels [Lloyd 1991].

In order to fabricate high quality PMMCs with desirable mechanical properties, important factors such as chemical reactions and the poor wettability between the matrix and the reinforcement, and the introduction of porosity during the incorporation of the particles require considerable attention [Oh et al. 1989, Naher et al. 2005]. Several researchers have investigated the wettability of reinforcement particles by the matrix alloy [Delannay et al. 1987], have studied the distribution of the reinforcement as affected by the interaction between the solidification conditions and the particles [Rohatgi et al. 1986, Naher et al. 2003] and have tried to optimise the process parameters and obtain a uniform distribution of the reinforcement [Naher et al. 2007, Ravi et al. 2007]. Another factor that has been found to significantly affect the final distribution is the size of the reinforcement particles. The high cohesive energy of ultrafine particles gives them a highly agglomerative nature and leads to an increase in the total surface area. Consequently their tendency to clump together forming agglomerates and clusters is increased and induces an unwanted brittle nature to PMMCs [Rumpf 1962, Tomas 2007].

1.1.2 Magnesium alloys

Being the lightest of all structural metallic materials and having excellent strength to weight ratio, magnesium alloys have found increased applications in the transport industry. A recent study [USGS 2008] has predicted an increase in the global demand for magnesium with a 7.3 % average annual growth rate until 2012. The same study showed that in 2007, 32 % of overall magnesium consumption in the United States was for die-casting applications. Typical applications in the transport industry for magnesium castings include components such as instrument panels, steering wheels, door and seat frames, which require optimisation of the quality and

performance of the castings.

The high-pressure die casting (HPDC) process is the most commonly used process offering efficient production with low cost. However, components can exhibit coarse and non-uniform microstructures, containing various casting defects and severe chemical segregation. A very common defect in HPDC Mg-alloy components is the formation of segregation and / or porosity bands, commonly referred to as 'defect' bands, which follow contours parallel to the surface of the casting [Dahle et al. 2001(b), Gourlay et al. 2007]. The occurrence of defect bands and other casting defects like shrinkage porosity and hot tearing can be reduced by grain refinement, also improving the machinability of cast products [Bamberger 2001]. Furthermore, as shown by the Hall-Petch equation, a fine grain structure is generally desirable to improve the mechanical properties [Hall 1951, Petch 1953].

Several researchers have pursued either a chemical or a physical approach for the grain refinement of Mg-alloys. The chemical route involves the inoculation of the alloys with addition of various alloying elements and several researchers have reported their results in this area [Emley 1966, Cao et al. 2006, Easton et al. 2006, Qian and Das 2006, Yang et al. 2008(b), Guang et al. 2009]. Although grain refinement by inoculation is a route easily applicable, a universal grain refiner for Mg-alloys has not yet been identified. Finding the right inoculants for different alloy systems is not always possible and although these elements can refine the microstructure, they give rise to various other problems. Therefore, a physical route that does not involve addition of any elements is necessary. Different approaches for the grain refinement of Mg-alloys so far have seen the application of electromagnetic stirring [Liu et al. 2008(a)], superheating [Cao et al. 2007] and ultrasonic vibration [Liu et al. 2008(b), Ramirez et al. 2008]. However, further research is required to reveal the mechanisms of grain refinement and these processes still need to be developed for large-scale industrial application.

The predicted increased usage of magnesium alloys is bound to lead to an increase in Mg-alloy scrap from both manufacturing sources (new scrap) and end-of-life vehicles (old scrap). About 50 % of the material used in magnesium diecasting is accumulated as scrap and handled by the foundry or an external recycler [Antrekowitsch et al. 2002]. At the same time, the European Union is pushing towards the recycling of the majority of end-of-life vehicles by 2015 [Fechner et al.

2007]. Several chemical routes have been approached for the recycling of Mg-alloy scrap [Javaid et al. 2006]. However, these recycling technologies remain complex, energy demanding and exhibit low productivity.

1.2 Aim and objectives

With Al-based PMMCs, the main objective of this thesis is to overcome problems that exist in the current processing technologies and produce composites with high quality microstructures, a uniform distribution of the reinforcement and good mechanical properties of the final product. The key idea is to apply sufficient shear stress (τ) on particle clusters embedded in the liquid metal to overcome the average cohesive force or the tensile strength of the cluster. Two commercially available casting Al-alloys, LM24 (USA designation A380) and LM25 (USA designation A356) were used as the matrix materials. The reinforcements used were black SiC with an average particle size equal to 4 μm and synthetic graphite powder with an average particle size less or equal to 20 μm.

With cast Mg-alloys, a grand challenge is to develop solidification processing technologies that can ensure a fine and uniform as-cast microstructure, free of macro-segregation and cast defects, so that the final products can be either directly used in the as cast state, or only require minimal thermo-mechanical processing. Both fresh and scrap magnesium alloys contain substantial amounts of inclusions and oxides. These could act as potential nucleation sites for primary magnesium grains hence intensive shearing could prove beneficial to disperse them uniformly throughout the melt volume and activate them in the solidification process. The grain refining potential of intensive shearing has been studied on the AZ91D, AM60B and AJ62 magnesium alloys. AZ91D alloy, as the most commonly used cast Mg-alloy, has been studied in further detail and its mechanical properties have been evaluated after the implementation of intensive shearing. Finally, a mixture of AM50 and AM60B die casting scrap has been used to investigate the potential of intensive shearing as a means of physical recycling for magnesium alloys.

The implementation of the shearing is carried out by the melt conditioning by advanced shear technology (MCAST) process, involving a specially designed twin screw machine which can be directly attached to a standard HPDC machine. The

twin-screw mechanism is used to impose the high shearing dispersive mixing action to the melt, which is treated in such a way that its uniformity in chemistry and temperature is improved. In the melt conditioned high-pressure die casting (MC-HPDC) process intensive shearing is directly imposed on the alloy melt prior to die filling. Inside the barrel of the twin-screw machine, there is a pair of specially designed screws, co-rotating, fully intermeshing and self-wiping, creating an environment of a high shear rate and high intensity of turbulence for the alloy melt. The sheared melt is expected to offer unique solidification behaviour, improved fluidity and die filling when subsequently cast by the conventional HPDC process.

1.3 Thesis Outline

The remainder of this thesis is subdivided into six chapters. In the following chapter a literature review of the current status of relevant research areas is presented. A review of material selection and production processes for PMMCS is provided, focusing more on the stir casting technology. Also, an overview of the different magnesium alloy systems with their processing and applications is given. Chapter 3 provides the experimental processes and techniques utilised in the present investigation. The materials, processing technologies, characterization techniques and equipment used are described. In Chapter 4 the results of this thesis on Al-based PMMCs are presented and discussed. The general microstructure of PMMCs is provided first and discussed with and without the implementation of intensive shearing. A quantitative analysis of the effect of intensive shearing on the microstructure is conducted and the mechanical properties are evaluated. Chapter 5 provides the results of processing magnesium alloys under intensive shearing. The effect of the MCAST process on the microstructure of commercially available cast Mg-alloys is studied. The MC-HPDC process is compared to conventional HPDC and the potential of the MC-HPDC process as a physical recycling route is also investigated. At the end of this chapter, the solidification behaviour of magnesium alloys under intensive shearing is discussed. Finally, concluding remarks for this thesis and recommendations for future work are provided in Chapters 6 and 7 respectively.

CHAPTER 2

LITERATURE REVIEW

2.1 Metal Matrix Composites

2.1.1 Introduction to composite materials

There is constant need for improved performance in the ground transportation, aerospace, industrial, recreational and infrastructure industries which leads to materials' development and commercialization. Weight saving requirements conflict with the fact that other properties such as strength, stiffness, wear resistance, machinability, electrical and thermal conductivity and corrosion resistance are of significant technological importance. Composite materials have emerged as ideal candidates and can be tailored to offer improved properties in a wide variety of applications [Schwartz 1984, Kelly 1989, Hull and Clyne 1996, Hunt Jr 2009].

Schwartz [Schwartz 1984] gives a working definition of composite materials as: '*A composite material is a materials' system composed of a mixture or combination of two or more macroconstituents differing in form and/or material composition and that they are essentially insoluble in each other.*' Many natural biological materials like the coconut palm leaf, wood, bone and teeth are effectively composites [Matthews and Rawlings 1994, Hull and Clyne 1996]. In engineering, the term composite originally arose when two or more materials were combined in order to overcome shortcomings of traditional materials [Kelly 1989]. Over the last three decades, active research and development efforts in composite materials led to their increased application in fields as diverse as transportation, energy and civil construction [Rawal 2001, Miracle 2005, Chawla and Chawla 2006].

According to the definition given above, a composite consists of two or more distinct constituents or phases. The constituent that is continuous, and often but not always present in the greater quantity in the composite, is termed the *matrix*. The composite matrix can be ceramic, metallic or polymeric [Chawla 1998]. Although there has been increased interest in metal matrix composites (MMCs) and various industrial applications have been developed, most composites used in industrial

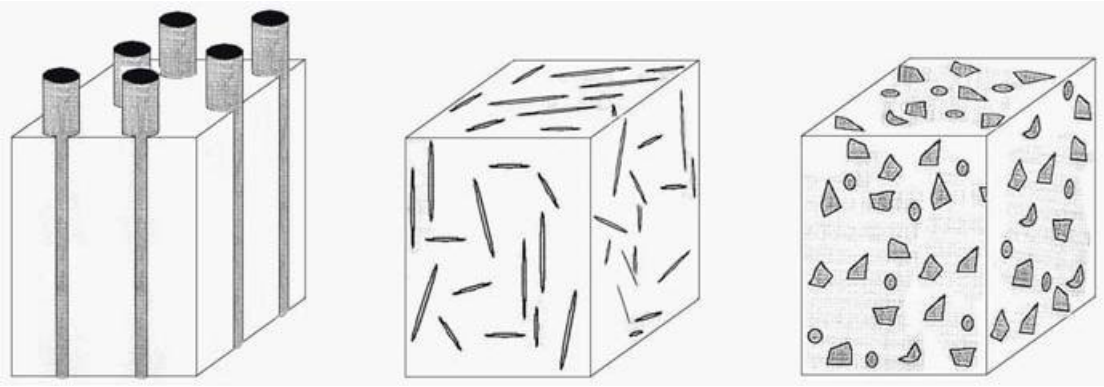

Figure 2.1 Classification of composites depending on size and shape of reinforcement [Rohatgi 2001].

applications are still polymer matrix composites (PMCs) whilst ceramic matrix composites (CMCs) have not seen extensive commercial applications [Hull and Clyne 1996, Chawla 1998]. The other constituent of composite materials is referred to as the *reinforcement* and can be in the form of particles, flakes, whiskers, short fibres, continuous fibres or sheets. Examples of typical composite microstructures can be grouped, as shown in Figure 2.1 according to the reinforcement shape. Further distinctions can be made if one considers fibre diameter or orientation distribution [Clyne and Withers 1993]

2.1.2 Metal matrix composites (MMCs)

When the matrix of the composite material is of a contiguous metallic nature, then these composites are termed metal matrix composites. They offer high strength, toughness and stiffness compared to unreinforced metals, but often they suffer from low ductility. The reinforcement is usually a ceramic material, although refractory metals have occasionally been used. A less restrictive MMC definition could also include materials such as oxide dispersion strengthened alloys or Al-Si eutectic alloys [Miracle 2005]. Based on the type and nature of the reinforcement, MMCs can be broadly classified into three basic types:

- Dispersion strengthened
- Fibre reinforced

- Particle reinforced.

A dispersion strengthened composite is characterised by a microstructure consisting of an elemental matrix and uniformly dispersed particles with a diameter range between 0.01 and 0.1 μm and volume fraction ranging between 1 and 15 % [Matthews and Rawlings 1994]. Dispersion strengthened systems such as dual-phase steels are strong, tough and formable materials finding applications in the automotive industry. They lie very close to particle reinforced composites as their structure consists of relatively coarse, hard martensite particles distributed in a soft ferrite matrix [Clyne and Withers 1993].

Fibrous metal matrix composites were the first to attract attention in the 1960s, when high volume fractions of tungsten and boron fibres were added in aluminium and copper [Clyne and Withers 1993]. The reinforcing phase in fibre composite materials can be either long, continuous fibres or short, discontinuous fibres as shown in Figure 2.1. In fibre reinforced composites, the mechanical properties are directional and the degree of anisotropy depends primarily on the fibre orientation. Production limitations and high cost have caused research on fibre reinforced metal matrix composites to slow down during the 1970s.

The success of dual phase steels encouraged researchers to work on the particles reinforced metal matrix composites concept. In the 1980s, efforts in discontinuously reinforced composites revived the research and development of MMCs [Miracle 2005]. In PMMCs both matrix and reinforcement bear substantial proportions of the load. Particle reinforced composites offer superior performance where isotropic mechanical and physical properties, strength-to-weight ratio, volume and life cycle costs are important considerations. They are distinguished from the dispersion hardened systems by the fact that the reinforcement is larger, ranging between 1 and 100 μm. In addition, since volume fraction is relatively high at 5 to 40 %, load transfer from the matrix is significant [Taya and Arsenault 1989, Clyne and Withers 1993].

2.1.3 Materials selection

The advantage offered by MMCs is that they can be tailored to offer the desirable properties depending on the application, which offers an advantage over

unreinforced metal alloys. When designing the metal matrix composite, an engineer aims to combine the desirable attributes of the metal and the reinforcing phase. Important considerations during materials' selection should be the desirable properties the MMC needs to possess and the interaction between metal matrix and reinforcement, expressed by their interface.

2.1.3.1 Property development

The opportunity offered by composite materials to alter the properties of the metal matrix in favour of the intended application is unique. Under ideal MMC production conditions, the principal mechanical, thermal, physical and tribological properties that the composite will exhibit are defined by the *rule-of-mixtures* [Rohatgi 1993]:

$$P_c = P_m V_m + P_f V_f \tag{2.1}$$

where P_c is the property of the composite material, P_m is the property of the matrix, P_f is the property of the reinforcement , V_m is the volume fraction of the matrix phase, and V_f is the volume fraction of the reinforcement phase. The rule of mixtures gives very good estimates of the properties for continuously reinforced composites.

On the other hand, for particle reinforced MMCs, it is preferable to consider the properties of a two phase composite in terms of a dielectric constant ε_c. The Hashin - Shtrikman bounds [Kelly 1989] predict the range of the effective dielectric constant of an isotropic composite according to:

$$\varepsilon_1 + \frac{V_2}{\frac{1}{(\varepsilon_2 - \varepsilon_1)} + \frac{V_1}{3\varepsilon_1}} < \varepsilon_c < \varepsilon_2 + \frac{V_1}{\frac{1}{(\varepsilon_1 - \varepsilon_2)} + \frac{V_2}{3\varepsilon_2}} \tag{2.2}$$

where ε_1 and ε_2 the dielectric constant of each phase, with $\varepsilon_2 > \varepsilon_1$, and V_1, V_2 the volume fraction of each phase. These are the best possible bounds for the dielectric constant of an isotropic, two-phase material when the volume fractions of each phase are known. The properties of an isotropic composite are expected to fall within these two bounds. However, since the mechanical properties are highly sensitive to reinforcement size, volume fraction, distribution, processing defects, brittle reaction zones and the matrix structure [Llorca and Gonzalez 1998], it is very

common for composite materials to exhibit properties that are lower than those defined by the Hashin – Shtrikman bounds.

One of the major challenges when producing MMCs is to achieve a homogeneous distribution of the reinforcement particles in the matrix. To obtain a specific mechanical/physical property, ideally, the MMC should consist of fine particles distributed uniformly in a ductile matrix, with clean interfaces between particle and matrix. However, the current processing methods often produce agglomerated particles in the ductile matrix and as a result they exhibit extremely low ductility [Segurado et al. 2003, Deng and Chawla 2006]. Clustering leads to a non-homogeneous, anisotropic response and lower macroscopic mechanical properties. Particle clusters act as crack or decohesion nucleation sites at stresses lower than the matrix yield strength, causing the MMC to fail at unpredictable low stress levels [Nair et al. 1985, Lloyd 1991].

2.1.3.2 Interface

The interface between the matrix and reinforcement is a very important microstructural feature of composite materials and has been recognised in the early studies of composites [Metcalfe 1974]. It is a transition zone where compositional and structural discontinuities can occur over distances varying from an atomic monolayer to over five orders of magnitude in thickness [Asthana 1998(b)]. Interfacial characteristics in metal matrix composites reinforced with ceramic reinforcements play a significant role in determining the mechanical properties, such as strength, ductility, toughness and fatigue resistance.

A weak interface results in a low stiffness and strength but a high resistance to fracture, whereas a strong interface produces high stiffness and strength but often a low resistance to fracture [Clyne 1997]. Reactive solutes in the matrix can attack the reinforcement during processing and/or service and deteriorate the interfacial strength [Tham et al. 2001]. The addition of alloying elements in the matrix has been found to limit the chemical reaction [Revzin et al. 1996] and more specifically, the addition of silicon (Si) to aluminium and aluminium alloy matrices prevents the formation of Al_4C_3 at the interface in Al-SiC or Al-graphite composites [Landry et al. 1998, Lee et al. 1988].

Wettability is a key concept in the context of interfacial bonding due to adhesion between the reinforcement and the matrix. The contact angle formed by a liquid droplet resting on a solid substrate as seen in Figure 2.2 can be used to describe the wettability [Delannay et al. 1987]. According to the Young-Dupré equation [Dupré 1869], the contact angle θ can be expressed as:

$$\gamma_{lv} \cos\theta = \gamma_{sv} - \gamma_{sl} \qquad (2.3)$$

where γ_{sv} is the surface energy of the solid, γ_{sl} the solid liquid interfacial energy and γ_{lv} the surface energy of the liquid and θ the contact angle.

In molten metal and ceramic particle systems, the high surface tension of the metals, of the order of 1000 mJ/m², makes wetting very difficult [Eustathopoulos et al. 1974]. Poor wettability results in inadequate bonding between the metal and the reinforcement particles. In practice, to improve wettability between the metal and the ceramic particles, the following actions can be taken:

- Application of a metallic coating on ceramic particulates [Rajan et al. 1998]
- Varying the matrix alloy composition [Pai et al. 1995]
- Heat treatment of the ceramic particulates [Asthana 1998(b)].

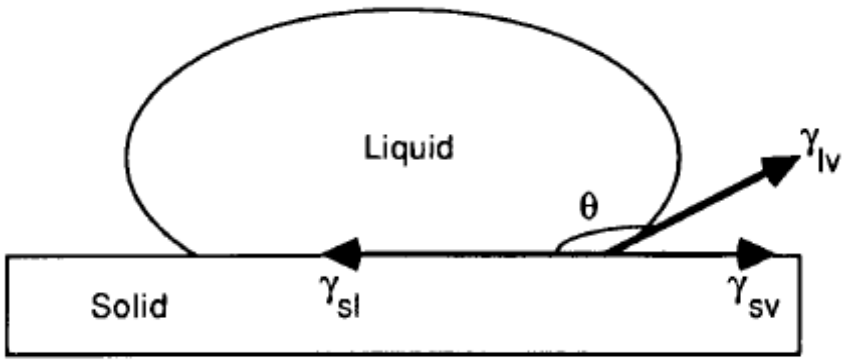

Figure 2.2 Schematic diagram of a liquid drop on a solid surface showing interfacial forces and wetting angle [Oh et al. 1989].

2.1.3.3 The Al-SiC system

There is a wide range of matrices and reinforcements that can be combined to produce PMMCs. Of these, the aluminium alloy based matrix SiC reinforced composites have found extensive applications in the aerospace, military and civil industries as they offer a good combination of high strength, high elastic modulus, increased wear and fatigue resistance [Clyne and Withers 1993, Kaczmar et al. 2000]. Addition of SiC particles should in principle increase the tensile strength and elastic modulus of the matrix, but on the other hand decrease the ductility [Deng and Chawla 2006, Song 2009]. There have been several attempts by researchers to produce high quality Al-SiC composites following different fabrication routes, and Table 2.1 presents the properties of some of the Al-SiC PMMCs reported in the vast literature.

2.1.4 Fabrication processes

There is now a wide variety of processing routes and technologies that have been developed for the production of MMCs. The selection is made upon the effect the process will have on the microstructure and properties of the composite materials. However, for the process to be rendered successful and suitable for industrial application, the cost parameter must be taken into consideration. The fabrication methods that are currently used to optimise the structure and properties of MMCs can be grouped into three main categories according to the temperature of the metallic matrix during processing:

- Solid state processes
- Semi-solid state processes
- Liquid processes

There is a vast literature available for the fabrication processes of MMCs. Several authors [Ibrahim et al. 1991, Clyne and Withers 1993, Ray 1993, Rohatgi 1993, Lloyd 1994, Miracle 2005] have summarised these processes according to the three different processing routes. This section briefly lists and describes the different MMC fabrication processes.

Table 2.1 Mechanical properties of PMMCs from the Al-SiC system produced by various fabrication routes, as presented in the literature.

Material	Fabrication route	UTS (MPa)	ε (%)	Reference
6061 – 15 vol. % SiC	Extrusion	421	6.7	[Zhao et al. 1991]
Al-2Cu – 13.9 vol. % SiC	Stir Casting	61±21.3	1.2 ± 0.3	[Gupta et al. 1996]
Al-2Cu – 13.9 vol. % SiC	Disintegrated Melt Deposition	152.3 ±19.1	0.6 ± 0.3	
Al – 4 vol. % SiC	Powder metallurgy	91	14.1	[Song 2009]
Al – 8 vol. % SiC	Powder metallurgy	96	12.5	
Al – 12 vol. % SiC	Powder metallurgy	103	9.5	
Al–6Ti–6Nb – 10 vol. % SiC	Powder Metallurgy	177	0.28	[Jia 2000]
Al–5Cu – 15 vol. % SiC	Powder Metallurgy	212 ± 29.0	7.6 ± 0.66	[Ogel and Gurbuz 2001]
Al-g. 5Fe- 1.3V-1.7Si – 14.5 vol. % SiC	Powder Metallurgy	452	2.4	[Ma et al. 1994]
7010 – 10 vol. % SiC	Mechanical Alloying	468	0.68	[Bhaduri et al. 1996]
7075 – 15 wt. % SiC	Stir Casting	63.62	1.13	[Dasgupta and Meenai 2005]
A1 – 10 vol. % SiC	Sintered	11.00 ± 4.2	0.055 ± 0.01	[Ling et al. 1995]
A1 – 10 vol. % SiC	CIP Sintered	15.25 ± 4.6	0.085 ± 0.01	
A1 – 10 vol. % SiC	HIPed	32.80 ± 5.9	0.534 ± 0.22	
A1 – 10 vol. % SiC	Sinter/HIPed	45.60 ± 7.8	1.149 ± 0.75	

2.1.4.1 Solid state processes

The two main solid state processes developed for the fabrication of MMCs are *powder metallurgy* (PM) and the *XD process*. The PM route involves high shear mixing of powder metal matrix and reinforcement which is usually followed by cold compaction, canning, degassing and a final consolidation stage by hot isostatic pressing (HIP), extrusion, forging, rolling or another high temperature method [Ibrahim et al. 1991, Clyne and Withers 1993]. Several commercial manufacturers, such as Alcoa (Pennsylvania, PA), Ceracon Inc. (Sacramento, CA), DWA Composites Specialties Inc. (Chatsworth CA) and the American Composites (Greenville, SC) have been using the PM route, and a more detailed description of their processes is available in the literature [Ibrahim et al. 1991, Rohatgi 1993]. Powder metallurgy is used for specific applications in the motorsport and aerospace industries and is more expensive than other routes used in MMC fabrication

The XD process is a patented in situ composite manufacturing method developed by Martin Marietta Corp. [Lloyd 1994].The matrix alloy and reacting constituents are mixed in the solid state and ignited to generate a self-propagating reaction throughout the mixture [Ray 1993]. A compound is added to a solvent metallic matrix, such as aluminium and aluminium alloys, and will react exothermally to produce the required reinforcing particles. Different compound reinforcing particles can be formed by this process, but the two which have received most attention are TiB_2 and TiC [Lloyd 1994]. The XD process offers the advantage of producing reinforcing particles inherently wetted by the matrix and can therefore provide high interfacial strength.

2.1.4.2 Semi-solid state processes

Compocasting or *rheocasting* is a very simple and effective semi-solid processing method to produce MMCs [Clyne and Withers 1993]. The extensive research that was carried out in the last few decades on the field of semi-solid processing of metals [Fleming 1991, Kirkwood 1994, Fan 2002] was inevitably transferred to the MMC production. In rheocasting, the ceramic reinforcement is progressively added into the metal matrix which is vigorously agitated at a temperature within the solid-liquid range of the alloy. The high viscosity of the semi-solid slurry allows the

addition of the reinforcement particles which are mechanically entrapped by the primary alloy solid particles, before subsequently interacting with the liquid matrix for bonding. Although rheocasting has all the advantages of semi-solid metal processing, the process is restricted to alloys with a long freezing range and the mechanical agitation can lead to particle agglomeration, excessive interfacial reactions and particle fracture.

Another semi-solid process for the fabrication of MMCs is the *Osprey process*, a spray deposition technique introduced in the late 1970s by Osprey LTD (Neath, UK) [Clyne and Withers 1993]. A spray gun creating a high speed inert gas jet is used to fragment a molten metal stream while the reinforcement is simultaneously injected. Both streams are directed towards a substrate where the droplets recombine forming a high-density deposit, with particle engulfment in molten or partially solid metal droplets taking place either during flight, or upon the high-energy impact over the substrate [Ray 1993]. Common features of MMCs produced by the Osprey process are strong interfacial bonding with limited reactions, inhomogeneous distribution of the reinforcement and porosity levels of around 5 % which can be eliminated by secondary processing [Clyne and Withers 1993].

2.1.4.3 Liquid state processes

Liquid state processes are very favourable and the two most common processes are *melt infiltration* and *stir casting*. In the melt infiltration process, inert gas or a mechanical device is used as a pressurizing medium to introduce a molten alloy into a porous ceramic preform. The metal alloy matrix composition, the preform material, the surface treatments and the geometry of the preform, as well as atmosphere, temperature and time are some of the parameters that determine the wetting of the ceramic preform by the liquid alloy. [Clyne et al. 1985, Clyne and Mason 1987]. Process variables that affect the quality of the final composite are the die pre-heat temperature, the applied pressure and the packing density of the reinforcement particles in the preform [Ray 1993]. The infiltration process is very widely used in industrial applications; however some drawbacks of this process can be identified as preform compression, reinforcement damage, microstructural non-uniformity and undesirable interfacial reactions [Ibrahim et al. 1991].

Stir casting is essentially the same process as rheocasting, only in this case the metal alloy matrix is in a fully liquid state when the reinforcement is being added into it. Because of the ease of operation and attractive economical aspects, stir casting is extensively used to synthesise composites reinforced with particulates of a wide variety of ceramic materials. The major problem in the synthesis of PMMCs by stir casting is to obtain a homogeneous distribution of the reinforcing phase. In composites produced by this method, the particle distribution will change significantly depending on process parameters during both the melt and solidification stages. A more detailed description of the stir casting process is given in the next section.

2.1.5 Stir casting

Stir casting is a cost effective, simple and flexible method that has seen commercial application in large scale production [Hashim et al. 1999]. The process emerged in the late 1960s when Ray developed aluminium – alumina MMCs by stirring molten aluminium alloys with an impeller while adding alumina particles [Ray 1993]. In general, during the stir casting process the molten metal alloy matrix is stirred using a mechanical stirrer and reinforcement particles are added through the vortex created by stirring. The negative pressure differential existing at the vortex helps to suck externally added particles and incorporate them into the liquid metal during stirring [Harnby et al. 1997]. A schematic illustration of the mixing set-up during stir casting process is shown in Figure 2.3.

The stir casting method is attractive because, in principle, it only requires the use of conventional metal processing routes and hence minimises the cost. It is easily applicable to conventional aluminium alloys, using uncoated ceramic particles of about 10 μm and larger and reinforcement levels up to 25 vol.% [Lloyd 1994].The main process variables in the stir casting are the size, shape, position and speed of stirrer. Once the particles are successfully transferred into the molten metal, the distribution of the reinforcement in the composite mixture is strongly affected by certain flow transitions [Beck et al. 1991]. Despite the advantages offered by the stir casting process, some difficulties exist and need considerable attention. Stirring causes the entrapment of air bubbles and other impurities from the surface of the melt, resulting in high porosity of the cast product. The reinforcement particles tend

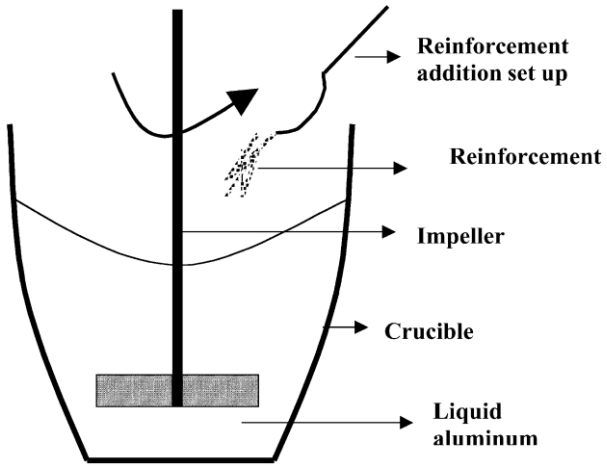

Figure 2.3 Schematic illustration of MMC mixing set-up during the stir casting process [Aniban et al. 2002].

to agglomerate and form clusters, especially in the case of fine and highly cohesive powders, and settling or floating of the particles has been observed. Finally, prolonged stirring times promote the chemical reactions between the reinforcement and the melt.

The macroscopic casting defects such as porosity and inclusions influence the tensile properties [Rohatgi et al. 2005]. Limitations also exist in terms of the volume fraction additions and the size of the reinforcement, because the viscosity of the melt increases with increasing particle content and decreasing particle size [Ravi et al. 2008]. To date, the lack of a cost effective mixing technology capable of achieving a uniform distribution of fine size reinforcement within the metal matrix has slowed down the widespread commercial application of PMMCs.

2.1.6. Impeller design

As described above, effective mixing of the reinforcement added in the molten metal during the stir casting process is the most important requirement. The impeller design will have a significant effect on the quality of mixing and the uniform dispersion of the particles in the melt prior to solidification. According to the direction of induced flow, impellers are classified into axial flow and radial flow impellers. In axial flow impellers, the impeller blade creates an angle smaller than 90° with the plane of impeller rotation. They induce a vertical upward or downward

flow parallel to the shaft and away from the blades. Radial flow impellers have blades parallel to the shaft and discharge the fluid in a horizontal direction, away from impeller blades. Whilst both impeller designs have been used in stir casting, axial flow impellers have an edge over radial flow impellers. An axial flow impeller will create more discharge than shear while radial flow impellers have more shear than flow for a particular power specified [Aniban et al. 2002]. Several researchers have analyzed the effect of the impeller design and suggested that for solid suspension applications, the impeller diameter, d_i, to vessel inner diameter, D_v, ratio should vary between 0.35 and 0.6, depending on the viscosity [Nagata 1975, Aniban et al. 2002, Hashim et al. 2002(b)]. The ratio of impeller width, w_i, to impeller diameter has also been found to have a significant role and it is advisable to have an impeller with a w_i/d_i ratio of 0.35 [Aniban et al. 2002].

Different designs of mechanical impellers as shown in Figure 2.4 have been studied [Beck et al. 1991, Harnby et al. 1997]. Propellers, turbines, and paddles, seen in Figure 2.4(a), (b) and (c) respectively, are generally used with relatively low viscosity systems and operate at high rotational speeds. For high viscosity liquids, anchor impellers, Figure 2.4(d), with a small wall clearance are often used. To promote top-to-bottom circulation or strong axial flow, helical ribbon or screw impellers, seen in Figure 2.4(e) and (f), are more suitable. But the shear stresses generated by these impellers are not adequate to break up and disperse agglomerated particles. In such cases, it is necessary to use a high shear mixing device operating at high speed. The effect of conventional impellers in the distribution of reinforcement particles in MMCs is discussed in section 2.1.9.

2.1.7 Twin screw mechanism

Twin screw processing is an effective method to produce a high shear flow environment. First developed in Italy just before World War II [Janssen 1978], twin screw processing has been well established mainly in the polymer industry as a dispersive mixing process before the mould or extrusion die, and also for food processing. Twin screw mechanisms can be classified according to the direction of screw rotation relative to each other, screw shape and speed and whether the screws are intermeshing or non-intermeshing [White 1990].

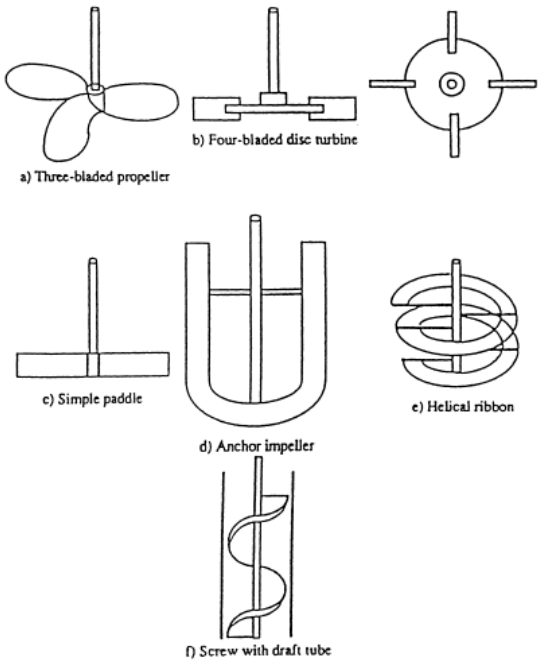

Figure 2.4 Different designs of mechanical stirrers [Harnby et al. 1997].

Fan and co-workers at Brunel Centre for Advanced Solidification Technologies (BCAST), Brunel University, have amongst others developed a patented twin-screw mechanism with fully intermeshing, self wiping and co-rotating screws [Fan et al. 1999]. The twin screw design is schematically presented in Figure 2.5. The unique characteristics of this twin-screw mechanism offer excellent metallurgical microstructural characteristics and have been extensively used on research of semi-solid and immiscible alloys [Fan et al. 2001, Fan 2005, Fan and Liu 2005, Fan et al. 2005].

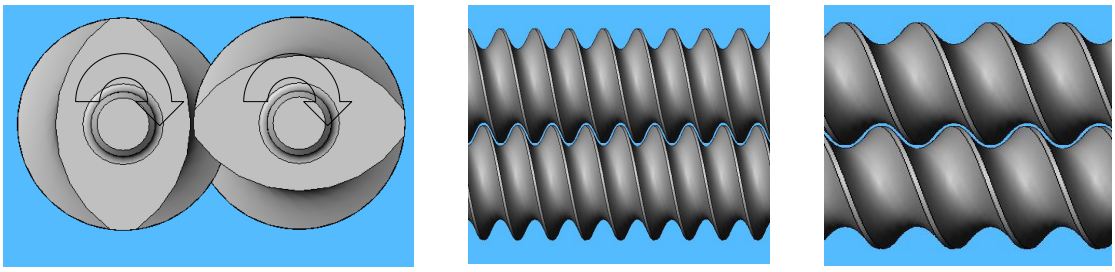

(a) (b) (c)

Figure 2.5 Twin screw design; (a) co-rotating, (b) fully intermeshing and (c) self wiping screws [Fan et al. 1999].

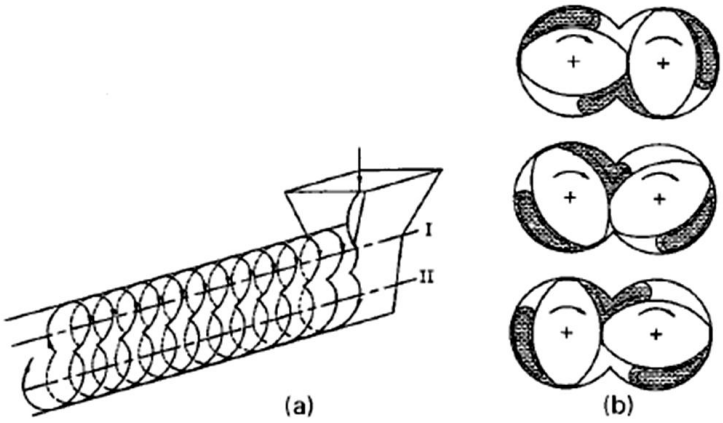

Figure 2.6 Schematic illustrations of flow pattern in a closely intermeshing, self-wiping and co-rotating twin screw mechanism; (a) ‘figure 8’ flow pattern in screw channels and (b) Movement of the melt from one screw to the other [Fan et al. 2001].

The exact mixing mechanism of a twin screw machine is quite complex and difficult to describe. Erdmenger was one of the first reported researchers to study the fluid flow mechanism of an intermeshing, co-rotating twin screw [Erdmenger, as cited *in* Ji et al. 2001]. Results of his study indicated that the fluid moved in ‘figure 8’ motions around the periphery of the screws in what is being referred to as a positive displacement pumping action. A schematic illustration can be seen in Figure 2.6(a). The movement of the alloy melt from one screw to the other, as seen in Figure 2.6(b), indicates that the whole volume of the melt will undergo a cyclic variation of shear rate, due to the continuous change of the gap between the screw and the barrel. Considering the viscosity of liquid metal alloys and composites, the turbulence inside the barrel of the twin screw mechanism is expected to be very high. The high intensity of the turbulence and the high shear dispersive mixing action make the twin screw a highly efficient tool to produce a homogeneous distribution of the reinforcement in MMCs.

2.1.8 Tensile strength of agglomerates

Several researchers [Rumpf 1962, Lee et al. 1993, Hansen et al. 1998, Tomas 2007] have studied the dispersion of solid particles in a viscous media. When solid reinforcement particles are added into a molten metal matrix, particle clusters are

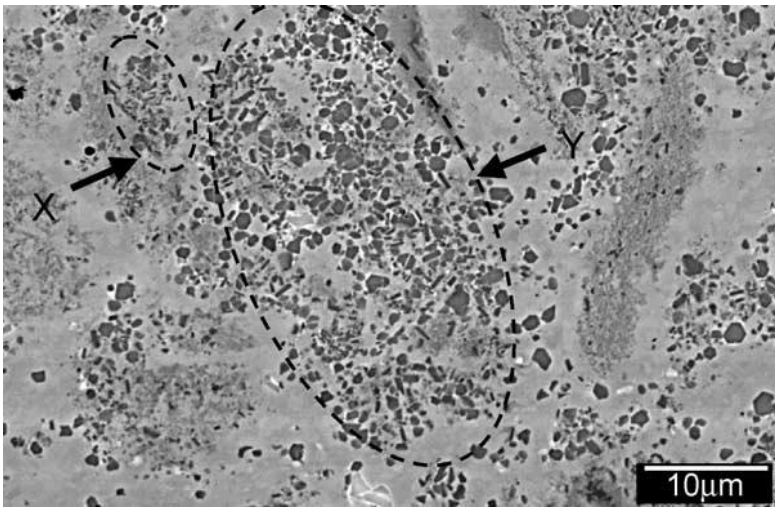

Figure 2.7 Back-scattered Field Emission Gun (FEG) SEM image showing small (X) and large (Y) clusters of TiB_2 particles in a commercial purity Al-matrix [Watson et al. 2005].

formed as seen in Figure 2.7. Their dispersion can be determined by factors such as the cohesivity of agglomerated particles, the applied shear stress and interfacial interactions between the agglomerates and melt. The dispersion of the particles is attributed to two modes of break up: rupture, which refers to the fragmentation of clusters and erosion, which refers to the gradual shearing off of particles from the cluster.

The hydrodynamic forces required to disperse particle clusters can be characterised by the fragmentation number F_α [Hansen et al. 1998], which is the ratio of the applied shear stress to the strength of the agglomerate and is given by:

$$F_a = \frac{\eta\tau}{T_c} \tag{2.4}$$

where τ is the shear stress, η is the viscosity of the liquid matrix and T_c is the cohesive strength of the agglomerate. The agglomerate strength is not a material property and is determined by interparticle bonds due to electrostatic charges, van der Waals forces or moisture [Hansen et al. 1998]. According to Rumpf's model [Rumpf 1962] which considers the agglomerate as a collection of cohesive particles, the strength of the agglomerate is given by:

$$T_c = \frac{9}{32}\frac{\phi}{\pi\alpha_p^2} n_b F_b \quad (2.5)$$

where ϕ is the volume fraction of the particles in the agglomerate, α_p is the radius of the particle, F_b is the average binding force of a single bond and n_b is the average number of bonds per particle. Another model used to determine the agglomerate strength of cohesive powders is given by Kendall [Kendall 1988] and assumes that the agglomerate will break at a strength limiting flaw. The agglomerate strength this time is given by:

$$T_c = 11.03\frac{\phi^4 \Gamma_c^{5/6} \Gamma^{1/6}}{\sqrt{l_f d_p}} \quad (2.6)$$

where Γ_c and Γ are the fracture surface energy and equilibrium surface energy, l_f *is* the flaw size and d_p is the particle diameter. For finer reinforcement size additions the particle size diameter is smaller and the interparticle distance is smaller, resulting in stronger interparticle bonds. According to both Rumpf's and Kendall's models, a smaller particle size and higher binding force will give a higher agglomerate tensile strength. This means that for reinforcement particles of a very fine size, smaller than 10 μm, high hydrodynamic forces are needed to break up agglomerates held together by high cohesive forces.

2.1.9 Distribution of reinforcing particles

For the stir casting process to produce MMCs that can replace conventional metal alloys, it is important that the final microstructure consists of reinforcement particles uniformly distributed in the matrix. Reinforcement agglomerates are known to have detrimental effects on the mechanical properties [Kennedy and Wyatt 2000, Hong et al. 2003, Murphy et al. 1998]. The reinforcement distribution in stir casting can be distinguished in three different stages which will be described in the following sections.

2.1.9.1 Distribution in the liquid as a result of mixing

In the stir casting process, after the reinforcement particles are introduced in

the molten metal matrix, the objective of mechanical stirring is to break up agglomerates to individual particles and then distribute the particles throughout the flow. The melt temperature, the amount and nature of the particles, the shape and size of the stirrer, its speed and its position relative to the melt surface and walls and bottom of the crucible are some of the main factors to be considered when investigating particle distribution during mixing and there have been extensive studies trying to optimise the stir casting process [Rana et al. 1989, El-Kaddah and Chang 1991, Rohatgi et al. 1998, Ravi et al. 2007].

However, further experimental effort is required to improve the microstructure of stir cast MMCs through a uniform distribution of particles, especially for reinforcements with a very fine size. As discussed in section 2.1.8, high hydrodynamic forces are needed to break up agglomerates held together by high cohesive forces. The maximum force, F_p, acting on a particle cluster rotating in a shear flow in the vicinity of a stirrer is given by [Harnby et al. 1997]:

$$F_p = 6\pi\eta\alpha_p^2\dot{\gamma} \qquad (2.7)$$

where $\dot{\gamma}$ is the shear rate in the surrounding liquid medium. In conventional stir casting, the degree of mixing is governed by the momentum transfer from the position of the stirrer to the clusters located away from the stirrer position. Whilst high local shear forces can be applied on the clusters in the near vicinity of the impeller, the shear forces diminish as we move towards the walls of the crucible or the surface of the melt.

2.1.9.2 Distribution in the liquid after mixing

The particle distribution in cast composites may become inhomogeneous even when a homogeneous state of suspension is maintained in the slurry during stirring. After mixing and prior to solidification, the dynamics of particles in a melt will be governed by gravitational and buoyancy forces. If the specific gravity of the particles is different from that of the molten metal, particles can start settling or floating resulting in agglomeration before solidification.

Richardson and Zaki [Richardson and Zaki 1954] have obtained a relation for the velocity of fall (V_c) as:

$$V_c = V_{tf}(1-C_f)^m \quad (2.8)$$

where V_{tf} is terminal falling velocity, C_f is the volumetric concentration of particles and m is the exponent. Ourdjini and co-workers [Ourdjini et al. 2001] studied the settling of SiC particles in molten aluminium alloy matrices considering the expression developed by Stokes:

$$V_0 = \frac{d_p^2(\rho_p - \rho_l)g}{18\eta} \quad (2.9)$$

where V_0 is the settling velocity of a single spherical particle moving relative to a continuous flow, ρ_p is the density of the spherical particle, ρ_l is the density of the liquid and g is the acceleration due to gravity. They concluded that factors such as particle density, size, shape and volume fraction play important roles in the settling phenomenon.

2.1.9.3 Redistribution as a result of solidification

The last stage of reinforcement particle distribution is the final solidification of the composite mixture melt containing suspended particles. Solidification under selected conditions can help obtain the desired distribution of the reinforcement phase in the cast matrix. During solidification of a liquid matrix alloy containing second phase particles, the particles in the melt can migrate towards or away from the freezing front. The interactions between the advancing solidification front and the particles change the distribution of particles. A schematic illustration of the forces acting on the reinforcement particle can be seen in Figure 2.8.

Stefanescu and co-workers have studied the behaviour of reinforcement particles in the liquid-solid metal interface during solidification of metal matrix composites [Stefanescu et al. 1988, Stefanescu et al. 1990]. They have suggested that factors which affect the behaviour of particles include:

- The particle size and shape
- The viscosity of the melt
- The interfacial energy between the particle, liquid and solid
- The particle aggregation
- The convection level in the melt

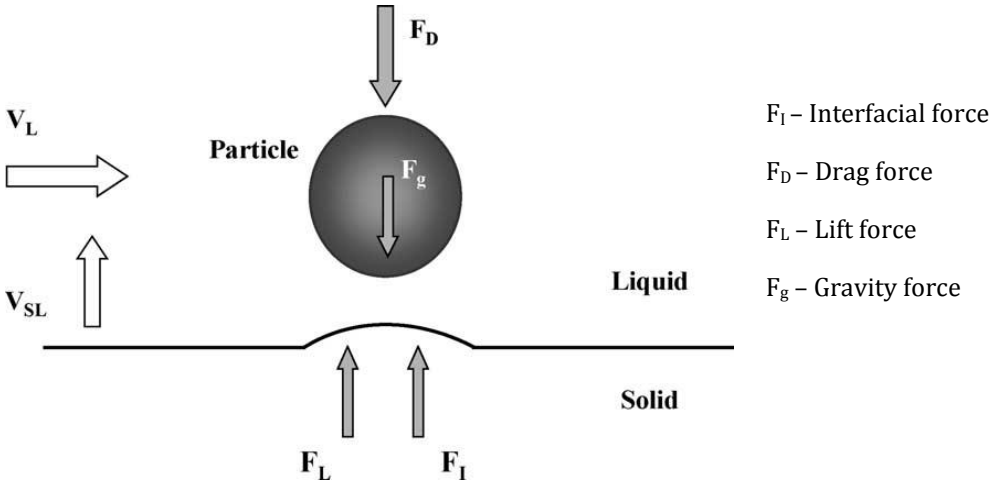

Figure 2.8 A schematic illustration of the forces acting on a particle in the vicinity of the solid–liquid interface [Youssef et al. 2005].

- The density of the melt and particles
- The liquid-solid interfacial shape
- The volume fraction of particles at the interface
- The temperature gradient in the melt ahead of the solidification interface.

The actual distribution of particles in a solidified material will largely depend on the morphology of the interface that is present under the given experimental conditions. A particle near the freezing front will either be rejected or engulfed [Rohatgi et al. 1986] and these two phenomena will lead to a redistribution of particles during solidification. When particles are entrapped by the solidification front, the distribution remains similar to that present in the liquid prior to solidification. On the other hand, pushing of the particles by the solidification front can lead to particles agglomerating between the grain boundaries. A final dendritic structure after solidification can lead to a particle distribution in the solid which will be significantly different from that in the liquid after mixing.

The theoretical critical velocity U_c above which the particle should be entrapped by a moving solid/liquid interface, can be calculated from the following equation [Uhlmann et al. 1964]:

$$U_c = \frac{\eta}{2}\left(\frac{La_0\Omega D}{k_B T a_p^2}\right) \qquad (2.10)$$

where n is a constant roughly equal to 5, L is the latent heat of fusion, a_0 is the atomic radius, Ω is the atomic volume, D is the diffusion coefficient, T is the temperature and k_B is Boltzmann constant. Surappa and Rohatgi [Surappa and Rohatgi 1981] have proposed an alternative empirical heat diffusivity criterion, according to which a particle is captured by the solidification front if:

$$\left(\frac{\lambda_p C_p \rho_p}{\lambda_l C_l \rho_l} \right) > 1 \qquad (2.11)$$

where λ_p, λ_l, C_p, C_l, ρ_p and ρ_l are the thermal conductivities, specific heats and densities of the particle and liquid respectively.

2.1.10 Characterization of reinforcement distribution in MMCs

The reinforcement distribution plays an important role in various aspects of the processing and final mechanical behaviour of particulate metal matrix composites. Therefore it is very important to quantify the distribution of the reinforcement in order to assess the quality of the fabricated MMCs. Several techniques have been used by researchers to characterise the reinforcement distribution in metal matrix composites. The *Lacey index* [Lacey 1954], *nearest-neighbor distance* and *mean free path* [Karnezis et al. 1998] are insensitive to mixture quality and fail to differentiate between distinctly different microstructures. A *finite body tessellation* [Boselli et al. 1998] provides a more meaningful description of the spatial distribution compared to a *Dirichlet tessellation* [Kurzydlowski and Ralph 1995]. *X-ray microtomography* (XMT) [Watson et al. 2005] shows three-dimensional distributions of reinforcement particles, whereas *reinforcement area fraction contour maps* [Ganguly and Poole 2002] capture the position, size, shape and reinforcement area fraction in a cluster. The *radial distribution function* and the *Quadrat method* [Karnezis et al. 1998] are found to be effective methods in detecting pronounced changes in the MMC microstructure.

The quantitative results provided by these methods can be related to the mechanical properties of a particular MMC system and provide an alternative method for understanding the factors that affect MMC failure. For example the mechanical properties are found to be a function of the nearest neighbor distance and it would be reasonable to assume that fracture is affected by the distance between contiguous

particles and not the macroscopic distribution of SiC particles. On the other hand, if a correlation existed between mechanical properties and the skewness of a distribution, it would be probable that the mechanical properties would be affected by the size of particle clusters rather than the distance between individual particles.

2.2 Magnesium alloys

2.2.1 Introduction to magnesium and magnesium alloys

Magnesium (Mg) takes its name from the Greek word *Magnesia*, an ancient Greek city and nowadays a prefecture in Thessaly, central Greece. It was first extracted in England by Sir Humphry Davy in 1808, but it was only until the early 19th century and the developments in lightweight flying machines that magnesium attracted interest [Polmear 1995]. It is an alkaline earth metal and constitutes about 2% of the Earth's crust by mass, which makes it the eighth most abundant element in the Earth's crust by mass [Housecroft and Sharpe 2007]. Magnesium is highly reactive and therefore not found in nature in elemental form, but only as magnesium compounds found in abundance both as solid deposits and aqueous solutions [Polmear 1995, Kainer and Von Buch 2003]. The most common minerals are dolomite ($MgCO_3$ $CaCO_3$), magnesite ($MgCO_3$) and carnallite (KCl $MgCl_2$ $6H_2O$), whilst the largest aqueous solution of magnesium is seawater. Magnesium can be recovered by various methods from all of the above, meaning the supply is virtually unlimited [Polmear 1995, Eliezer et al. 1998, Kainer and Von Buch 2003].

Magnesium has a hexagonal close packed (HCP) crystal structure, with lattice parameters a=0.3202 nm and c=0.5199 nm. The principal planes and directions in its unit cell can be seen in Figure 2.9. Plastic deformation of the magnesium crystal occurs by slip in the <1 1 $\bar{2}$ 0> directions on the basal planes and by twinning on the pyramidal {1 0 $\bar{1}$ 2} planes at temperatures below 498K. However, deformation is easier when the temperature is increased above 498K, as additional pyramidal {1 0 $\bar{1}$ 1} slip planes become operative. This explains why magnesium alloys have limited cold formability but are readily hot worked.

The lattice parameter of the magnesium unit cell (a=0.3202 nm) is such that it allows the addition of a wide range of solute elements, such as aluminium (Al), zinc (Zn), manganese (Mn), zirconium (Zr), strontium (Sr), calcium (Ca), etc., which can

be found in commercial magnesium alloys. The American Society for Testing Materials (ASTM) norm is most commonly used to identify magnesium alloys, according to which each alloy is marked with letters to indicate the main alloying elements and rounded whole numbers representing the nominal composition of each weight in percentage terms. Suffix letters following the last identification number are used to indicate the stage of alloy development or variations in composition [Polmear 1995, Kainer and Von Buch 2003]. The letters used for the main alloying elements in commercial magnesium alloys are summarised in Table 2.2.

Magnesium alloys have excellent specific strength and stiffness, very good machinability and processability, dimensional stability, high damping capacity and good weldability under a controlled atmosphere [Mordike and Ebert 2001, Kainer and Von Buch 2003, Yang et al. 2008(a)]. However, there are certain disadvantages that limit the application of these alloys, mainly identified as limited cold workability, limited strength and creep resistance at elevated temperatures, high chemical reactivity, high solidification shrinkage and in some cases low corrosion resistance [Eliezer et al. 1998, Mordike and Ebert 2001, Kainer and Von Buch 2003].

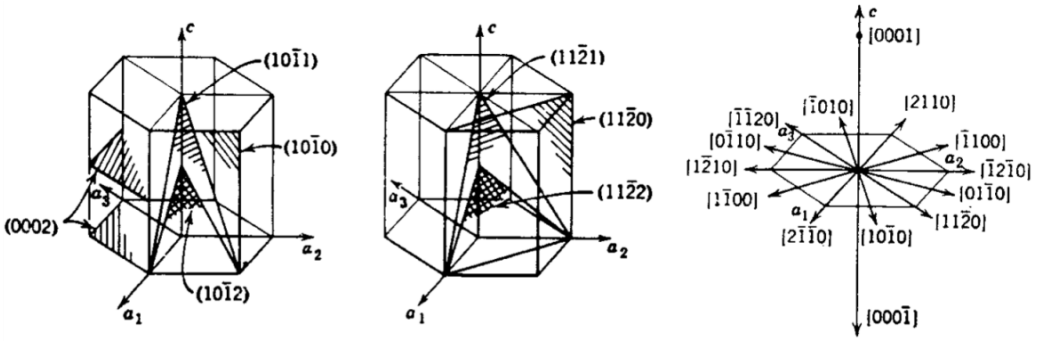

(a) (b) (c)

Figure 2.9 Magnesium unit cell crystal. (a) Principal [1 $\bar{2}$ 1 0] planes , basal plane, face plane (b) Principal [1 $\bar{1}$ 0 0] planes. (c) Principal directions [Polmear 1995].

Table 2.2 ASTM designations for alloying elements used in magnesium alloys.

Abbreviation letter	Alloying element	Abbreviation letter	Alloying element	Abbreviation letter	Alloying element
A	Aluminium	J	Strontium	R	Chromium
B	Bismuth	K	Zirconium	S	Silicon
C	Copper	L	Lithium	T	Tin
D	Cadmium	M	Manganese	W	Yttrium
E	Rare earths	N	Nickel	X	Calcium
F	Iron	P	Lead	Y	Antimony
H	Thorium	Q	Silver	Z	Zinc

Since these shortcomings of magnesium alloys were identified, several attempts have been made to improve their properties by employing different alloying elements to achieve strengthening by solid solution and/or precipitation hardening. The effects of the main alloying elements can be summarised as follows [Avedasian and Baker 1999, Kainer and Von Buch 2003]: aluminium causes an increase in tensile strength and hardness, improves castability but induces a higher tendency for microporosity; calcium refines the grain structure and aids creep resistance, but deteriorates castability in terms of tool sticking and hot cracking; manganese increases the tensile strength, offers grain refinement and improves weldability; rare earth additions raise the creep resistance, corrosion resistance and high temperature strength but increase the cost; silicon increases the creep resistance but deteriorates castability, zinc has a similar effect to aluminium, increasing the tensile strength and improving castability, but also induces a tendency to microporosity and hot cracking; finally zirconium leads to an increase in tensile strength and is very effective for grain refinement, but cannot be added to alloys containing aluminium or silicon.

Cast magnesium alloys can be classified in two broad groups depending on whether they contain zirconium: zirconium free alloys and zirconium bearing alloys. The reason for this classification is that Zr can effectively act as a grain refiner only in

the absence of Al, Mn, Si and Fe, as it forms stable compounds with these alloying elements [Emley 1966, Polmear 1995].

2.2.1.1 Zirconium free casting alloys

The most common commercially used zirconium free cast alloys are based on the magnesium– aluminium system [Avedasian and Baker 1999], such as the AZ (magnesium – aluminium – zinc) series and AM (magnesium – aluminium – manganese) series alloys, offering a good combination of mechanical properties, corrosion resistance and castability. As described earlier, aluminium increases the strength and castability of magnesium alloys, however, the presence of more than 2% Al inevitably leads to the formation of the β-phase $Mg_{17}Al_{12}$. The β-phase is located along the grain boundaries and leads to a decrease in ductility. Small additions of zinc further improve the strength of the alloys, but are limited because of an increased susceptibility to hot cracking. The most widely used cast magnesium alloy belongs to the AZ alloys series and is the AZ91D alloy, offering excellent castability even for complex and thin-walled shapes. When there are specific requirements for higher ductility and fracture toughness, zinc is replaced by manganese creating the AM alloys series. The presence of Mn and the reduced levels of Al in these alloys lead to a reduction in the amount of the β-phase and an increase in the alloy ductility. At the same time, manganese leads to an increase in the corrosion resistance. AM series alloys are widely used in the automotive industry, with alloys AM50A and AM60B being the most common examples.

What has been identified as an important drawback of the alloys based in the magnesium-aluminium system is their poor properties at elevated temperature and their unacceptable creep performance [Polmear 1995, Bamberger and Dehm 2008, Yang et al. 2008(a)]. The creep mechanisms of magnesium are mainly dislocation climb and grain boundary sliding and the limited creep resistance of commercial AM and AZ series alloys is attributed to the poor thermal stability of the β-phase and the accelerated diffusion of aluminium [Yang et al. 2008(a)]. Attempts have been made to reduce the Al content in magnesium alloys and use different alloying elements to replace Zn and Mn and improve their creep resistance. The addition of calcium is known to have a positive effect on the creep resistance of magnesium alloys and this lead to the development of the magnesium-aluminium-calcium (AX)

alloy system. However, these alloys are prone to hot cracking and casting defects such as misruns and die-sticking [Powell et al. 2001]. Reducing the levels of aluminium and alloying with silicon will reduce the amount of $Mg_{17}Al_{12}$ and lead to the formation of hard Mg_2Si intermetallic particles at the grain boundaries. The magnesium-aluminium-silicon (AS) alloy series exhibit improved creep performance, but still lower than that of competing aluminium alloys such as A380 [Polmear 1995, Avedasian and Baker 1999]. As a result the addition of rare earth (RE) elements was investigated and the magnesium-aluminium-RE (AE) alloy series were found to have increased creep resistance, although the use of RE elements leads to a significant increase in cost. Finally, the addition of strontium has been investigated [Pekguleryuz and Baril 2001] and the results were highly promising. The developed magnesium-aluminium-strontium (AJ) alloy series has shown superior creep resistance, elevated temperature properties and castability [Baril et al. 2003]. However, the room temperature properties of the AJ series alloys are not optimum.

2.2.1.2 Zirconium bearing casting alloys

Castings made with early magnesium alloys suffered from poor mechanical properties and microporosity, mainly attributed to their large and variable grain size. It was in 1937 in Germany that the intense grain refining effect of zirconium on magnesium was discovered, but several years later that a reliable method was found to produce zirconium bearing magnesium alloys [Polmear 1995]. The main reason for this was that zirconium was removed from solid solution by forming stable compounds with elements widely used in magnesium alloys, such as aluminium and manganese. Since then, new series of alloys containing zirconium have evolved and become of significant interest.

The first alloys to be developed belonged to the magnesium-zinc-zirconium (ZK) series, which had a fine grain structure and high strength, but were non-weldable and susceptible to microporosity. Addition of RE elements to the ZK series alloys improved their casting characteristics. The magnesium-zinc-RE-zirconium (ZE) series and magnesium-RE-zinc-zirconium (EZ) series have been commercially used in the aircraft industry and exhibit good mechanical properties and creep resistance. Another magnesium alloy series that has shown good creep resistance and elevated

temperature properties is the magnesium-thorium-zirconium (HK) alloy series, which however is considered obsolete today for environmental issues [Polmear 1995]. Finally, two magnesium alloy series that have excellent tensile properties and improved creep performance respectively are the magnesium-silver-RE-zirconium (QE) series and magnesium-yttrium-RE-zirconium (WE) series. However both these alloys are relatively expensive and have found limited automotive and aeronautical applications.

2.2.2 Processing and applications of magnesium alloys

2.2.2.1 Melting

Magnesium alloys are usually melted inside steel crucibles under the presence of a suitable flux or protective atmosphere. Contrary to aluminium and aluminium alloys, the oxide that forms on the surface of molten magnesium does not protect it from further oxidation and magnesium alloys tend to oxidise or burn in air rapidly [Avedasian and Baker 1999]. The first protective means against oxidation used during magnesium melting were salt fluxes containing $MgCl_2$, KCl, $BaCl_2$, CaF_2 and MgO [Ricketts et al. 2003]. The presence of chlorides in the flux that are retained in the melt after casting deteriorates the corrosion resistance of magnesium alloys and in the 1970s the fluxless method became more popular [Polmear 1995, Avedasian and Baker 1999]. A protective atmosphere comprising a single gas like argon (Ar) and SO_2, or a mixture of an active gas and diluting gas like CO_2, N_2 and air replaced fluxes. The active gas most widely used has been sulphur hexafluoride (SF_6) [Cahn et al. 2005, Bartos et al. 2007], an active gas that is non-toxic, odourless, colourless and effective at low concentrations. However, SF_6, which is a relatively expensive gas, was proved to have an enormous potential as a green house gas and several attempts have been made to replace it [Polmear 1995, Cahn et al. 2005, Bartos et al. 2007, Dieringa et al. 2007].

2.2.2.2 Casting

Magnesium alloys, as the lightest of all structural metallic materials, have found increased application, especially in the automotive industry, triggered by the demand for vehicle weight reduction. Almost every conventional casting method can be used

for the production of magnesium alloy products and factors such as the intended application, the required properties or the number of castings determine the method of choice [Avedasian and Baker 1999]. Sand casting and permanent mould casting produce components with low porosity and complicated shapes, while squeeze casting has been used to produce high quality castings from alloys that could not be cast by conventional methods [Polmear 1995, Eliezer et al. 1998].

The most commonly used fabrication process for magnesium components is high pressure die-casting [Cole 2007, Dieringa et al. 2007]. It is an economical process capable of producing high volumes of cast magnesium components with a wide range of sizes and shapes. Cold chamber high pressure die-casting machines are used for the production of large castings because of the high injection speed and pressure, whilst hot chamber machines are used for most applications, but are more competitive for small sizes because of the shorter cycle times obtained [Polmear 1995]. In 2007, 32% of overall magnesium consumption in the United States was for die-casting applications whilst the global demand has been expected to increase at a 7.3% average annual growth rate until 2012 [USGS 2008]. However, high pressure die-casting components usually suffer from high levels of porosity which limit the possibility of further property enhancement via heat treatment [Polmear 1995]

2.2.2.3 Applications

Commercial production of magnesium started in France in the middle of the 19th century but only reached 10 tonnes per annum by the end of the 19th century. The unlucky events of World War I and World War II and the extensive use of magnesium for German aircraft rose production of magnesium to around 300,000 tonnes per annum by the middle of 1940s. The annual production fell to about 250,000 tonnes for most of the 1990s and there has recently been an increase to more than 400,000 tonnes as reported in 2004 [Polmear 1995].

Although initially used mostly as an addition to various aluminium alloys [Polmear 1995, Mordike and Ebert 2001], magnesium is now finding increased applications as a structural material, mainly in the automotive industry. The main driving forces for this have been the attractive mechanical properties of magnesium, the continuous demand for weight savings, fuel economy and environmentally friendly cars with

reduced emissions, whilst there has been a decrease in the production cost of magnesium.

The increasing environmental concerns and tight regulations on CO_2 emissions render weight reduction a matter of crucial importance [Brungs 1997]. Mass reduction between 1.5 and 3.0 % is required in order to achieve a 1 % reduction in fuel consumption which in turn would reduce the CO_2 emissions of a vehicle [Cole 2007]. Compared to other fuel efficiency procedures such as diesel/hybrid powertrains and six/seven-speed automatic transmissions, mass reduction is more cost-effective and as such stimulates more interest [Bezdek and Wendling 2005]. At the same time, the price of magnesium has been decreasing over the years and the price ratio of magnesium compared to aluminium has ranged between 1.5:1 and 2.5:1. It is being estimated that if this ratio falls below 1.5:1, the use of magnesium will increase exponentially [Polmear 1995].

As mentioned earlier, the first applications of magnesium were in the aeronautical industry, used extensively in aircraft engines, airframes and landing wheels [Emley 1966]. New designs of airframes have completely eliminated the use of magnesium, which is now restricted to engine cases and transmission housings [Polmear 1995]. However, in the automotive industry magnesium is finding increased applications. In the 1950s and 1960s the Volkswagen Beetle was the largest single market for magnesium alloys [Emley 1966, Polmear 1995]. Since then, magnesium usage as a structural part in the automotive industry has been increasing and components such as die-cast steering wheels and steering columns, instrument panels, seat frames, motor housings, door handles, pedals and various brackets are produced from magnesium alloys. Other potential powertrain, chassis, body and interior applications have been summarised by Luo [Luo 2002] and are presented in Table 2.3.

The high strength to weight ratio and light density of magnesium have been exploited in applications such as thin walled computer housings and mobile telephone casings [Polmear 1995, Avedasian and Baker 1999]. Magnesium has also been used to manufacture sporting equipment like the frames of light-weight bicycles [Polmear 1995]. Finally, a very intriguing application for magnesium and

Table 2.3. Potential applications for magnesium alloys in the automotive industry.

Application	Product	Application	Product
Interior	Airbag housing	Body	Door frame (Inner)
	Window regulator housing		Hatchback frame
	Glove box		Spare tyre jack
Chassis	Wheel	Powertrain	Automatic transmission case
	Control arm		Engine block, engine mount
	Rack and pinion housing		Crankcase
	Bracket for rail frames		Oil pan, oil pump housing
	Spare tyre rim		Starter housing

magnesium alloys would be the use as orthopedic biomaterials. Magnesium has mechanical properties similar to natural bone; it is essential to the human metabolism and is found in bone tissue; it would degrade *in vivo* via corrosion in the electrolytic environment of the body and could serve as biocompatible, osteoconductive, degradable implants for load bearing applications. However, a great deal of research is still required in this area [Staiger et al. 2006].

2.2.3 Grain refinement

As described above, magnesium alloys are finding increased applications in several industries. With their low density, high strength to weight ratio and excellent castability, they have been spotlighted as the materials of choice for the production of automotive components that will enable weight savings [Lee 2007(b)]. However, conventional casting processes introduce coarse grain structures and characteristic defects like shrinkage porosity and hot tearing. Such casting defects can be reduced by grain refinement, also improving the machinability of cast products [Bamberger 2001].

The mechanical properties of magnesium alloys are highly affected by the grain size. As shown by the Hall-Petch equation [Hall 1951, Petch 1953]:

$$\sigma_y = \sigma_0 + k_y / d_g^{1/2} \quad (2.12)$$

where σ_y is the yield strength, σ_0 is the resistance of the lattice to dislocation motion (or the yield strength of a single crystal), k_y is the strengthening coefficient and d_g is the grain diameter, a fine grain structure is generally desirable to improve the mechanical properties. Magnesium alloys have a higher strengthening coefficient compared to aluminium alloys [Mabuchi et al. 2000] and grain refinement represents a very efficient way to improve their mechanical performance. As a result, since the late 1930s several researchers have pursued either a chemical or a physical approach for the grain refinement of Mg-alloys [StJohn et al. 2005].

2.2.3.1 Chemical route

The chemical route involves inoculation of the alloys by adding elements or compounds such as carbon (C) [Emley 1966, Polmear 1995, Qian and Cao 2005, Lu et al. 2006], zirconium (Zr) [Polmear 1995, Qian and Das 2006], silicon carbide (SiC) [Easton et al. 2006, Lu et al. 2006], strontium (Sr) [StJohn et al. 2005, Liu et al. 2008(a), Yang et al. 2008(b)], calcium (Ca) [Lee et al. 2000, Du et al 2008] and manganese (Mn) [Cao et al. 2006]. Addition of anhydrous $FeCl_3$ has also been considered historically and is known as the Elfinal process [Farbenindustrie 1942]. This process leads to obvious grain refinement, however, Fe is detrimental to the corrosion resistance of magnesium alloys and, in addition, the release of Cl or HCl is of great concern [StJohn et al. 2005, Fan et al. 2009(b)].

As described in section 2.2.1, zirconium is a potent grain refiner for magnesium alloys in the absence of Al, Mn, Si, and Fe, as zirconium forms stable compounds with these elements [Emley 1966]. Zirconium has been identified as an efficient grain refiner for magnesium alloys such as ZK, ZE and WE series alloys which can be easily grain-refined to a few tens of micrometres through minor addition of Zr containing master alloys under normal solidification conditions [Emley 1966]. For Mg-Al based alloys on the other hand, carbon inoculation has proved to be an effective approach for grain refinement. It involves the introduction of carbon into the alloy melt through either direct addition of carbon-based materials or organic

compounds, such as graphite, C_2Cl_6 and Al_4C_3, or bubbling the alloy melt with carbonaceous gases, such as CO and CH_4 [Emley 1966]. Grain refinement with carbon inoculation has been attributed to Al_4C_3 particles that act as nucleation sites for magnesium grains [Polmear 1995, Qian and Cao 2005]. This process has been used effectively, but inconsistency and contamination of the alloy melt still remain as important issues.

Although grain refinement by inoculation is a route easily applicable, a universal grain refiner for Mg-alloys has not yet been identified. Finding the right inoculants for different alloy systems is not always possible and although these elements can refine the microstructure, they give rise to various other problems. A number of grain-refining methods have been developed but they suffer from a number of problems making them unsuitable for commercial casting operations [StJohn et al. 2005]. Therefore, a physical route that does not involve addition of any elements would be favourable.

2.2.3.2 Physical route

Different physical approaches for the grain refinement of Mg-alloys so far have seen the application of superheating [Cao et al. 2007] and ultrasonic treatment [Abramov 1994]. Superheating was one of the first methods devised to control the grain size of Mg-Al based alloys as disclosed in a patent in 1931 [Farbenindustrie 1931]. It involves heating the alloy melt to a temperature well above the alloy liquidus (usually 180–300 °C of superheat) for a short time followed by fast cooling and a short holding at the pouring temperature prior to casting. Both the process variables and the alloy composition affect the efficiency of superheating [StJohn et al. 2005]. There are several proposed mechanisms for grain refinement with superheating, which involve Al–Mn–Fe-based intermetallics [Emley 1966, Cao et al. 2004] and aluminium carbides (Al_4C_3) [Emley 1966, Cao et al. 2007] acting as nucleation sites for magnesium grains. Owing to the severe oxidation at high temperatures and the requirement of rapid cooling, grain refinement by superheating is not very practical for commercial use. Other shortcomings include excessive consumption of time and fuel/electricity and a shortened life of the alloying vessels used in superheating [StJohn et al. 2005].

The grain refining potential of an ultrasonic treatment was first demonstrated by investigations carried out between 1960 and 1990 [Abramov 1994]. The renewed interest in magnesium alloys in recent years, together with the attempts to find an efficient physical approach for their grain refinement, have resulted in increased attention in the ultrasonic treatment of magnesium alloys [Zhang et al. 2007(b), Liu et al. 2008(b), Ramirez et al. 2008], particularly for Mg–Al-based alloys. However, the mechanisms of grain refinement with this approach are not yet clear and further research and development is needed to speed up its industrial application.

2.2.4 Recycling

The tight government regulations for sustainable economic development and the increasing concerns for environmental protection are the main driving forces for the attempts made by the automotive industry to improve fuel consumption and reduce greenhouse gas emissions. There is a general consensus that for every 10% reduction in vehicle weight there will be a corresponding 6–8% decrease in fuel consumption, also leading to reduced CO_2 emissions [Liu et al. 2008(c)]. The increasing usage of magnesium alloys aimed at weight savings will inevitably lead to a fast increase in Mg-alloy scrap from both manufacturing sources (new scrap) and end-of-life vehicles (old scrap).

The European Union has launched a directive on end-of-life vehicles, which states that 85 % of the vehicles weight will have to be recycled by 2015 [Fechner et al. 2007]. According to a German magnesium inventory analysis up to 2020 [Scharf et al. 2004], the major source of magnesium scrap is end-of-life vehicles. The general picture of this magnesium inventory is expected to be similar in the rest of the developed countries [Liu et al. 2008(c)]. In addition, the source for new scrap is also growing rapidly. In typical magnesium die-casting operations only around 50% of the material input ends up as finished products, and the remaining 50% of magnesium alloys is accumulated as scrap and handled by the foundry or an external recycler [Antrekowitsch et al. 2002]. Recycling scrap magnesium alloys requires less than 10% of the energy required for primary production [Scharf 2003]. Hence, the application of recycled magnesium can lead to a substantial reduction of greenhouse gas emissions and help the automotive industries conform to the tight government regulations for sustainable economic development. Therefore, recycling

magnesium alloys is becoming a major technical, economical and environmental challenge.

Both new and old magnesium alloy scrap contain substantial amount of inclusions and impurity elements which cause severe loss of strength and ductility and significantly reduce the corrosion resistance. Thus, a major barrier to overcome in magnesium recycling is dealing with the increased inclusions and impurity elements. Chemical approaches have been followed in order to reduce the amount of such inclusions and impurities [Javaid et al. 2006]. However, these recycling technologies remain complex, energy demanding and exhibit low productivity.

CHAPTER 3

EXPERIMENTAL PROCEDURES

3.1 Materials

3.1.1 Metal Matrix Composites

3.1.1.1 Matrix

Commercially available cast Al-alloys LM24 (USA designation A380) and LM25 (USA designation A356) supplied by *Norton Aluminium Ltd., Staffordshire, UK* were used as the matrix materials for the current study. The LM25 alloy was slightly modified with iron (final composition shown in Table 3.1) using an Al-46Fe master alloy. The small additions did not affect the alloy composition other than the Fe levels and were used to facilitate ejection and help die release in high-pressure diecasting [Fang et al. 2007]. The LM24 alloy was used as received from the supplier and the composition is given in Table 3.2. The specific alloys were chosen because a sufficient Si content is required to prevent or delay interfacial reactions between the matrix and the reinforcement during processing. More specifically, a Si content of at least 7 wt. % can prevent the formation of aluminium carbide (Al_3C_4) up to a temperature of 750 ºC in Al/SiC composites [Chernyshova and Kobeleva 1985, Lee et al. 1988].

Table 3.1 Chemical composition in wt. % of the modified LM25 alloy used.

Cu	Mg	Si	Fe	Mn	Zn	Ti	Al
0.003	0.30	7.5	0.5	0.005	0.003	0.11	Balance

Table 3.2 Chemical composition in wt. % of the as received LM24 alloy.

Cu	Mg	Si	Fe	Mn	Ni	Zn	Pb	Sn	Ti	Al
3.37	0.13	8.54	1.20	0.19	0.04	1.36	0.07	0.03	0.04	Balance

3.1.1.2 Reinforcement

The reinforcements used were black SiC_p (average size 4 μm) supplied by *Electro Abrasives Corporation, NY, USA*, and synthetic graphite powder (particle size ≤ 20 μm) supplied by *Sigma-Aldrich Company Ltd., Dorset, UK*. The size distribution of the SiC is shown Figure 3.1. The observed SiC particle size distribution in the cast samples was examined using an optical microscope (Carl Zeiss Axioskop 2 MAT0) equipped with image analysis software and compared with the supplier's data. Since the contact angle between liquid aluminium and SiC or graphite is higher than 90° [Eustathopoulos et al. 1974, Laurent et al. 1987] resulting in poor wettability, treatment of the reinforcement particles prior to addition in the molten metal matrix is considered beneficial. As a clean surface provides a better opportunity for the melt - particle interaction, the reinforcements were preheated at 400 °C for approximately one hour to remove moisture and surface impurities. The reinforcement was then transferred directly to the mixing setup and added in the molten matrix via gravity according to the following formula:

$$m_R = \frac{X m_M \rho_R}{(1-X)\rho_M} \tag{3.1}$$

Where X is the volume fraction of the reinforcement, m_R is the added mass of the reinforcement, m_M is the added mass of the matrix, ρ_R is the density of the reinforcement and ρ_M is the density of the matrix.

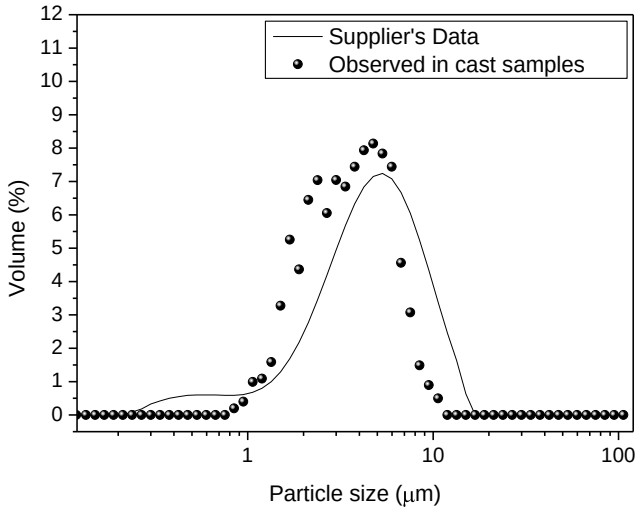

Figure 3.1 SiC particle size distribution used in this study.

3.1.2 Magnesium alloys

A range of magnesium alloys was investigated in the present study, covering the magnesium-aluminium-zinc (AZ), magnesium-aluminium-manganese (AM) and magnesium-aluminium-strontium (AJ) series. More specifically, these were AZ91D alloy supplied by *Magnesium Electron, Manchester, UK,* AM60B alloy supplied by *Meridian Technologies United Kingdom, Nottingham, UK,* and AJ62 alloy (Mg - 6 Al – 2.3 Sr in wt. %) supplied by *Magnesium Electron* and a mixture of AM50 - AM60B die casting high-grade scrap supplied by *Meridian Technologies United Kingdom*. Tables 3.3 to 3.5 show the chemical composition of alloys AZ91D, AM60B and AM50A according to the ASM Specialty Handbook [Avedasian and Baker 1999]. The designated letters after the numbers in the Mg nomenclature (i.e. A, B and D) are used to distinguish between alloys with the same nominal composition. Table 3.6 provides the chemical composition of the AJ62 alloy as given by the supplier. All alloys were melted in a *Carbolite* top loaded electrical resistance furnace at a temperature of 680 ºC. A protective atmosphere of 0.5 vol. % SF_6 in pure N_2 gas was maintained in both the melting furnace and the twin-screw mechanism, in order to avoid oxidation of the molten Mg-alloy.

Table 3.3 Chemical composition specification of AZ91D Mg-alloy (wt. %).

Al	Mn	Si	Zn	Fe	Cu	Ni	Others (each)	Mg
8.3-9.7	0.15-0.50	<0.10	0.35-1.0	<0.005	<0.030	<0.002	<0.02	Balance

Table 3.4 Chemical composition specification of AM60B Mg-alloy (wt. %).

Al	Mn	Si	Zn	Fe	Cu	Ni	Others (each)	Mg
5.5-6.5	0.25-0.6	<0.10	<0.22	<0.005	<0.010	<0.002	<0.2	Balance

Table 3.5 Chemical composition specification of AM50A Mg-alloy (wt. %).

Al	Mn	Si	Zn	Fe	Cu	Ni	Others (each)	Mg
4.4-5.4	0.26-0.6	<0.10	<0.22	<0.004	<0.010	<0.002	<0.2	Balance

Table 3.6 Chemical composition of AJ62 Mg-alloy (wt. %) as given by the supplier.

Al	Mn	Sr	Mg
6.3	0.36	2.5	Balance

3.2 Melt Processing

The process employed for the fabrication of the composites consists of two steps. The first step is conventional mechanical stirring offering distributive mixing of the reinforcement added in the matrix. The second and novel part of the process is dispersive mixing under intensive shearing, implemented by the MCAST process [Fan et al. 2009(a)]. For magnesium alloys, the melt was conditioned in the MCAST process prior to shape casting, in order to investigate the effects of intensive shearing on the solidification microstructures and mechanical properties. Table 3.7 provides the liquidus temperature of all alloys studied.

Table 3.7 Liquidus temperature of the aluminium and magnesium alloys studied in this work.

Alloy	LM25	LM24	AZ91D	AM60B	AM50A	AJ62
Liquidus temperature (° C)	615	596	598	615	620	612

3.2.1 Distributive mixing of metal matrix composites

Conventional mechanical stirring of Al alloys while adding reinforcement particles is being used to fabricate Al-based metal matrix composites [Ibrahim et al. 1991, Ray 1993]. The method is commonly known as stir casting and offers distributive mixing of the reinforcement particles in the metal matrix. The distributive mixing equipment used in this study is schematically shown in Figure 3.2. The setup consisted of a driving motor to create the torque on the impeller, a control part for the vertical movement of the motor and the attached stirrer assembly and a transfer tube for the introduction of the reinforcement particles into the melt. Properly cleaned metal alloy ingots were melted in cylindrical crucibles using a top loaded resistance furnace set at 650 ºC. Accurately measured reinforcement volume fractions were heated at 400 °C inside an electrical resistance furnace. With the help of the transfer tube, the preheated reinforcement was added by gravity in the melt through the vortex created by stirring.

It is well known [Beck et al. 1991] that the impeller design plays a crucial role in the mixing process. To ensure a uniform distribution and based on previous work [Nagata 1975, Aniban et al. 2002], the impeller was designed to have a d_i / D_v ratio equal to 0.4 and a w_i / d_i ratio equal to 0.35, where d_i is the diameter of the impeller, w_i is the width of the impeller and D_v is the inner diameter of the crucible

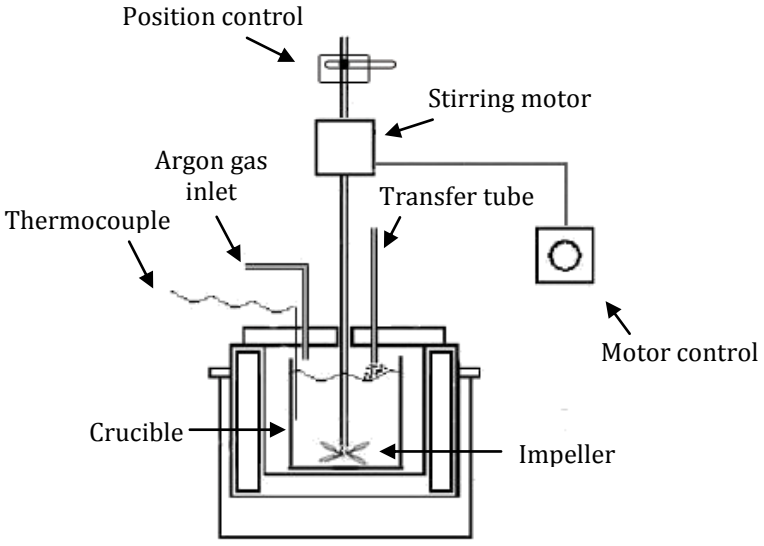

Figure 3.2 Schematic diagram of the distributive mixing equipment.

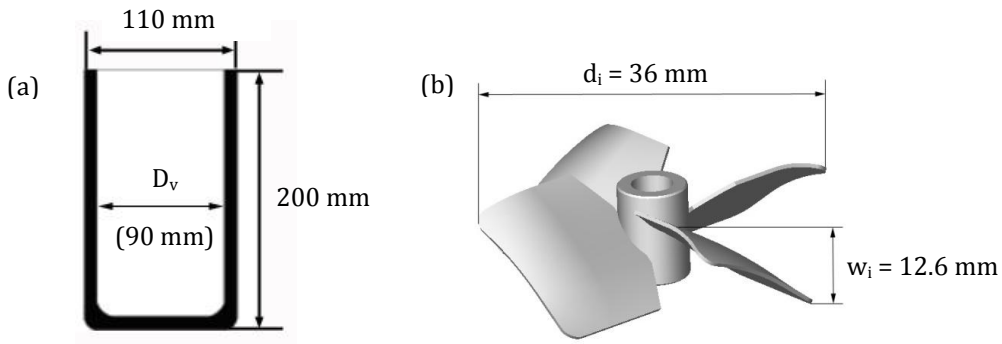

Figure 3.3 Schematic illustration of the geometry of (a) the clay graphite crucible and (b) the stainless steel impeller used for distributive mixing.

(90 mm). Schematic diagrams of the flat bottom cylindrical clay graphite crucible and the impeller geometry are shown in Figure 3.3. The four-bladed stainless steel impeller was coated with boron nitride to prevent reaction with the molten aluminium. A controlled argon atmosphere was maintained inside the furnace throughout the whole experiment to prevent melt oxidation. The reinforcement particles were transferred slowly and continuously into the melt which was mechanically stirred at 600-800 rpm. Stirring of the mixture was carried out in both liquid and semi-solid regions to achieve spatial homogeneity of the reinforcement particles (similar volume fraction in any part of the mixture).

3.2.2 Dispersive mixing of metal matrix composites

The first stage of MMC fabrication, the distributive mixing, is necessary in order to introduce the reinforcement particles in the melt. However, due to a diminishing velocity gradient in the melt as we move away from the impeller, the degree of mixing is limited. The lack of sufficient shear force during distributive mixing results in agglomeration of the reinforcement in relatively stagnant zones such as areas near the crucible walls. To break up these agglomerates into individual particles in the liquid metal, the applied shear stress (τ) on particulate clusters should overcome the average cohesive force or the tensile strength of the cluster. Molecular dynamics studies [Falk and Langer 1998, Schuh and Lund 2003, Mayr 2006] suggest that intensive shearing can displace the position of atoms that are held together with high strength bonds. Under high shear and high intensity of

turbulence, liquid can penetrate into the clusters and displace the individual particles within the cluster. The implementation of intensive shearing is done with the MCAST process.

3.2.3 Melt Conditioning by Advanced Shear Technology (MCAST) process

The MCAST process is a novel technology for conditioning liquid metal prior to solidification processing. In the MCAST process, liquid metal is fed into a twin screw device, in which a pair of co-rotating and fully intermeshing screws is rotating inside a heated barrel with accurate temperature control resulting in the melt being subjected to intensive shearing under a high shear rate and high intensity of turbulence [Fan et al. 1999, Ji et al. 2001]. A schematic illustration of the basic functional unit of the MCAST process, the twin screw machine, can be seen in Figure 3.4. After the MCAST process, the conditioned liquid metal has an extremely uniform temperature, uniform composition and well dispersed inclusion particles. These individual particles will have a fine size and narrow size distribution, and more importantly, they are believed to be completely wetted by the liquid metal under the intensive forced convection (referred to as forced wetting). The MCAST unit can be operated at temperatures either above the alloy liquidus to provide conditioned liquid metal, or below the alloy liquidus to provide semisolid slurry. The temperature is monitored using six K-type thermocouples with an accuracy of ±2.5 ºC. In the latter case, the semisolid slurry contains a well controlled solid fraction of primary solid particles with a fine size and a spherical morphology.

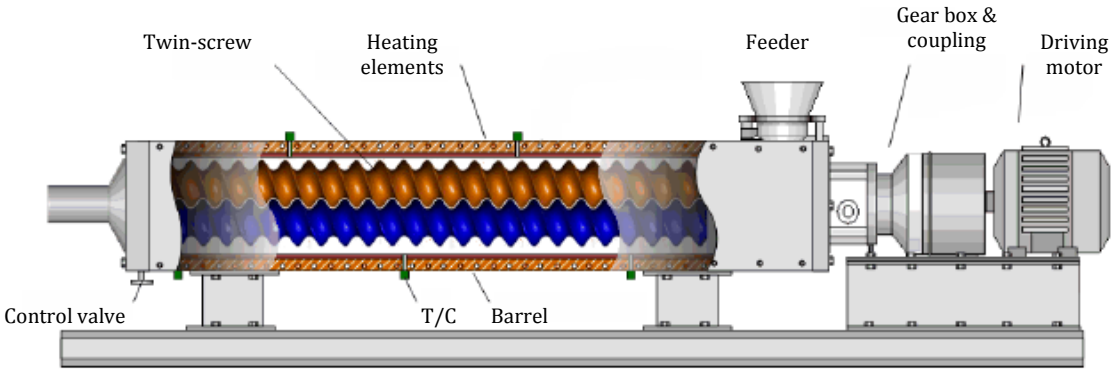

Figure 3.4 Schematic illustration of the twin-screw mechanism used in the MCAST process.

3.3 Casting processes

Various casting methods were used in order to examine the effect of intensive shearing on the microstructure and mechanical properties of the metal matrix composites and the magnesium alloys studied. The Aluminium Association Test Procedure-1 (TP1®) mould was used for casting the sheared and non-sheared magnesium melts under similar conditions. A pressurised filtration technique (Prefil®, N-Tec Ltd, UK) was used to collect oxides and other inclusions for optical and scanning electron microscopy. Al-based PMMC and Mg-alloy components were also high pressure die cast for optical and scanning electron microscopy, as well as mechanical property testing. A small cylindrical steel mould was also used for general microstructural observations of the Al-based PMMCs.

3.3.1 Test Procedure -1 (TP-1®) mould

There are various factors that can affect the solidification microstructure of a given alloy and perhaps the most important is the cooling rate. The grain size for a given alloy depends on the cooling rate and in order to study the effect of intensive shearing on the microstructure of various magnesium alloys, a standard Test Procedure-1 (TP-1®) mould technique was used, to maintain a constant cooling rate. The experimental steps followed in this casting process are:

a) The magnesium alloy was melted inside a steel crucible in an electrical resistance furnace at a preset temperature. A protective atmosphere of 0.5 vol. % SF_6 gas in pure N_2 was maintained to avoid oxidation. The melt was held for 1 hour to homogenise.
b) The TP1® mould ladle (Figure 3.5) was placed inside a furnace for preheating at 350°C.
c) The water flow rate of the TP1® mould quench tank was set at 1 gallon $minute^{-1}$ (3.8 l $minute^{-1}$). This flow rate resulted in 25 mm submersion from the bottom of the ladle.
d) Sample preparation for microstructural study: The test sample removed from the TP-1 conical mould was cut according to the standard procedure (38 mm above the base) as illustrated in Figure 3.5. The cooling rate at this position corresponds to 3.5 K s^{-1}.

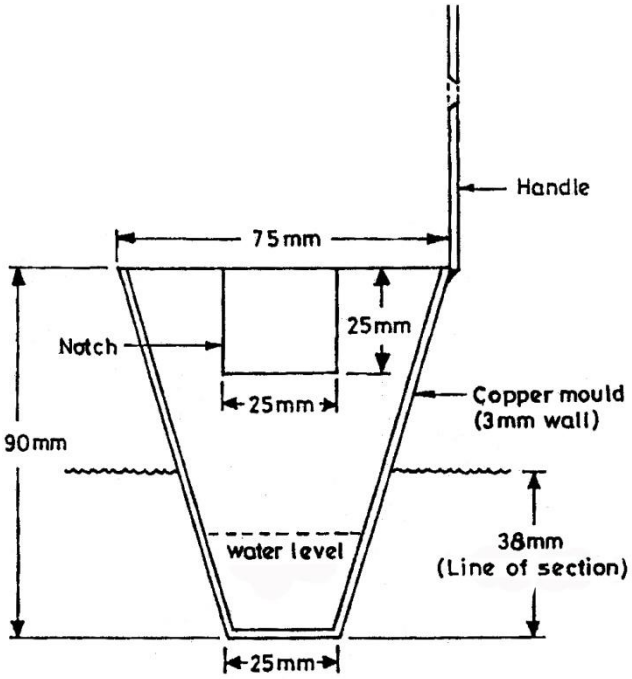

Figure 3.5 Schematic diagram of TP-1 grain refining test mould ladle [The Aluminium Association 1990].

3.3.2 Pressurised filtration technique – Prefil®

In order to investigate the nucleation mechanisms of the solidifying magnesium alloys, a pressurised filtration technique was used to collect possible heterogeneous nucleating particles for various alloy melts with and without intensive shearing. Figure 3.6 shows a schematic illustration of the Prefil® technique developed by N-Tec Ltd, UK, which was used in this study. The experimental steps followed during the pressurised filtration technique are:

a) The magnesium alloy was melted inside a steel crucible in an electrical resistance furnace at 680 °C. A protective atmosphere of 0.5 vol. % SF_6 gas in pure N_2 was maintained to avoid oxidation. The melt was held for 1 hour to homogenise.
b) A clean Prefil® crucible with an iron filter of approximately 3 μm mesh size was pre-heated.
c) The weigh ladle was emptied and placed in its position.
d) The Prefil® crucible with the filter was placed in the pressure chamber.

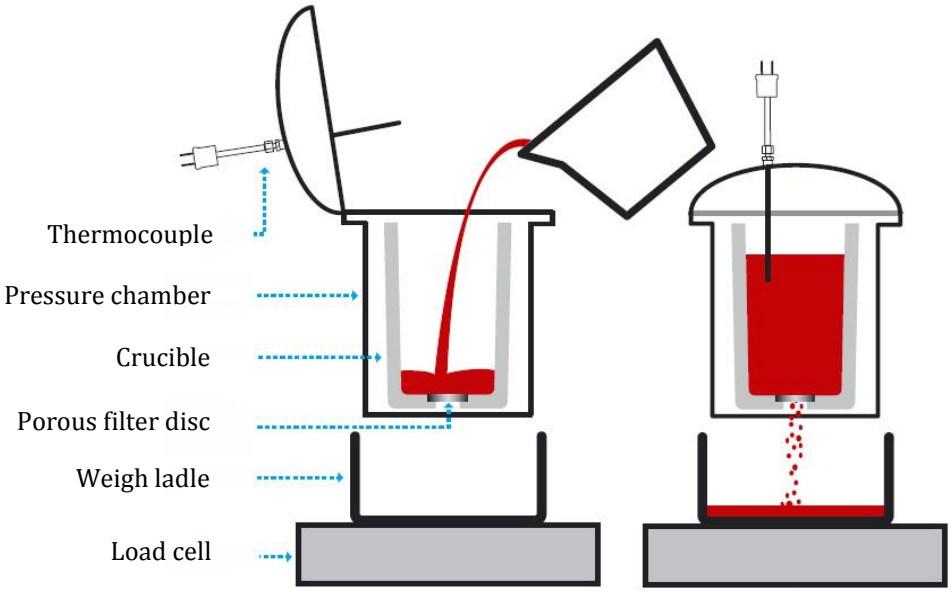

Figure 3.6 Schematic illustration of the Prefil® equipment used for the pressurised filtration of the Mg-alloys in this study.

e) 0.7 kg of melt either with or without intensive shearing was transferred to the Prefil® crucible.
f) The pressure chamber was closed and pressure was applied to the metal pushing it through the filter at the bottom of the crucible.
g) When a pre-determined amount of melt was filtered and collected at the weighing ladle, the test was stopped and pressure was released from the chamber, allowing the lid to open.
h) A cubic sample with a 10mm side was cut from the metal that solidified inside the Prefil® crucible, consisting of the filter and the metal right above the filter. The sample was then prepared for metallographic characterization.

3.3.3 The High Pressure Die-Casting (HPDC) process

In order to study the microstructure of samples cast at high cooling rates, as well as being able to evaluate their mechanical properties, high pressure die casting was used to produce standard mechanical property test samples. The HPDC process is well established and widely used as an effective manufacturing technique, especially in the automotive industry. A more detailed understanding of the process and its applications are given by Street [Street 1977].

A standard cold chamber HPDC machine by *LK® Machinery Co. Ltd., Hong Kong* was used and a schematic illustration of the equipment is shown in Figure 3.7. The diameter of the plunger is 60 mm, and it has a maximum accelerated shot speed of 6.22 m/s, with the maximum shot distance being 405 mm. The dies were clamped at a load of 280 tonnes and pre-heated using 8 cartridge heaters embedded symmetrically inside the two halves of the die-block maintaining a uniform temperature across the die-cavity. A thermocouple was also embedded inside the die block to feed the heating control unit on the machine with a temperature reading and an external thermocouple was used to measure the temperature of the die-cavity surface prior to any casting. The steps followed for the HPDC process are:

a) Carefully clean the die surfaces of any material left from previous castings and coat with 'Hotemp 2000' lubricant to aid ejection of cast samples.
b) Pour a pre-determined amount of melt at a pre-set temperature into the shot sleeve of the HPDC machine
c) Activate the HPDC machine to apply the shot according to the set profile of the plunger speed, position and pressure. The machine automatically runs through the cycle of injection, intensification, dwelling (while the casting fully solidifies) and finally ejection of the cast component.

The die used for the test samples consists of four cavities, two are tensile test samples (labelled A and C) and two are fatigue test samples (labelled B and D) as shown in Figure 3.8. The exact dimensions of the tensile test specimens and the fatigue test specimens are 6.4 and 6.3 mm in gauge diameter respectively, 25 mm in gauge length and 12 mm in diameter of the grip section.

3.3.4 The Melt Conditioned High Pressure Die Casting (MC-HPDC) process.

The MC-HPDC process is a combination of the MCAST and HPDC processes. Figure 3.9 shows a schematic illustration of MC-HPDC process. As described in section 3.2.3, the twin screw machine used in the MCAST process consists of a barrel and a pair of closely intermeshing, self-wiping and co-rotating screws. The barrel is divided into separate heating and cooling zones and the temperature control, achieved by balancing the heating power input by a central control unit, has an accuracy of ± 1°C. The thermocouples are fitted in the barrel liner perpendicular to its axis ensuring the nearest temperature reading. Thermocouples are also fitted on

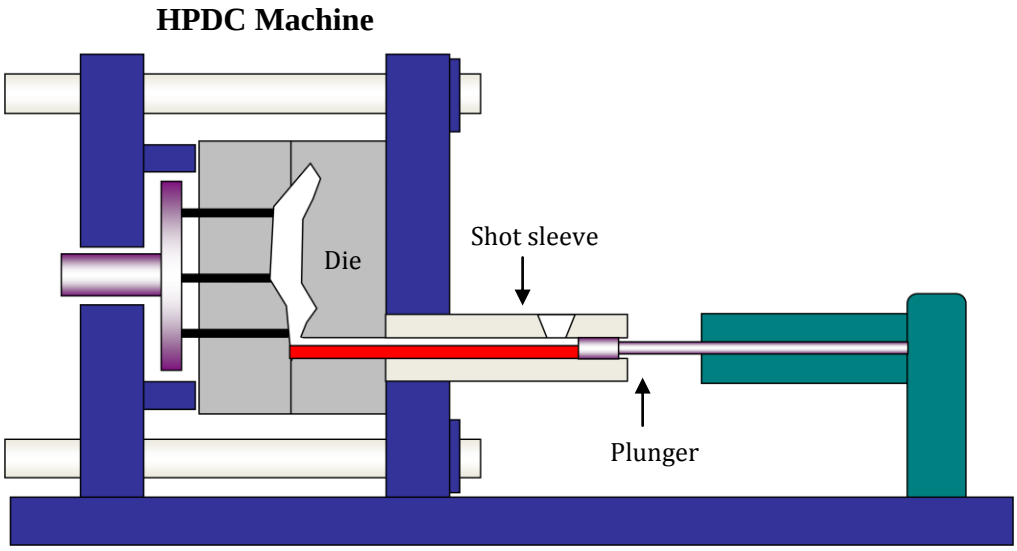

Figure 3.7 A schematic illustration of the cold chamber high pressure die-casting (HPDC) set-up.

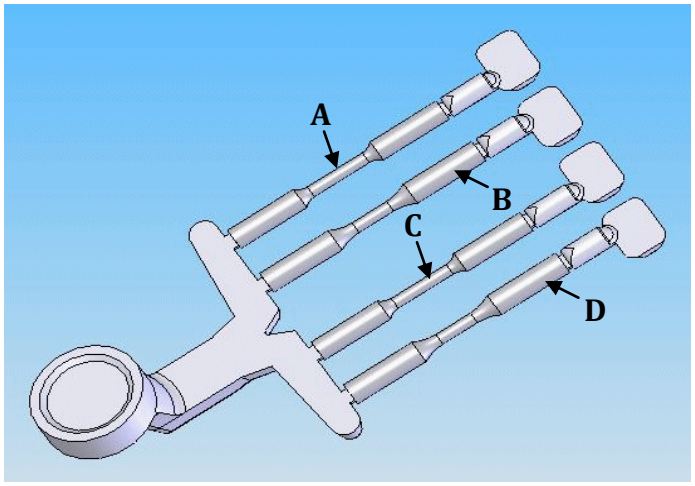

Figure 3.8 Schematic illustration of the die-cast component produced by the HPDC machine, showing the two tensile test specimen (labelled A and C) and the two fatigue test specimen (labelled B and D).

the feeder and the transfer valve area. The central control unit consists of temperature controls for all the heating zones, a dial to indicate screw rotations per minute (rpm), a torque reading of the screws, a timer, and switches to control the transfer valve.

The machine heaters are switched on and set to the preferred temperature. Sufficient time is allowed for the machine to reach the set temperature from room temperature. The transfer tube is heated to the same temperature as the processing temperature set in the MCAST machine. The rotating speed and running time of the screws can be controlled until discharge of the conditioned melt in the shot sleeve of the HPDC machine, before applying the plunger to cast a component. The entire sequence can be set on automatic mode including opening and closing of the transfer valve, where the discharge time can also be controlled. The MC-HPDC process can be fully automated by an electronic connection between the control panel of the MCAST machine and that of the die caster. The cycle time is mainly dictated by the shearing time allowed in the MCAST machine and dwell time allowed for complete solidification of the die-cast component during the die-casting process. The discharge time is dependent on the amount of melt processed inside the MCAST machine.

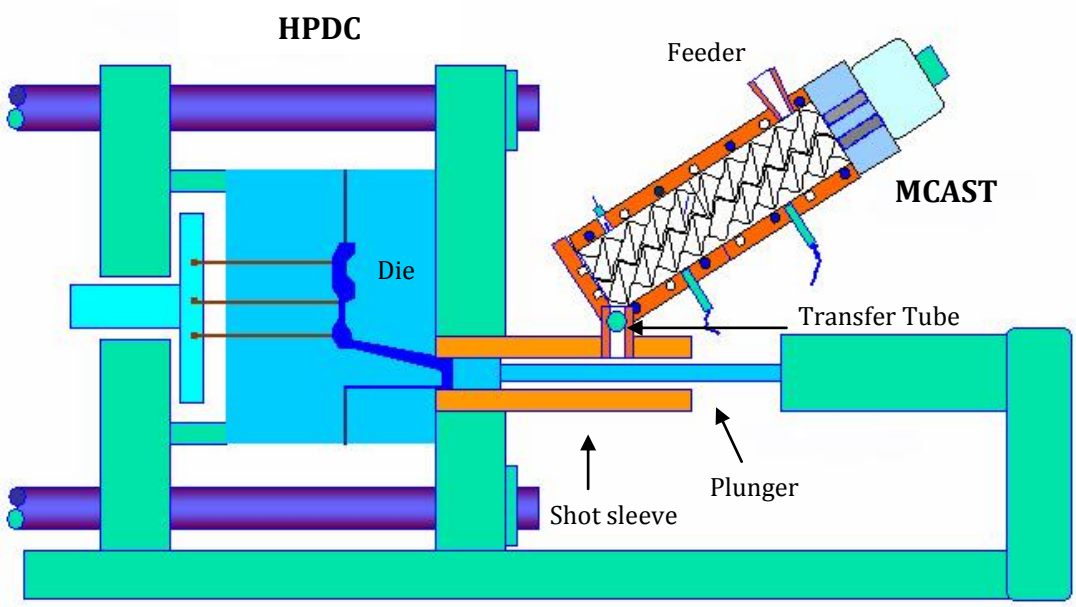

Figure 3.9 Schematic illustration of the MC-HPDC process.

The fluid flow inside the MCAST machine is characterised by a cyclic variation of shear rate and high intensity of turbulence. It is rather difficult and complex to determine the exact shear rate, but based on viscous flow, the shear stress τ between the screw and the barrel can be estimated from [Rauwendaal 1994]:

$$\tau = \eta \, \pi \, N_s \left(\frac{D_s}{G_s} - 2 \right) \tag{3.2}$$

where N_s is the rotation speed of the screw, D_s is the outer diameter of the screw, in our case equal to 36 mm, and G_s is the gap between the screw flight and the barrel surface, in our case 1 mm. For simplicity, the screw rotation speed N_s is being used in this investigation to determine the shearing intensity. Based on reported data for the viscosity of aluminium matrix PMMCs [Quaak and Kool 1994, Quaak et al. 1994], at different processing temperatures and different rotation speeds, the shear stress produced by the MCAST unit was estimated from equation 3.2 to vary from as little as 300 Pa up to 5000 Pa or more.

3.3.5 Processing Conditions

The investigated MCAST processing parameters used in this study together with the HPDC parameters are listed in Table 3.8 for the MMCs and the Mg-alloys. The results and the effect of the processing parameters are presented and discussed in Chapter 4 for the MMCs and Chapter 5 for the Mg-alloys.

3.4 Microstructural Characterization

3.4.1 Metallographic sample preparation

Samples were cut from various locations of the final cast components for microstructural characterization, as indicated in Figure 3.9b. The microstructures presented throughout this thesis are all from specimens taken from location CC´. The specimens were prepared by the standard technique of mounting in Bakelite followed by grinding using 120, 500, 800, 1200, 2400 and 4000 grit SiC papers. The MMC specimens were polished on a cloth with a silica suspension and 1 μm and 0.25 μm diamond suspensions. The microstructures were examined without etching. The Mg-alloy specimens were polished on a cloth with a silica suspension followed

Table 3.8 The investigated MCAST and HPDC processing parameters.

Parameter	Metal Matrix Composites	Mg-Alloys
Shearing Temperature (ºC)	600 – 630	605 - 650
Shearing Speed (rpm)	400 - 800	500 - 800
Shearing Time (seconds)	60 - 240	45
HPDC Die Temperature (ºC)	200	170 - 250
Intensifier position (mm)	200	180 - 240
Shot Speed (%)	60	70 - 75
Intensifying Pressure (bar)	70	100
Intensifying Speed (%)	65	75 - 80
Dwell time (seconds)	30	30 - 60

by etching. A solution of 5 vol. % concentrated HNO_3 and 95 vol. % of ethanol was used for general observations of the microstructure. In order to obtain further microstructural information, colour etching in a solution of 70 ml ethanol, 10 ml water, 20 ml acetic acid and 4.2 grams picric acid was used, with the coloured orientation contrast being created under polarised light of the optical microscope.

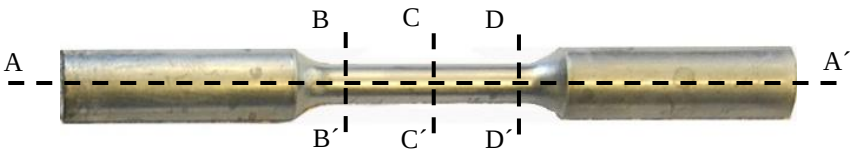

Figure 3.10 Identification of the locations where the cast tensile specimen where cut for the preparation of metallographic specimen for microstructural characterisation. The samples were sectioned along the length as indicated by line AA´ and at three different cross-sections in the gauge length, as indicated by lines BB´, CC´ and DD´.

3.4.2 Optical microscopy (OM)

A Carl Zeiss Axioskop 2 MAT optical microscope equipped with image analysis software, a camera and a computer was used for the OM observation and the quantitative measurements of microstructural features. A software application was used to acquire images from the camera and to perform image analysis. This microscope has 2.5, 10, 20 and 50 objective lenses. The size and area fraction of reinforcement particles in the MMC specimens and primary particles in the Mg-alloy specimens were measured. In the bright field (BF) mode, a polished surface shows bright in contrast and the surface irregularities such as grain boundaries, reinforcement particles and intermetallics appear dark in contrast. Plane polarised light (PP) is most commonly used for grain size measurements.

3.4.3 Scanning electron microscopy (SEM)

Some of the specimens used for optical microscopy were subsequently carbon-coated and SEM examinations were performed using a Zeiss Supra 35VP FEG scanning electron microscope. For chemical composition analysis, the SEM was equipped with an energy dispersive X-ray spectrometer (EDX), Oxford Instruments Inca and data were ZAF corrected. The advantage of SEM over optical microscopy is the large depth of field and higher resolution, thus producing high resolution images at high magnification (up to 50,000 times). A good explanation of the procedures and uses of SEM and EDX are given by Watt [Watt 1997].

3.4.4 Quantitative metallography

Quantitative metallographic analysis was carried out on OM images using image processing software Axioskop 2 MAT0. The equivalent circle diameter d_c was calculated by:

$$d_c = \sqrt{\frac{4A_p}{\pi}} \tag{3.3}$$

where A_p is the total area occupied by the particle. For the quantitative analysis of the distribution of the reinforcement particles in the MMCs, two statistical methods were used: the Lacey Index [Lacey 1954] and the Quadrat method [Rogers 1974].

The two extremes of a mixture can be described as completely segregated when any sample withdrawn from the mixture will be composed of a pure component, or fully randomised when the probability of finding a constituent in every point is identical. According to Lacey [Lacey 1943], for a completely segregated mixture the variance S_0^2 can be expressed as:

$$S_0^2 = pq \tag{3.4}$$

where p and q are the proportions of the components estimated from the samples using image analysis. For a fully randomised mixture the variance S_R^2 is:

$$S_R^2 = \frac{pq}{N_p} \tag{3.5}$$

where N_p is the number of particles in the sample, estimated using the average particle size and the component proportions. The Lacey index M_L is defined as:

$$M_L = \frac{S_0^2 - S^2}{S_0^2 - S_R^2} \left(= \frac{\text{How much mixing has occured}}{\text{How much mixing could occur}} \right) \tag{3.6}$$

where S^2 is the variance of the mixture. The index should have a zero value for a completely segregated mixture and increase to unity for a fully randomised mixture. A criticism of the Lacey index is that it is insensitive to mixture quality. Practical values of the Lacey index are restricted to the range of 0.75 to 1.0 [Harnby et al. 1997].

With the quadrat method, the image to be studied was divided into a grid of square cells where the square quadrat size was approximately twice the size of the mean area per particle [Curtis and McIntosh 1950]. To minimise the edge effects, particles only inside and in contact with the left and bottom side of each quadrat were counted. A schematic illustration of the quadrat method is presented in Figure 3.10. The quadrat method was performed on a number of images of each specimen within square fields, 924 × 924 pixels in size. Each field was divided into 36 contiguous quadrats. A quadrat side of 20 μm (154 pixels) was chosen at 50X magnification and a number of 40 images was analyzed for each specimen of the Al-SiC PMMCs. A characteristic example of how the Quadrat method was applied on the micrographs can be seen in Figure 3.11. The area to be studied in LM24-graphite composites was divided into 25 contiguous quadrats with a quadrat side of 54 μm (168 pixels) at

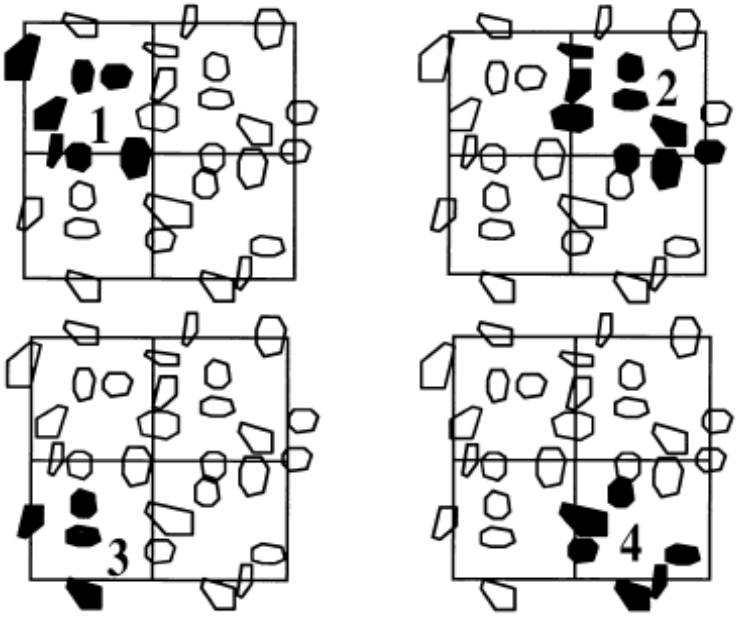

Figure 3.11 Schematic representation of the quadrat method, using four quadrats. Counted particles are denoted in black. [Karnezis et al. 1998].

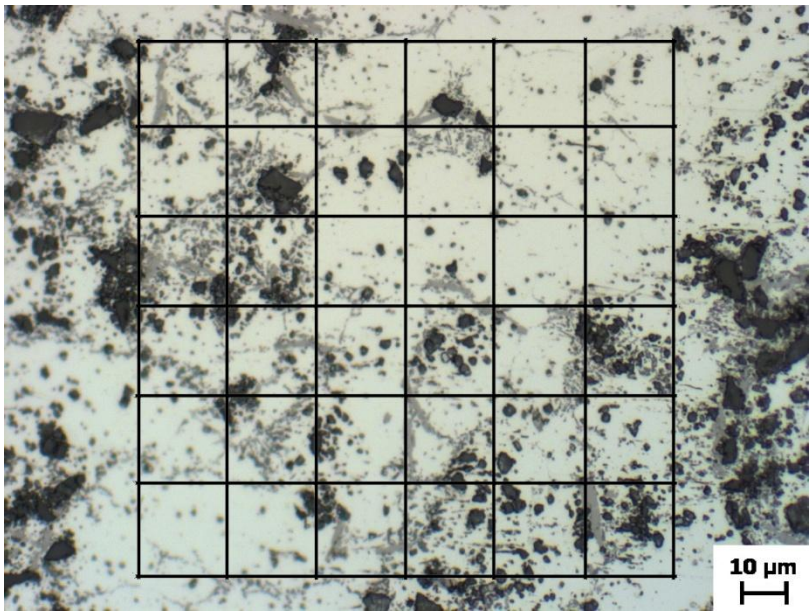

Figure 3.12 Application of the Quadrat method performed on the microstructure of a LM25 - 5 vol. % SiC_p composite.

20X magnification and analysis was performed on 40 images of each specimen. The number of particles in a quadrat, N_q, was measured and the degree of asymmetry of a statistical distribution around its mean can be quantified by its skewness β, which is defined by:

$$\beta = \frac{q_t}{(q_t - 1)(q_t - 2)} \sum \left[\frac{N_{qi} - N_q^{mean}}{\sigma_q} \right]^3 \qquad (3.7)$$

where q_t is the total number of quadrats studied , N_{qi} is the number of particles in the i^{th} quadrat (i = 1,2,…..q), N_q^{mean} is the mean number of particles per quadrat and σ_q is the standard deviation of the N_q distribution. According to a previous study [Karnezis et al. 1998] an increase in β indicates an increase in clustering.

The grain size measurements for the Mg-alloys were carried out on colour etched samples using a mean line intercept method as shown in Figure 3.12. Five horizontal and three vertical equidistant lines where used to estimated the grain size.

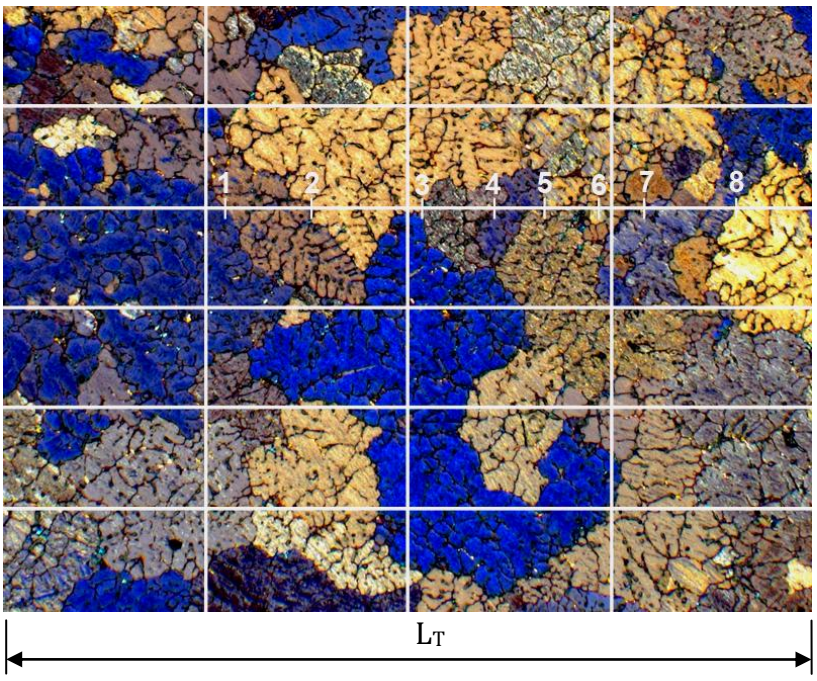

Figure 3.13 Schematic representation of the mean line intercept method performed on the microstructure of an AJ62 casting.

The mean intercept length $\bar{l}$ which is used as the grain size is then calculated using the following equation:

$$\bar{l} = \frac{L_T}{N_i} \tag{3.8}$$

where L_T is the total length of the test lines and N_i the total number of grain boundary intersections on each test line. The measured standard deviation from the average grain size measurements is used as the error in grain size measurements.

3.5 Mechanical properties testing

3.5.1 Tensile testing

The tensile property testing was carried out using a universal materials testing machine (Instron ® 5569) at a cross head speed of 2 mm minute^{-1} (strain rate: 1.33 $\times$ 10^{-3} s^{-1}) for the Al-based composites and 1 mm minute^{-1} (strain rate: 0.66 $\times$ 10^{-3} s^{-1}) for the Mg-alloys. The tensile testing system was connected to a PC for automated testing and calculation of tensile test results such as yield stress, ultimate tensile strength and Young's modulus. During the test, a sample was extended at constant rate, and the load needed to maintain this was measured. An external extensometer of 25 mm gauge length was attached to each test sample during testing to get accurate elongation results. The stress σ calculated from the load and the strain ε calculated from the extension were plotted as a stress-strain curve. The yield strength was measured as the 0.2% proof strength on the stress-strain curve. All samples were tested at room temperature.

3.5.2 Hardness testing

The Vickers diamond pyramid indentation technique was used to determine the macro-hardness of the composite materials. Samples prepared by the procedure described in section 3.4.1 were used for the Vickers hardness measurements. Each sample was placed on the platform of the test machine and the applied load on the pyramid makes an indentation point on the sample. The indentation diagonals are measured and the Vickers hardness is calculated using the average diagonal length

and reference tables converting the length to a hardness value. On an average, 10 indentations were measured for each sample. A Vickers pyramid hardness testing machine, *Vickers – Armstrongs Ltd., London & Crayford, UK*, was used, with an applied load of 20 kg.

CHAPTER 4

METAL MATRIX COMPOSITES (MMCs)

RESULTS AND DISCUSSION

4.1 General Microstructure

The PMMC microstructures obtained with or without the implementation of intensive shearing are presented in this section. Discussion is focused on the distribution of the reinforcement particles during melt processing, their redistribution during solidification and how intensive shearing affects the dispersion of these particles and the solidification behaviour of the materials. In Section 4.1.1 that follows, the microstructures presented and discussed are by conventional mixing, while in Section 4.1.2 the resultant microstructures after additional intensive shearing of the PMMCs are presented and discussed.

4.1.1 Distributive mixing – the HPDC process

4.1.1.1 LM25 – SiC_p composites

Figure 4.1 presents the microstructures of the distributive mixed composites, where no intensive shearing was imposed on the melt prior to casting either in a steel mould or by high pressure die casting. The reinforcement particles agglomerated forming clusters preferentially located at the grain boundaries or the interdendritic regions regardless of the casting method. This can be attributed to the pushing of the particles by the solidification front and is in accordance with various previous studies [Nagarajan et al. 1999, Gupta et al. 1996, Naher et al. 2003, Akhalaghi et al. 2004, Youssef et al. 2005]. The difference between the two casting methods is that with the HPDC process, the high cooling rates and application of pressure resulted in a more refined microstructure and the macroscopical segregation observed was significantly lower than in the composites cast in the steel mould. In addition, during the HPDC process the composite melt is forced to pass through the narrow gate of the die where the developed shear forces can result in partial cluster break

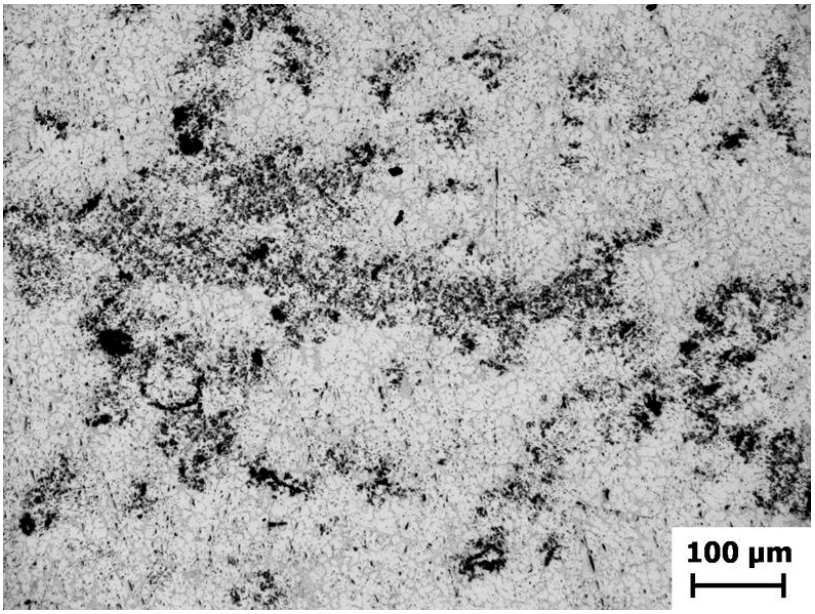

(a)

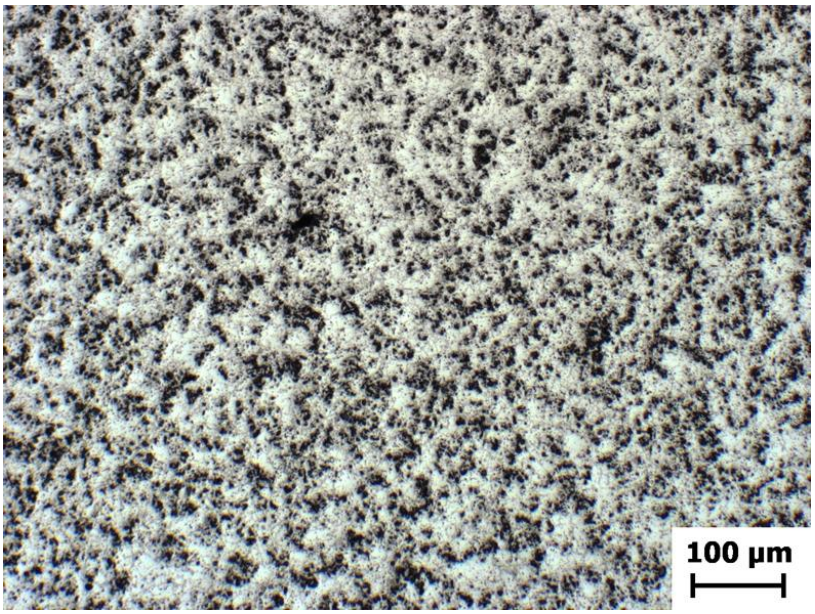

(b)

Figure 4.1 Typical microstructures of distributive mixed LM25 – 5 vol. % SiC_p composites cast at 630 ºC. (a) Cast in steel mould and (b) produced with the HPDC process.

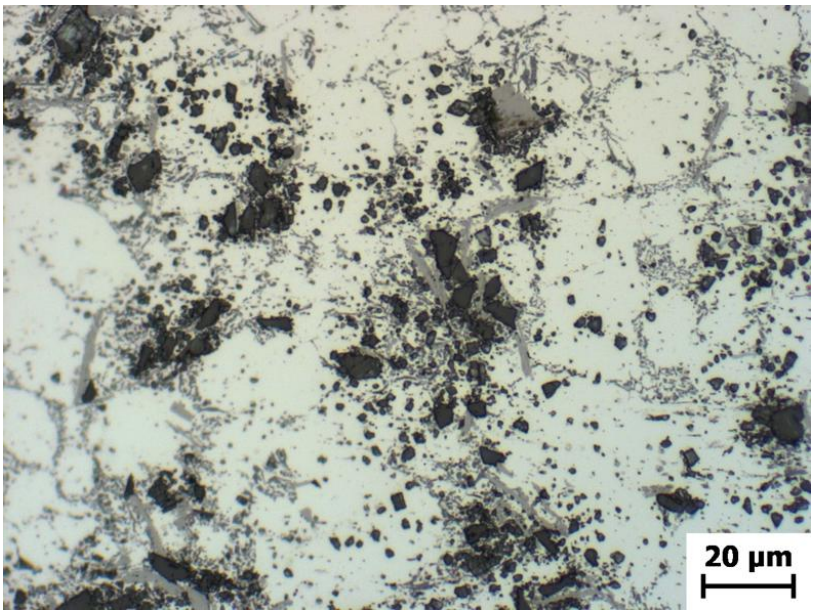

Figure 4.2 Higher magnification of a typical microstructure of LM25 – 5 vol. % SiC PMMC produced with the HPDC process at 630 ºC, revealing the presence of SiC particle clusters.

down. Thus, at lower magnifications, the HPDC samples seemed to have a more uniform distribution of the reinforcement, as seen in Figure 4.1.

However, an increase in the magnification revealed the presence of particle clusters, as presented in Figure 4.2. Another observation from Figure 4.1 was the high level of porosity in the samples cast in the steel mould. During the conventional mixing process, air bubbles are sucked into the melt via the vortex created whilst adding the ceramic powder to the melt, resulting in high levels of porosity in the composite. The particles tend to become attached to the air bubbles leading to the formation of particle-porosity clusters, especially in low volume fraction composites [Bindumadhavan et al. 2001]. Also, there is normal casting porosity resulting from dissolved gases or shrinkage. With the HPDC process, due to the application of high pressure the levels of porosity are reduced. As the metal solidifies and the dendritic structure grows, the paths for the flow of the remaining liquid become more tortuous. The application of pressure during solidification allows liquid to flow between the solidifying dendrite branches and compensates to a certain extent for shrinkage, compared to casting in the steel mould.

4.1.1.2 LM24 – SiC_p composites

Figure 4.3 provides the microstructures of LM24 - SiC_p composites produced by conventional HPDC. Optical microscopy carried out on the composites containing 5 and 10 vol. % SiC_p revealed the presence of areas occupied by particle clusters and at the same time areas free of SiC particles. The highly agglomerated nature of the LM24-SiC PMMCs was a result of the ineffective mixing and a lack of sufficient hydrodynamic forces during conventional processing. These results are in agreement with numerous previous studies [Lin et al. 1998, Lin et al. 1999, Sevik and Kurnaz 2006, Zhang et al. 2007(a)] which reported the non-uniform reinforcement distribution in the cross sections of cast PMMCs, where particle clusters and segregation bands were observed.

4.1.1.3 LM24 – Graphite (C) composites

The soft nature of graphite particles can be utilised to improve the wear resistance and antifriction properties of Al-based graphite composites. Figure 4.4 presents a typical optical micrograph of LM24 - 5 vol. % graphite composite produced by conventional HPDC, where the agglomerates of the reinforcement particles are clearly visible. Lack of efficient mixing during the conventional process for the production of these components allowed the graphite particles to form clusters and remain as such in the final solidified microstructure.

4.1.1.4 Reinforcement distribution during distributive mixing

During the distributive mixing of PMMCs, the rotation of the stirrer generates a vortex through which the reinforcement particles are drawn into the melt. Physical wetting between liquid aluminium and SiC or graphite is in general very poor [Delannay et al. 1987]. The force provided by the impeller during mechanical stirring is required to overcome the surface energy barriers due to poor wettability of the reinforcement particles by the aluminium alloy matrix. Mechanical stirring helps promote wettability and once the particles are introduced into the melt, the reinforcement distribution is strongly affected by the fluid flow characteristics.

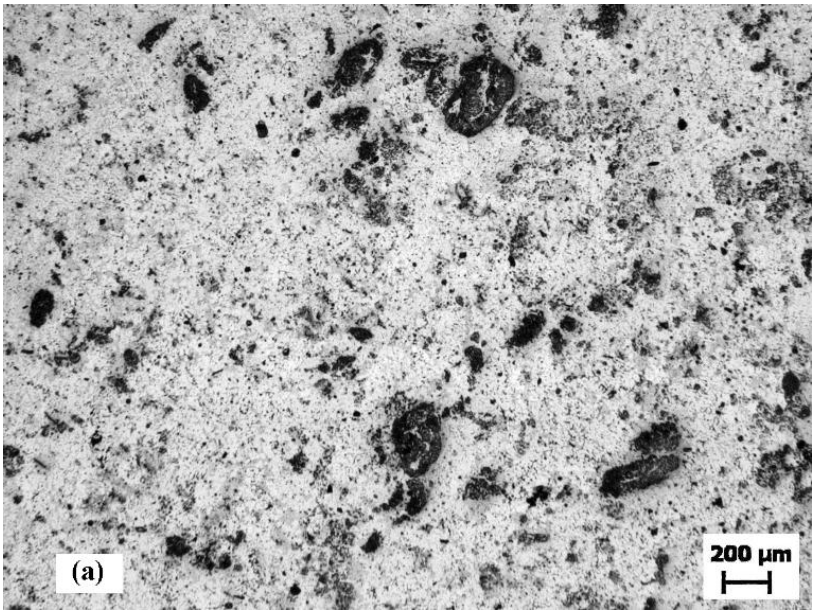

(a)

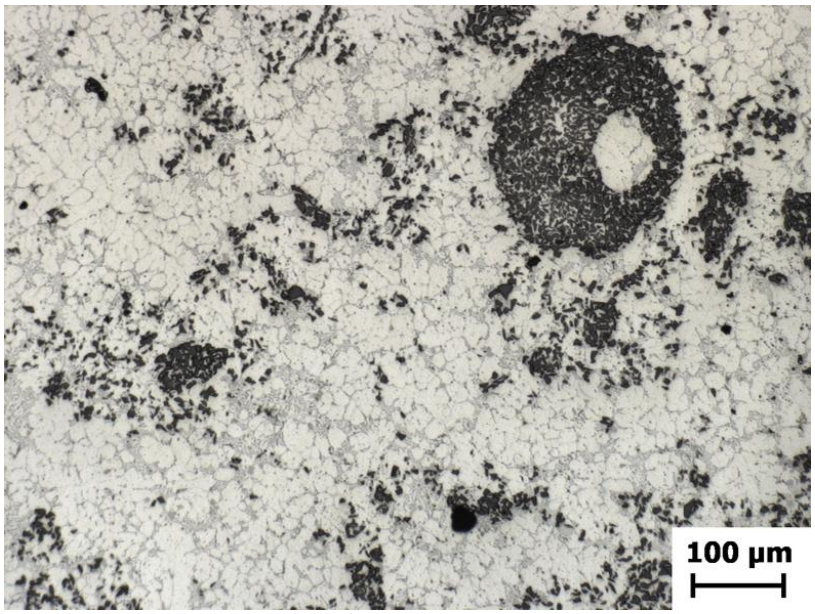

(b)

Figure 4.3 Representative optical micrographs of PMMC castings produced with the HPDC process at 610 ºC. (a) LM24 - 5 vol. % SiC_p and (b) LM24 - 10 vol. % SiC_p.

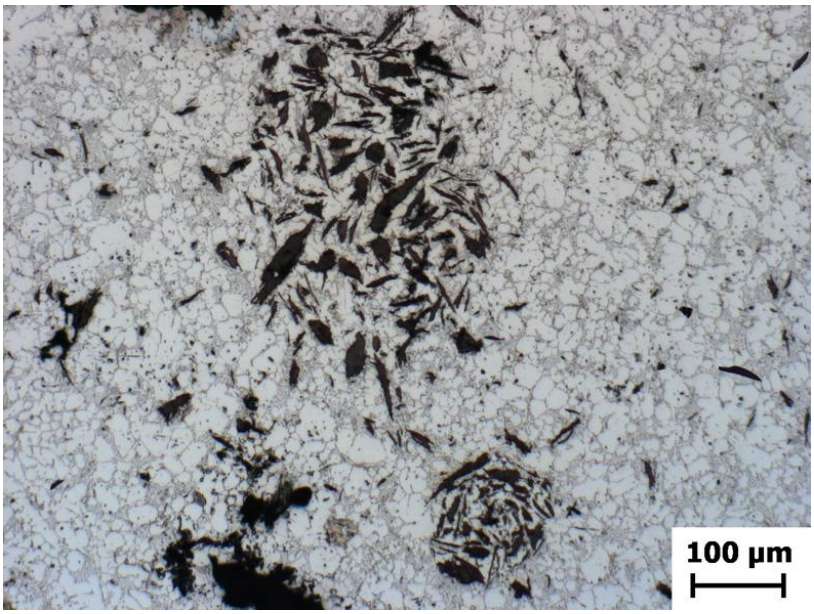

Figure 4.4 Typical optical microstructure of LM24 - 5 vol. % graphite composite produced with the conventional HPDC process at 610 ºC.

The very fine size of SiC particles used in this study, which were 4 µm in average size, and the low density of graphite particles which is 1.9 g/cc make any gravitational effects negligible and they are usually carried fully suspended in the liquid [Hashim et al. 2002(a)].

With the conventional stirring process, axial and radial flow components are the most dominant regarding the suspension of the reinforcement particles. The fluid flow characteristics during distributive mixing are schematically presented in Figure 4.5. Axial flow causes lifting of the particles due to momentum transfer and radial flow prevents particle settling. Several factors, such as the shape of the impeller, the rotational speed, and its position relative to the melt surface and walls of the crucible, can determine the final mixing quality. The optimum diameter of the stirrer helps distribute the solid particles in the central and peripheral parts of the flow at the same speed.

The objective of mixing is to break up agglomerated particles and then distribute them uniformly in the composite mixture. The application of a local shear force on the agglomerates of the bulk cohesive powder contributes to their distribution in the close vicinity of the stirrer. The force applied on a particle cluster is directly related to the viscosity of the medium. Harnby [Harnby et al. 1997] has described the

maximum force on a particle cluster rotating in a shear flow in the vicinity of a stirrer as given by Equation 2.7 and discussed in section 2.1.9.1. The degree of mixing is affected by the momentum transfer from the impeller to the clusters located away from the stirrer position. During distributive mixing velocity gradients are present within the liquid media. Whilst the shear force applied to the liquid that is in contact with the impeller is high, the overall shear force averaged out over the whole volume of the liquid medium is low and inadequate to break down particle agglomerates. A lack of sufficient hydrodynamic forces due to a variation in the velocity gradient results in accumulation of the agglomerates in relatively stagnant zones away from the impeller, such as the crucible walls, where they resist the shear forces of mixing and remain unaffected. These agglomerates are not transported back into the high shear regions and finally find their way as clusters into the cast structures, resulting in the characteristic microstructure seen in Figures 4.2, 4.3 and 4.4.

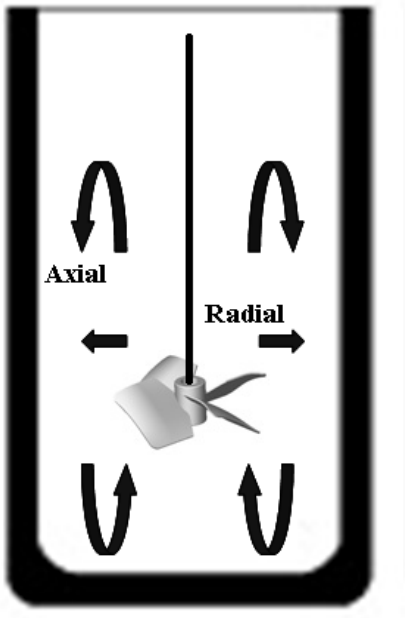

Figure 4.5 Fluid flow characteristics during distributive mixing. Axial component aids momentum transfer and radial component prevents settling.

4.1.2 Dispersive mixing – the MC-HPDC process

4.1.2.1 LM25 – SiC_p composites

Figures 4.6(a) and 4.6(b) present the microstructures of the dispersive mixed LM25 – 5 vol. % SiC_p composites cast in a steel mould and produced with the MC-HPDC process respectively. After the implementation of intensive shearing, the microstructures of the composites showed a more uniform distribution compared to the conventional distributive mixing process. The samples cast in the steel mould after intensive shearing had high levels of porosity similar to the ones cast in the steel mould after distributive mixing only. This was due to the fact that the distributive mixing process, used to introduce the particles in the liquid metal, caused the suction of air bubbles. Casting in a steel mould also results in higher levels of porosity in the samples. However, for the MC-HPDC samples the resulting microstructures were much improved. The uniform dispersion of the SiC particles in the matrix is clearly seen in Figure 4.6(b) and at higher magnification in Figure 4.7(a). For comparative purposes, a microstructure of LM25 – 5 vol. % SiC_p composite prepared with the HPDC process is also given in Figure 4.7(b).

Microstructural observations at intermediate magnifications, as presented by Figure 4.8 revealed that the majority of the SiC particles were present at the grain boundaries and the interdendritic regions. However, numerous SiC particles were observed inside the aluminium grains. The presence of these particles inside the aluminium grains is attributed to the high velocity of the solidification front, which must have been higher than the critical velocity required for the engulfment of the SiC particles. SEM analysis following the microstructural analysis of the MC-HPDC samples under the optical microscope, revealed interesting features of the microstructure. Two significant observations were made whilst examining the SEM microstructures:

- The particles observed under the optical microscope and assumed to be SiC, actually consisted of both SiC particles and α-AlFeMnSi compound particles as seen in Figure 4.9(a). This explains the higher concentration of the particles observed in Figure 4.1 and Figure 4.6.

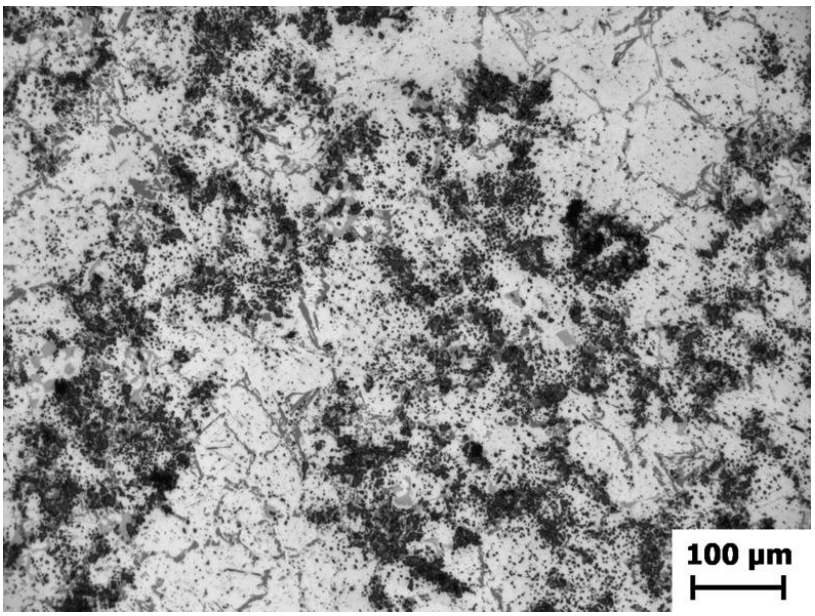

(a)

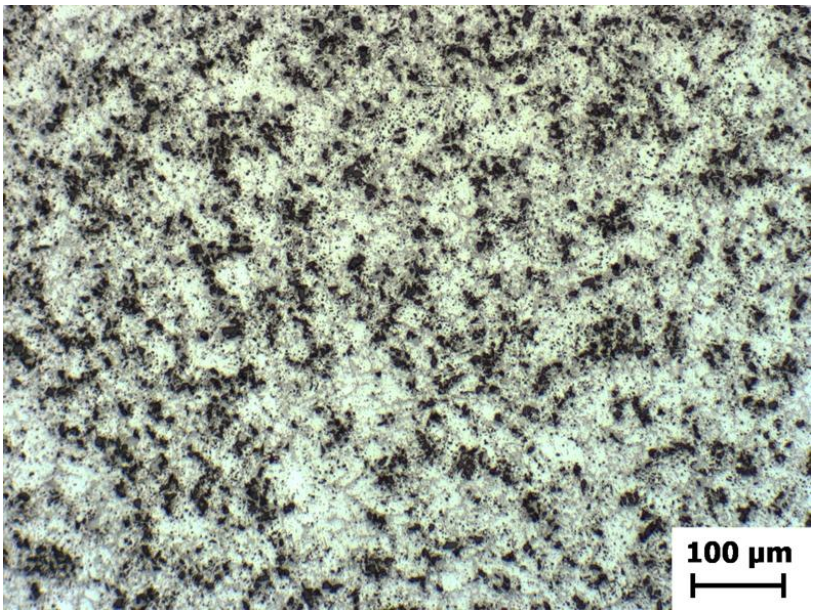

(b)

Figure 4.6 Typical microstructures of dispersive mixed LM25 – 5 vol. % SiC_p composites with the implementation of intensive shearing at 630 ºC. (a) Cast in steel mould and (b) produced with the MC-HPDC process.

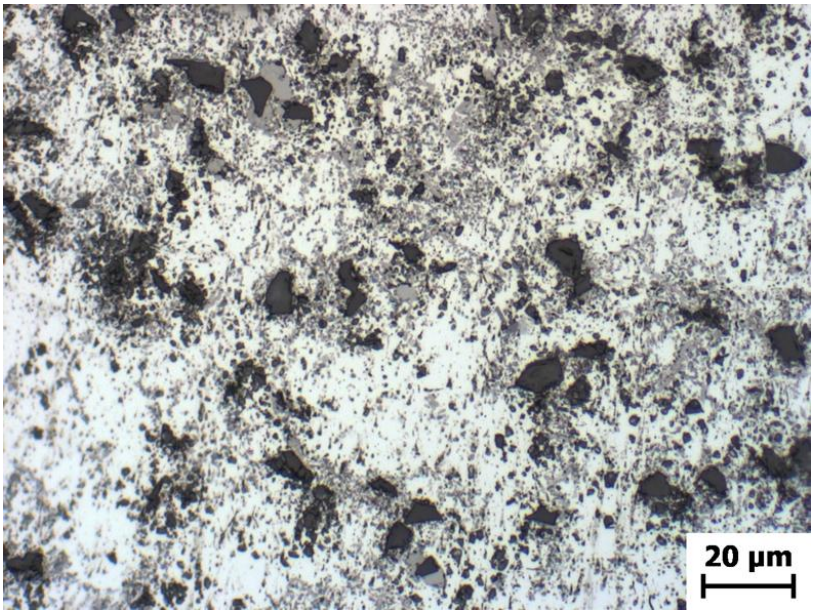

(a)

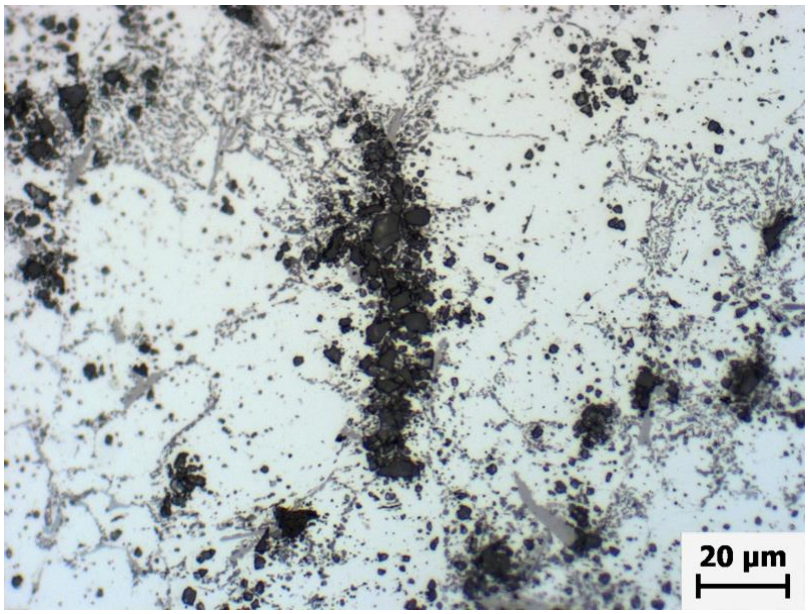

Figure 4.7 Higher magnification of a typical microstructure of LM25 – 5 vol. % SiC_p produced with (a) the MC-HPDC process at 630 ºC, showing uniform distribution of SiC particles and (b) the HPDC process at 630 ºC, revealing the clustering of SiC particles.

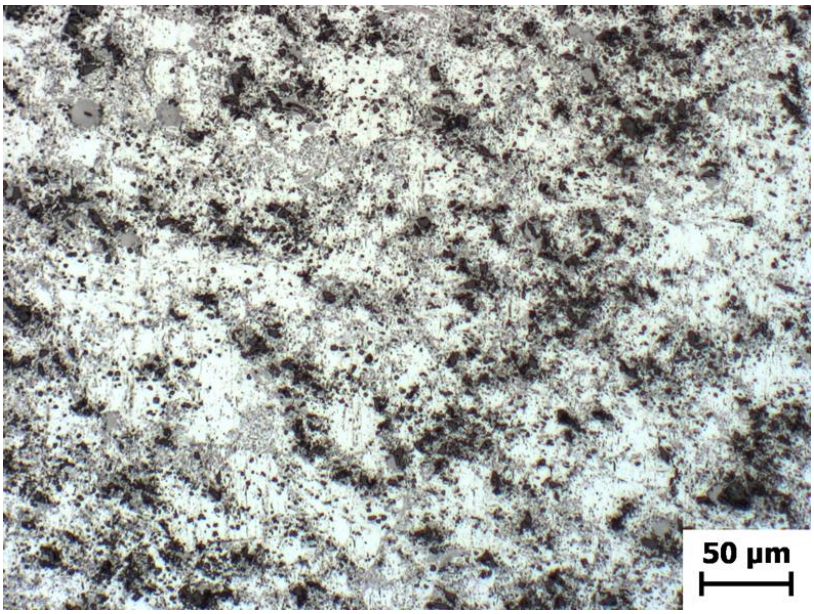

Figure 4.8 Microstructure of a MC-HPDC at 630 ºC LM25 – 5 vol. % SiC_p composite showing the presence of SiC particles in the aluminium matrix grains (dark in contrast particles inside the white Al-matrix).

- The eutectic Si has a very fine structure as seen in Figure 4.9(b). In this current study, the Si particles were considered to have an elliptical shape, with an average size of its major axis a_e = 0.7 µm and an aspect ratio of minor to major axis b_e/a_e = 0.66. To our knowledge, formation of such fine Si particles has not been observed before.

For the vast majority of Al alloys the presence of Fe is detrimental to the mechanical properties and ductility in particular. This is attributed to the low solubility of Fe in the α-Al solid solution phase (0.04 wt. %) and its strong tendency to form various Fe-containing compounds [Mondolfo 1976]. More specifically, ternary Al-Fe-Si phases, such as the hexagonal α-AlFeSi (Al_8Fe_2Si) and the monoclinic β-AlFeSi (Al_5FeSi), are of great importance in Al-Si based alloys. The presence of Mn is known to stabilise a cubic ternary α-AlMnSi ($Al_{15}Mn_3Si_2$) compound which consumes Fe by forming an equilibrium quaternary phase, α-AlFeMnSi ($Al_{15}(Fe,Mn)_3Si_2$) [Villars and Calvert 1991], which can be seen in Figure 4.9. Previous work [Fang et al. 2007] has shown that intensive shearing modifies the morphology of these primary intermetallic compound particles from dendritic to

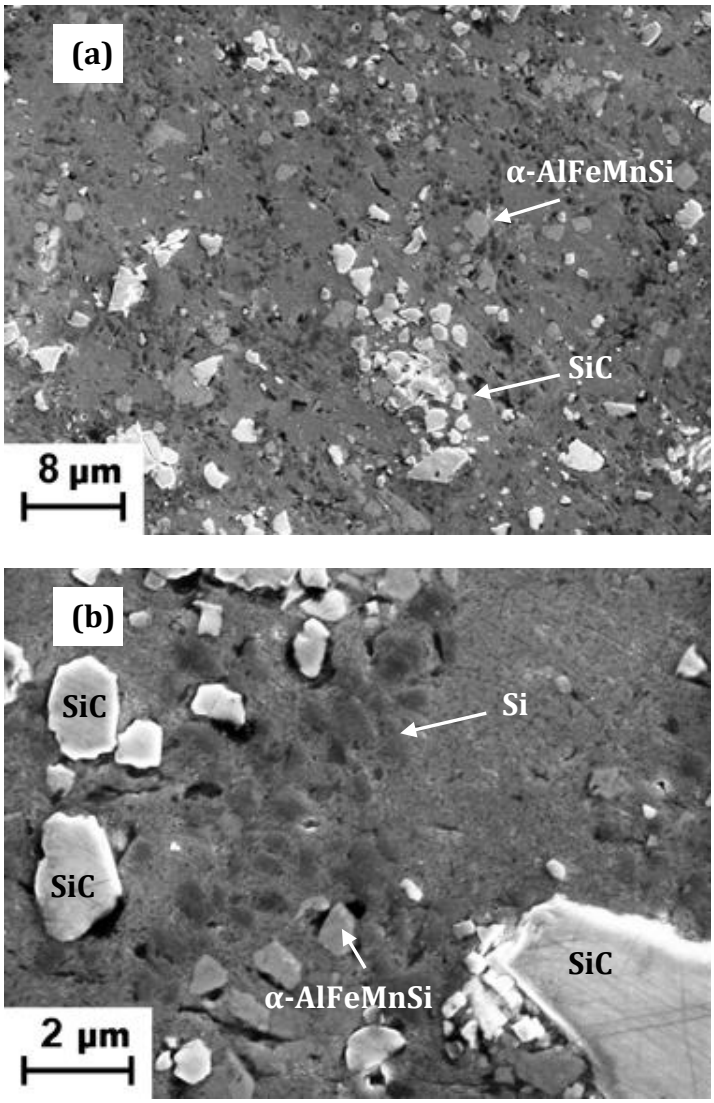

Figure 4.9 SEM microstructure of LM25 – 5 vol. % SiC PMMC produced with the MC-HPDC at 630 ºC, showing (a) the presence of α-AlFeMnSi intermetallic compounds in the microstructure and (b) the very fine, sub-micrometre eutectic Si particles.

equiaxed. Hence their uniform dispersion could improve the mechanical properties of Al-Si based alloys.

Several authors [Rohatgi et al. 1986, Ray 1993, Gupta et al. 1996, Nagarajan et al. 1999] have reported on the heterogeneous nucleation of eutectic Si on SiC particles. Solidification of the α-Al phase leads to SiC particle pushing in the interdendritic regions. At the same time, the growth of the α-Al nuclei leads to enrichment of the remaining liquid in Si, which is also concentrated at the interdendritic regions. SiC

has been shown to be a favourable site for heterogeneous nucleation of Si [Rohatgi et al. 1993] and solidification of the remaining liquid will start with the nucleation of Si. As the growing Al dendrites push the SiC particles in the eutectic liquid, the relative amount of SiC there is higher causing a severe refinement of the eutectic Si.

4.1.2.2 LM24 – SiC_p composites

Figure 4.10 presents typical microstructures of LM24 - SiC_p composites produced with the MC-HPDC process. Microstructural characterization of these castings revealed a more uniform distribution of SiC particles compared to the conventional HPDC microstructures provided by Figure 4.3. In addition, the difference between these microstructures and those presented in Figure 4.6 for LM25 – SiC, is due to the same contrast between the reinforcement and the intermetallic particles observed in LM25 during OM, which makes them difficult to distinguish. On the other hand, the intermetallic reinforcement particles in LM24 appear with different contrast during OM observations and are easily distinguished. The high shear rate, dispersive mixing action of the MCAST process results in a homogeneous dispersion of the reinforcement. Image analysis of the of LM24 - 5 % SiC_p and LM24 - 10 % SiC_p has shown the reinforcement volume fractions to be 5.26 ± 0.91 % and 10.35 ± 1.12 % respectively, confirming the reinforcement quantities added.

4.1.2.3 LM24 – Graphite (C) composites

A representative optical micrograph of LM24 – 5 vol. % graphite composite produced by MC-HPDC is shown in Figure 4.11. The implementation of intensive shearing in the MC-HPDC process resulted in a homogeneous distribution of the graphite particles. In comparison to the microstructure of the PMMCs produced with the HPDC process, presented in Figure 4.4, no particle clusters were present in the structure. A previous study [Narendranath et al. 1986] has shown that due to pinhole porosity and polishing defects, observation under the optical microscope fails to distinguish between graphite particles and micropores in composite materials. To ascertain the graphite distribution in the matrix and the surface details of composite materials, SEM analysis was utilised to assess the microstructure. Figure 4.12 presents a SEM micrograph of MC-HPDC LM24 - graphite composite produced

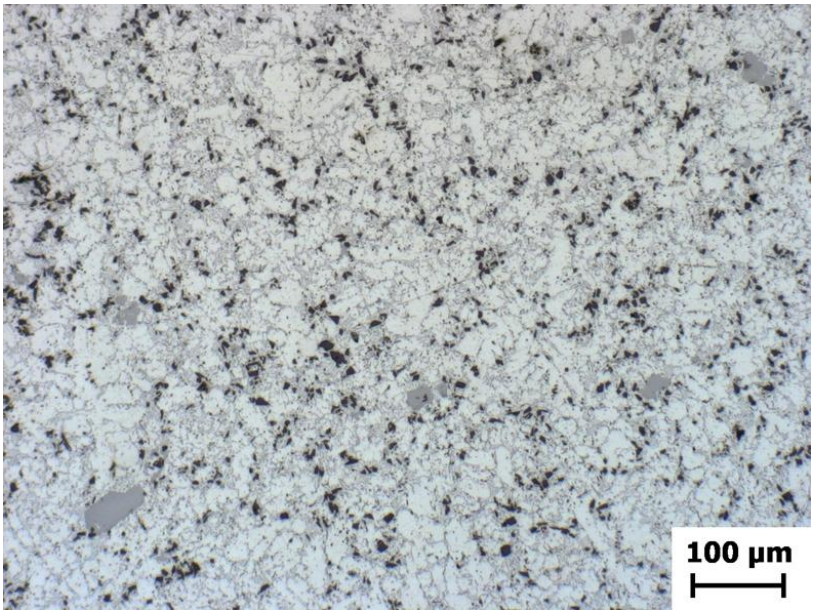

(a)

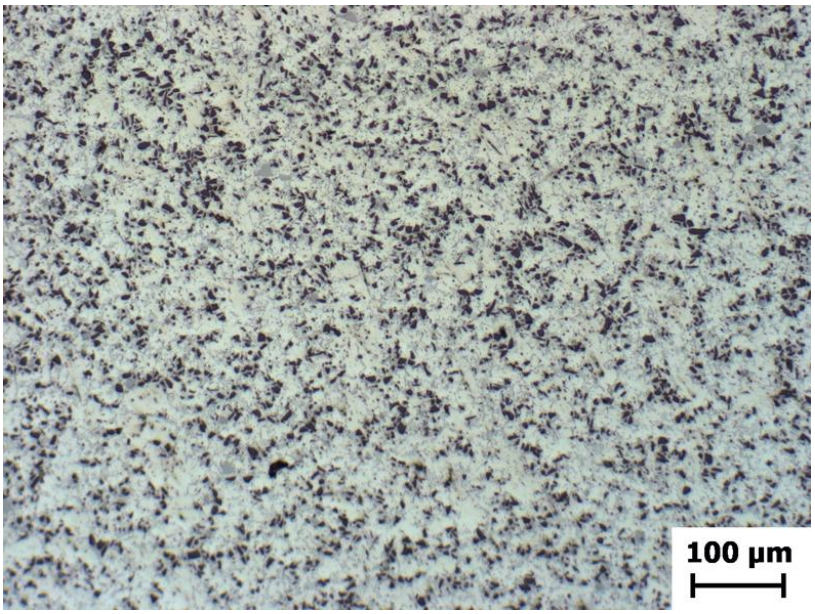

(b)

Figure 4.10 Representative optical micrographs of PMMC castings produced with the MC-HPDC process at 610 ºC. (a) LM24 - 5 vol. % SiC_p and (b) LM24 - 10 vol. % SiC_p.

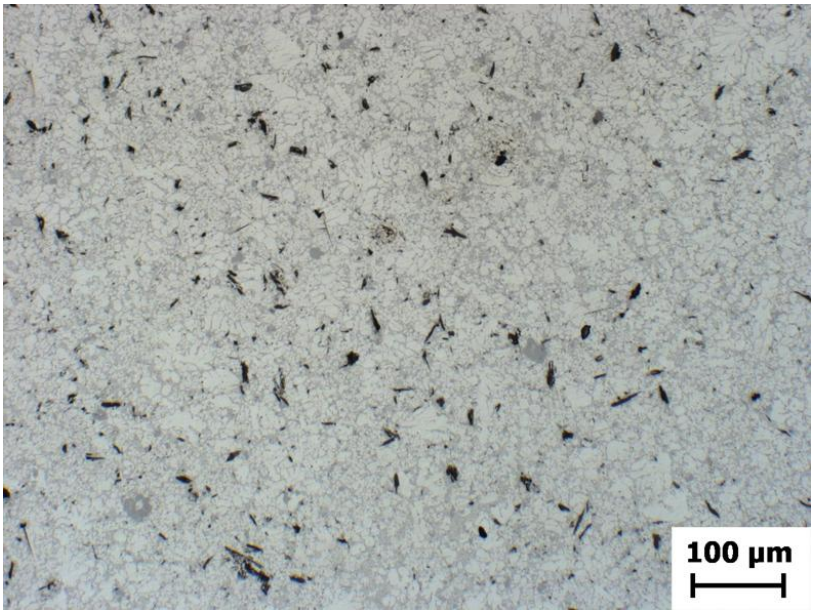

Figure 4.11 Typical optical microstructure of LM24 - 5 vol. % graphite composite samples produced by MC-HPDC at 610 ºC.

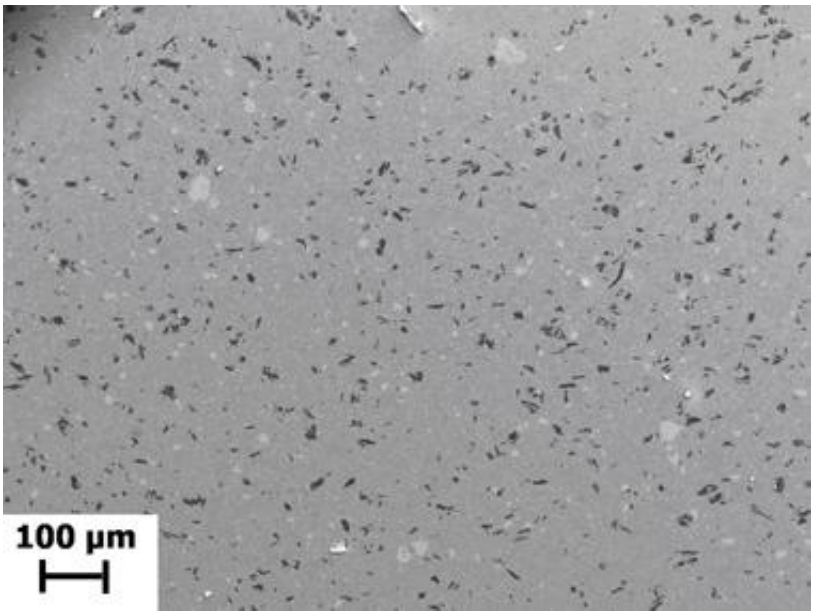

Figure 4.12 SEM micrograph of LM24 - 5 vol. % graphite composite produced by MC-HPDC at 610 ºC, showing a uniform distribution of graphite particles.

with the MC-HPDC process at 610 °C, confirming the uniform distribution of graphite particles, which are the dark in contrast particles seen in the microstructure. Image analysis of the microstructures of LM24 – 5 vol. % graphite PMMCs has shown the reinforcement volume fractions to be 4.93 ± 1.26 %. The density of the MC-HPDC composite sample, measured using Archimedes' principle as discussed by Clyne and Withers [Clyne and Withers 1993] and the rule of mixtures (ROMs) [Chawla 1998], was found to be 2.58 ± 0.06 g/cm^3 and 2.66 g/cm^3 respectively, indicating negligible porosity of the castings.

4.1.2.4 Reinforcement distribution during dispersive mixing

In section 4.1.1.4 we described how during distributive mixing the shear force applied on the composite mixture by the impeller is not enough to break down all of the SiC clusters. Intensive shearing is required to break down the agglomerates into individual particles by applying a shear stress that will overcome the average cohesive force or the tensile strength of the cluster. The two models by Rumpf [Rumpf 1962] and Kendall [Kendall 1988] for the calculation of the strength of a cluster were discussed in section 2.1.8 and Equations 2.5 and 2.6. Previous work has measured the tensile strength of highly cohesive particles to reach a maximum of 300 kPa [Lee et al. 1993]. According to Equations 2.5 and 2.6, for fine reinforcement powders, the smaller particle size and shorter interparticle distance result in significantly higher tensile strength making the application of a high shear stress necessary in order to break the clusters. This can be achieved by the implementation of intensive shearing in the MC-HPDC process.

The fluid flow in the MC-HPDC process is characterised by a cyclic variation of a high shear rate, high intensity of turbulence and positive displacement pumping action. The screws have specially-designed profiles and are co-rotating, fully intermeshing and self wiping. The lowest shear rate is found at the gap between the root of the screw flight and the inner surface of the barrel whilst the highest shear rate is offered by the intermeshing regions between the two screws. The high shear regions are schematically shown in Figure 4.13. Intensive shearing is implemented in order to break up the particle clusters embedded in the liquid melt and disperse the particles uniformly in the mixture.

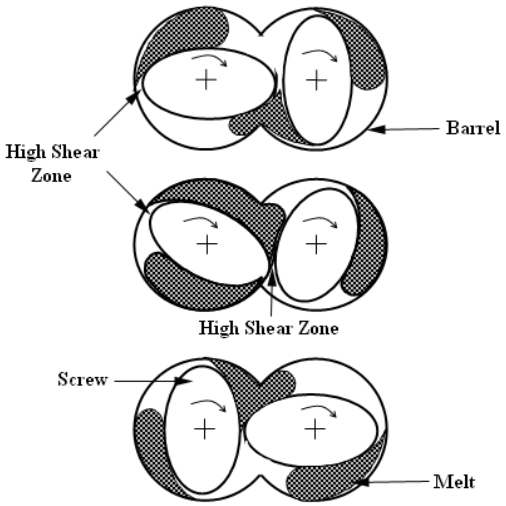

Figure 4.13 A schematic illustration of the high shear zones at the intermeshing regions of the screws and the fluid flow during intensive mixing.

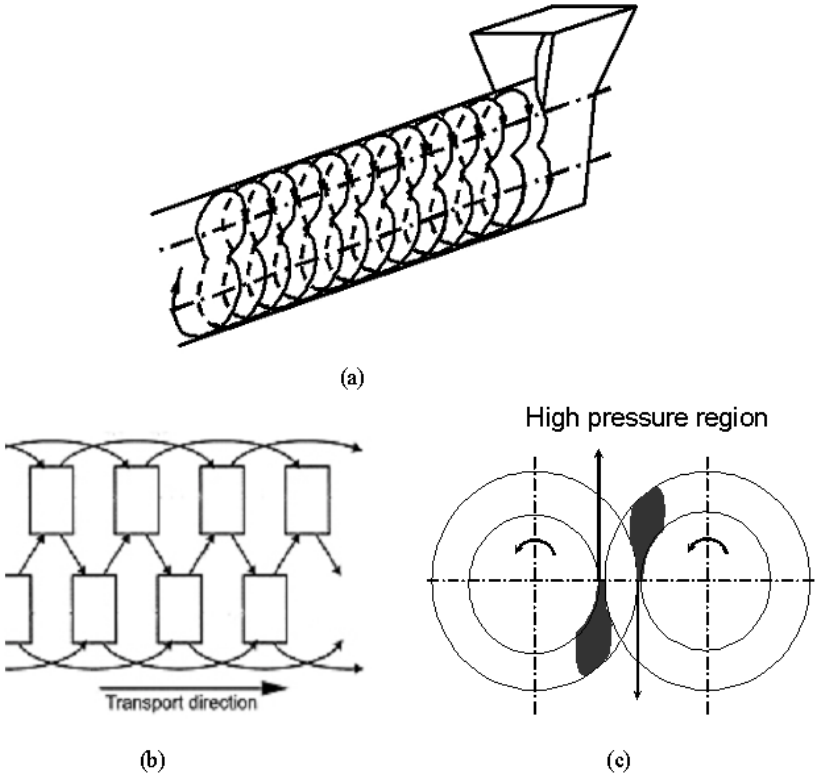

Figure 4.14 Fluid flow patterns inside the twin screw machine (a) figure ‘8’ motion of the slurry, (b) positive displacement and (c) high shear zones.

Ji *et al.* [Ji et al. 2001] described that the melt in the MCAST unit moves in the periphery of the screws in a 'figure of 8' motion, moving from one pitch to the next, to what is known as positive displacement. The fluid flow inside the MCAST unit is shown schematically in Figure 4.14. While cohesive forces hold the agglomerates together, hydrodynamic stresses developed due to the specially-designed profile of the screws break the agglomerates into individual particles and result in the homogeneous dispersion presented in Figures 4.7, 4.10 and 4.12.

For the MC-HPDC process, as described in section 3.3.4, the shear stress between the screws and the barrel in the twin screw machine has been described by Rauwendaal [Rauwendaal 1994] and is given by equation 3.1. Depending on the viscosity and rotational speed, an adequately high shear stress can be applied by the MCAST unit on particle clusters. An average tensile strength value for particle clusters has been reported equal to 660 Pa [Pierrat and Caram 1997], whilst intensive shearing with the MCAST unit at 800 rpm and above the liquidus temperature of Al – SiC PMMCs can produce a shear stress of approximately 1000 Pa. The combination of the fluid dynamics briefly described above and an enormous amount of ever-changing interfacial contact surface, compared to conventional stirrers, contribute to the high shear dispersive mixing action of the twin-screw mechanism used in the MC-HPDC process.

4.1.2.5 Reinforcement redistribution as a result of solidification

In the microstructures of the composites produced with the HPDC process, the reinforcement particles have agglomerated forming clusters preferentially located at the grain boundaries or the interdendritic regions, as seen in Figure 4.2. This is consistent with established particle pushing theories [Stefanescu et al. 1988, Stefanescu et al. 1990, Youssef et al. 2005], which predict the existence of a critical velocity of the solidification front below which the particles are pushed ahead of the advancing solidification front. When the particle is rejected by growing crystals and pushed ahead of the advancing interface, a viscous force is generated which tends to prevent the pushing of the particle. The balance of these counteracting forces will decide the rejection or engulfment of the particle. Parameters such as relative density difference, relative difference in thermal conductivity and heat diffusivity between the particle and the metallic melt, and alloy composition will affect the shape of the

solidification front and determine the magnitude of these forces [Stefanescu et al. 1988, Stefanescu et al. 1990]. Any engulfment observed for LM25 – SiC PMMCs produced with either the HPDC or MC-HPDC processes, can be attributed to the high velocity of the solidification front due to the high cooling rate provided by the metallic die, which can be up to 10^3 K s^{-1} [Fan and Liu 2005]. This must have exceeded the critical velocity required for the engulfment of the SiC particles, resulting in the characteristic microstructure seen in Figure 4.8.

4.2 Quantitative Analysis

This section presents the results of the quantitative analysis carried out to describe the distribution of the various reinforcement particles in the metal matrix of the PMMCs produced with the HPDC and MC-HPDC processes. The experimental results are compared to theoretical distribution curves and the effect of processing parameters is discussed.

4.2.1 LM25 – SiC_p composites

The first statistical method used in this study to describe the distribution of SiC and α-AlFeMnSi intermetallic particles in the LM25 based composites was the Lacey Index *M*. The values of the Lacey index *M* for the distributive and the dispersive mixed LM25 – 5 vol. % SiC_p cast in a steel mould and by high pressure die-casting, both at 630 ºC, are presented in Figure 4.15 as a function of shearing time. The shearing speed was fixed at 800 rpm. As described in section 3.4.4, the Lacey index is insensitive to mixture quality. The Lacey index of the distributive mixed composites, represented in Figure 4.15 by a corresponding shearing time of 0 s, was 0.906 which is lower than that of the dispersive mixed, which ranged between 0.955 and 0.961. This is in agreement with the microstructural observations. For the HPDC and the MC-HPDC composites on the other hand, the results of the Lacey index are not representative of the microstructural observations. The distribution of the particles is definitely improved compared to the composites cast in the steel moulds as seen by the overall increase in the Lacey index. However, the improvement in the distribution of the PMMCs produced with the MC-HPDC

process was not reflected. To overcome this problem, further quantitative analysis was carried out on the HPDC and the MC-HPDC composites using the Quadrat method.

The results of the statistical analysis with the Quadrat method for the HPDC and MC-HPDC processed composites are in accordance with the optical observations made from the microstructure. They are given in Figure 4.16 as a frequency scatter of the number of particles per quadrat, *Nq*, together with the theoretical curves for a negative binomial, binomial and Poisson distribution. The magnitude of clustering affects the shape of the *Nq* distribution, with a higher clustering tendency making the *Nq* distribution less symmetric.

As proven mathematically [Rogers 1974], a clustered spatial distribution follows a negative binomial model, a random spatial distribution follows a Poisson model and a regular spatial distribution model follows a binomial model. The observed particle distribution for the HPDC samples lies closer to a negative binomial curve indicating clustering, whereas the MC-HPDC sample particle distribution bears more of a resemblance to the Poisson and binomial curves. These results reveal that

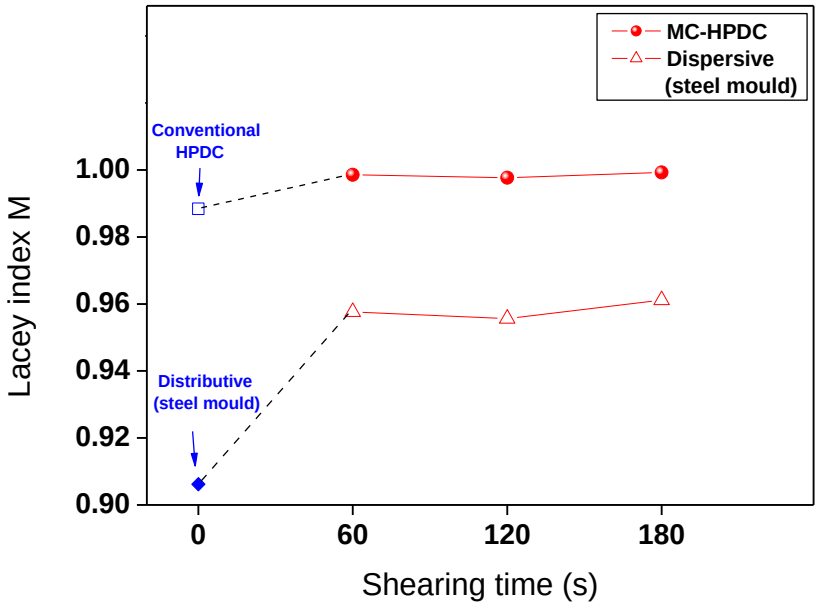

Figure 4.15 The Lacey Index M of LM25 – 5 vol. % SiC PMMCs processed with or without the implementation of intensive shearing, as a function of shearing time.

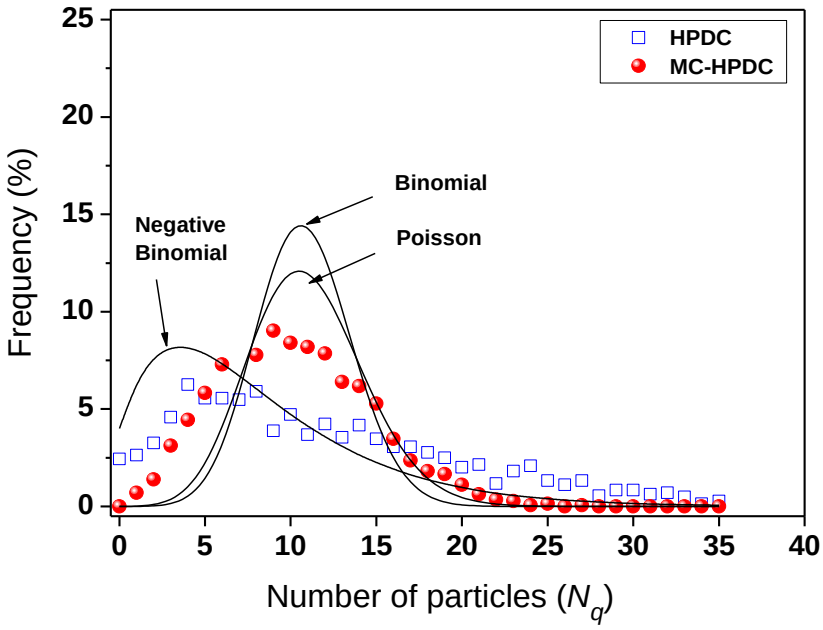

Figure 4.16 Experimental results from the Quadrat analysis for HPDC and MC-HPDC processed LM25 - 5 vol. % SiC PMMCs components and theoretical distribution curves.

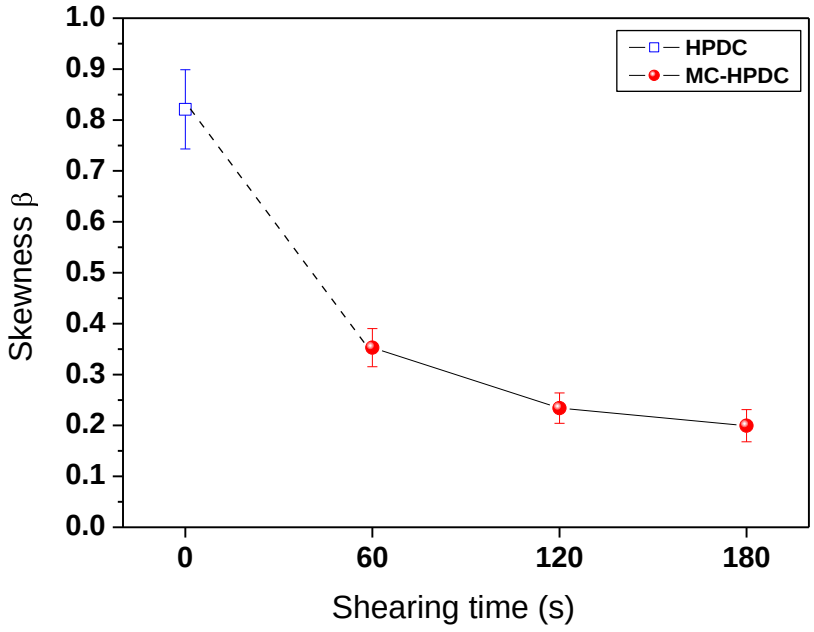

Figure 4.17 The effect of shearing time on the skewness β of the particle distribution in HPDC and MC-HPDC processed LM25 – 5 vol. % SiC PMMCs.

the MC-HPDC process offered a great advantage for the fabrication of PMMCs producing castings with a more uniform distribution of the particles compared to conventional HPDC, resulting in more homogeneous microstructures.

Figure 4.17 shows the variation of the skewness β of the reinforcement distribution, as a function of the shearing time, when the shearing speed and temperature were fixed at 800 rpm and 630 ºC respectively. The skewness, an indicative value of the degree of asymmetry, is a relative term used for comparison purposes. Lower skewness values correspond to more symmetric, thus uniform distributions. The calculated value for the HPDC processed castings was significantly higher than that for the castings produced with the MC-HPDC process, representing the observed clustering tendency. At a shearing time of 0 s, corresponding to the HPDC process, the skewness value was 0.821 which then drops to 0.353 after 60 s of intensive shearing. For 120 s of shearing the value of β was 0.234, whilst the lowest skewness value of 0.199 was obtained after intensive shearing of the composite melt for 180 s.

4.2.2 LM24 – SiC_p composites

Similar to the analysis carried out for LM25 – SiC_p composites, the experimental results of LM24 – 10 vol. % SiC_p composites are compared to theoretical distribution curves in Figure 4.18. The clustered distribution of the reinforcement particles in the HPDC composites was expected to result in a combination of empty quadrats, quadrats with a small number of particles and quadrats with a high number of particles during the Quadrat analysis. The observed distribution for a composite produced with the conventional HPDC process followed a clustered distribution expressed by a negative binomial curve, whereas the corresponding distribution for the MC-HPDC composite showed a pronounced deviation from the negative binomial distribution and lay closer to both the Poisson and the binomial curves, confirming the more uniform distribution.

The effect of shearing speed on the distribution of the SiC particles in the aluminium matrix, as indicated by the variation of the skewness β, is illustrated in Figure 4.19 for both 5 vol. % and 10 vol. % LM24 – SiC_p composites. The results demonstrate that intensive shearing with the MC-HPDC process had a significant positive effect on the distribution of SiC particles compared to the conventional distributive mixing

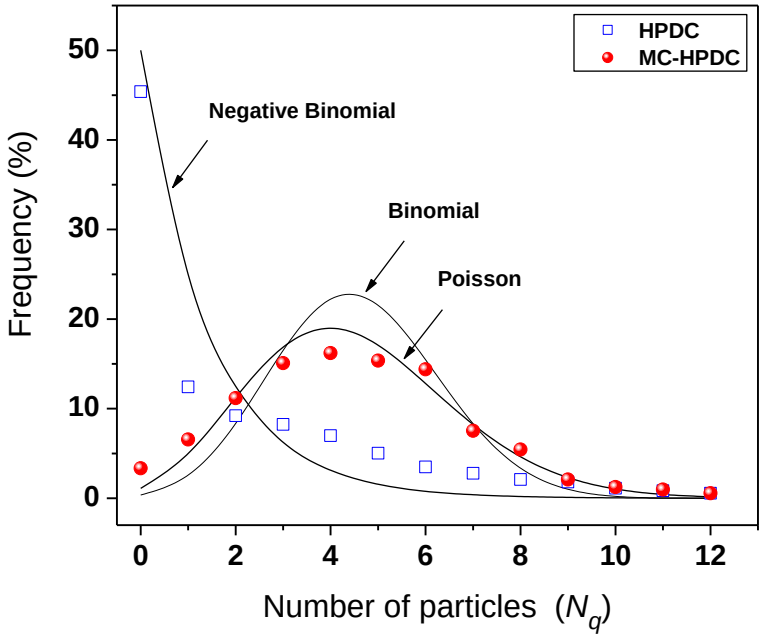

Figure 4.18 Experimental results from the Quadrat analysis for HPDC and MC-HPDC processed LM24 - 10 vol. % SiC_p PMMCS and theoretical distribution curves.

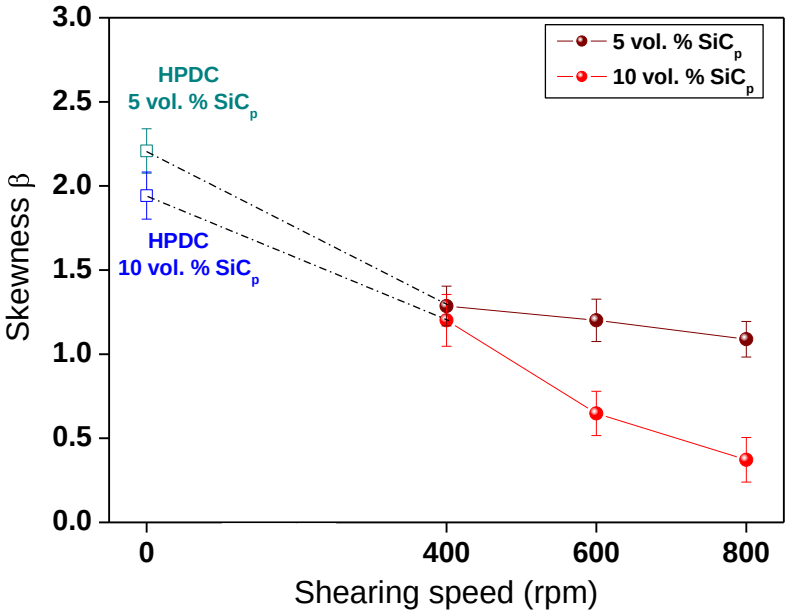

Figure 4.19 The effect of intensive shearing speed on the skewness of the reinforcement distribution of both 5 vol. % and 10 vol. % LM24 – SiC_p composites, produced at 610 ºC and a shearing time of 120 s.

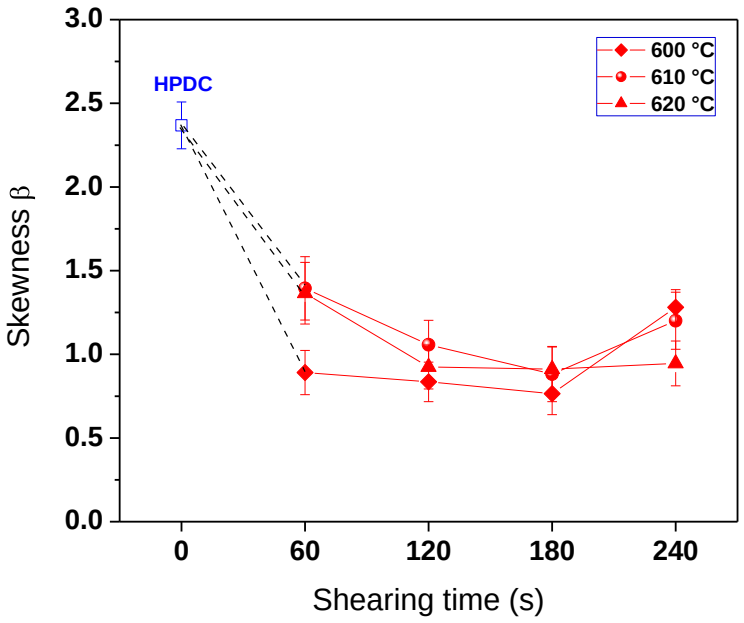

Figure 4.20 The effect of shearing time at various processing temperatures of LM24 – 5 vol. % SiC_p composites, at a shearing speed of 800 rpm.

process. The implementation of intensive shearing, even at the lowest speed of 400 rpm, caused an approximate 40 % reduction in the skewness value of the composites for both 5 vol. % and 10 vol. % SiC additions. Increasing the shearing speed resulted in a further reduction of the skewness value, with this reduction being more pronounced in the case of the LM24 – 10 vol. % SiC_p composites.

Other processing variables that can affect the distribution of the reinforcement are the shearing temperature and shearing time. The calculated skewness of SiC particle distribution in LM24 – 5 vol. % SiC_p composites is plotted as a function of shearing time for three different processing temperatures in Figure 4.20. The skewness value for the conventional HPDC composite was 2.37, whilst with the implementation of intensive shearing in the MC-HPDC process the skewness ranged from 1.39 for a sample processed at 610 ºC and 60 s, to 0.76 for a composite processed at 600 ºC and 180 s. When the shearing time was increased from 60 s to 180 s, the skewness β decreased and then increased again at 240 s. Figure 4.20 also indicates that mixing quality was enhanced by decreasing the processing temperature from 620 ºC to 600 ºC. HPDC castings were produced at approximately 630 ºC for improved processability and hence connected with dotted lines, as seen in Figure 4.20.

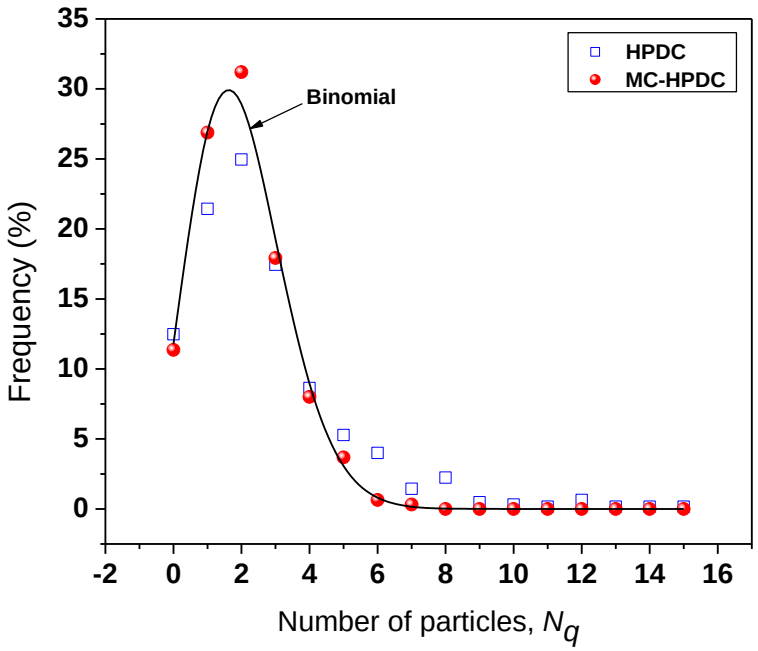

Figure 4.21 Experimental results from the Quadrat analysis for HPDC and MC-HPDC processes and Binomial distribution curve for LM24 - 5 vol. % C composites.

4.2.3 LM24 – Graphite (C) composites

The results of the Quadrat analysis for LM24 – 5 vol. % C composites are compared in Figure 4.21 with a theoretical binomial distribution curve, which is used as an indication of the homogeneity. Similar to the cases of LM25 – SiC_p and LM24 - SiC_p, the MC-HPDC process can produce composites with well dispersed reinforcement particles, resulting in a uniform distribution which lies closer to the binomial curve compared to the conventional HPDC process.

4.2.4 The effect of processing parameters

4.2.4.1 Processing temperature and processing time

The viscosity of a molten metal will increase with decreasing temperature following the Arrhenius relation [Brandes 1983]. Addition of any solid reinforcement particles will decrease the fluidity of the melt as the viscosity increases significantly and the liquid becomes non-Newtonian [Quaak and Kool 1994, Quaak et al. 1994]. Strong agglomeration at low shear rates produces a large amount of entrapped liquid in the

composite mixture and as a consequence, a considerable fraction of the liquid is immobilised increasing the effective fraction of the solid and resulting in an even higher viscosity. Stagnant boundary layers around the particles result in an increase in the total surface area of ultra fine size particles, which will in turn cause increased resistance to fluid flow [Ravi et al. 2008]. Equation (3.2) predicts that an increase in the viscosity of the melt will cause an increase in the shear stress τ. A lower processing temperature will increase the viscosity and the increased shear rate will break up the agglomerates of SiC_p and disperse the particles uniformly, as expressed by the decreased skewness at 600 °C in Figure 4.20. However, an adequately high processing temperature, above the liquidus temperature of the alloy – 596 °C for LM24 and 615 °C for LM25 - is required to increase the fluidity of the composite mixture and to improve its castability. Furthermore, an increased shearing time dissociates the inter-aggregate bonds but can also increase the frequency of collisions between these particles resulting in the formation of new agglomerates which impair the mixing quality [Rohatgi et al. 1998]. However, it is clear from Equation (3.2) that the shear stress produced by the MCAST unit is independent of shearing time. As expected, a significant variation was not observed with varying shearing time in Figures 4.17 and 4.20 for the skewness of MC-HPDC processed LM25 – SiC_p and LM24 – SiC_p composites, respectively.

4.2.4.2 Shearing intensity

When solid particles are dispersed in a liquid metal, two types of interactions can occur, both of which produce an increase in the apparent viscosity of the slurry:

- A hydrodynamic interaction between the liquid and the particles and
- A non-hydrodynamic interaction between the particles themselves.

Previous studies [Mada and Ajersch 1996(a), Mada and Ajersch 1996(b), Ravi et al. 2008] have shown that the viscosity increases with the volume fraction of the solid particles and with a decrease in the particle size. Owing to the increased shear forces with intensive shearing, particle agglomerates are dissociated. Under intensive shearing at a constant shear rate, an increase in the volume fraction of reinforcing particles will inevitably lead to increased inter-particle interactions. As a result, higher shear stresses are experienced by the particles in the LM24 – 10 vol. % SiC_p

composites, which explains the improved homogeneity of the reinforcement distribution seen in Figure 4.19.

Equation (3.2) also suggests that an increase in the rotational speed of the screws will increase the applied shear stress τ. An increased shear stress is expected to break up the agglomerates by overcoming the cohesive forces which hold them together. Under the high shear stress environment in the MCAST unit, the melt penetrates into the clusters and disperses the individual particles within the cluster, resulting in a more uniform distribution. This is expressed by the decreased skewness at higher shear rates in Figure 4.19, indicating an improvement in the homogeneity of the reinforcement distribution.

4.3 Mechanical Properties

4.3.1 LM25 – SiC_p composites

The improvement in the distribution of the reinforcement particles in the Al-matrix had a positive effect on the mechanical properties of the composites, expressed by the Vickers hardness measurements on the LM25-SiC PMMCs produced with and without intensive shearing. As seen from the results in Table 4.1, the improved distribution of the particles accounts for an increase in the hardness values after intensive shearing, regardless of the casting method.

Table 4.1 The average Vickers Hardness of LM25 – 5 vol. % SiC composites produced with and without the implementation of intensive shearing.

Processing conditions		Casting method	
		Steel mould	Die-casting
Distributive mixing	0 s	59	74
Dispersive mixing (MCAST-process)	60 s	61	78
	120 s	65	76
	180 s	70	79

As expected, die casting produced PMMCs with a higher hardness compared to the composites cast in the steel mould. However, the implementation of intensive shearing improved the hardness of the PMMCs produced with the MC-HPDC process, compared to the castings produced with the conventional HPDC process.

The composites produced by the MC-HPDC process have a much more homogeneous microstructure compared to the conventional HPDC composites, with the SiC particles being distributed uniformly throughout the whole volume of the samples. This was consequently reflected in the mechanical properties obtained by the tensile tests that were carried out. Figure 4.22 shows a comparison of the mechanical properties of LM25 – 5 vol. % SiC_p composite samples produced by the two different processes. The MC-HPDC composites show an increase in the tensile elongation together with an increase in the ultimate tensile strength, UTS, of the material, resulting from the effective dispersion of the particles. The magnitude of this increase is approximately 15%. Figure 4.23 shows that Young's modulus values of MC-HPDC composites fall within the Voigt's (upper) and Reuss' (lower) limits of the Hashin-Shtrikman bounds, indicating a uniform distribution of the SiC particles in the aluminium matrix.

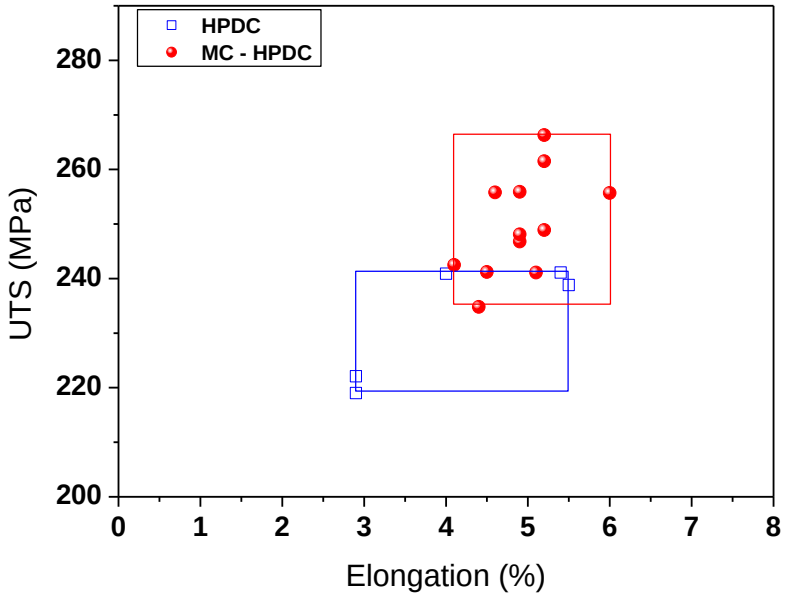

Figure 4.22 Comparison of the tensile properties of LM25 - 5 vol. % SiC PMMCs produced with the HPDC and MC-HPDC processes.

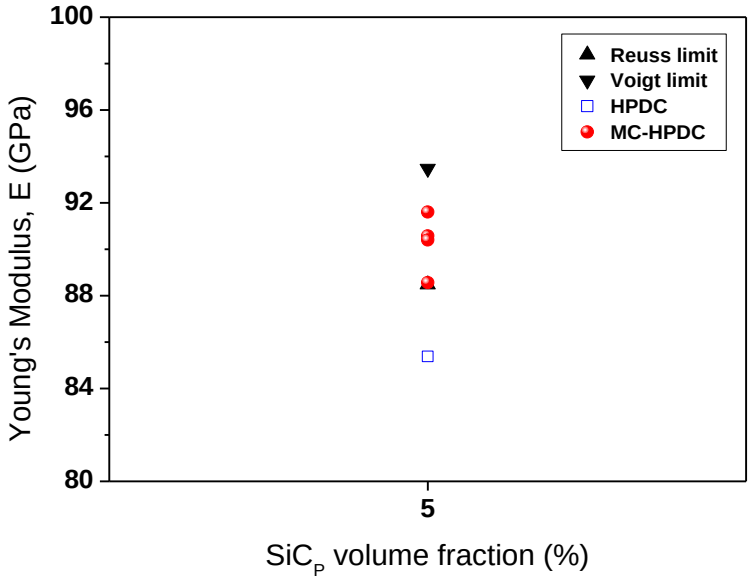

Figure 4.23 Hashin-Shtrikman bounds and measured average values of the Young's modulus for LM25 – 5 vol. % SiC PMMCs produced with the HPDC and MC-HPDC processes.

4.3.2 LM24 - SiC_p composites

The fabrication process is well known to affect both the structure and properties of cast composites. Figure 4.24 shows a comparison of the mechanical properties obtained from tensile tests for LM24 - 10 % SiC PMMC castings processed with conventional HPDC and MC-HPDC. The results clearly demonstrate that the MC-HPDC process offered improved tensile properties compared to the conventional HPDC process, expressed by a simultaneous increase in strength and ductility. The elongation of the MC-HPDC samples was approximately 25 % higher than that of HPDC samples. The mechanical properties of the melt-conditioned base LM24 aluminium alloy are also included in Figure 4.24.

The present study demonstrates that the MC-HPDC process is capable of producing composite materials which exhibit an increase in tensile strength whilst maintaining a reasonably comparable ductility with the unreinforced samples, when most conventional processes produce brittle products. Figure 4.25 provides the Young's modulus data for LM24-SiC PMMCS together with the theoretical Hashin-Shtrikman bounds. Similar to LM25-SiC PMMCs, the MC-HPDC process produced

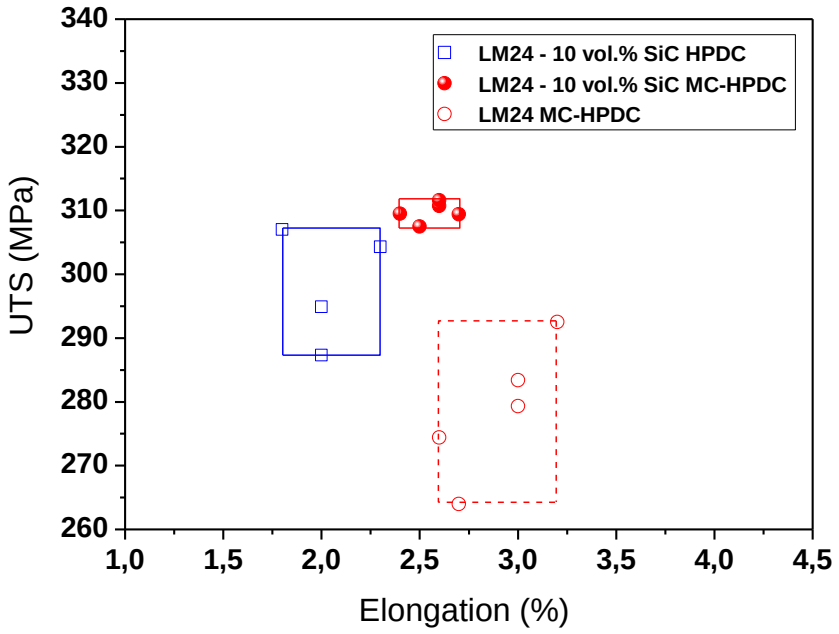

Figure 4.24 Comparison of the tensile properties of LM24 – 10 vol. % SiC_p composites produced with the HPDC and MC-HPDC processes. The properties of the base LM24 alloy produced with the MC-HPDC process are also included for comparison purposes.

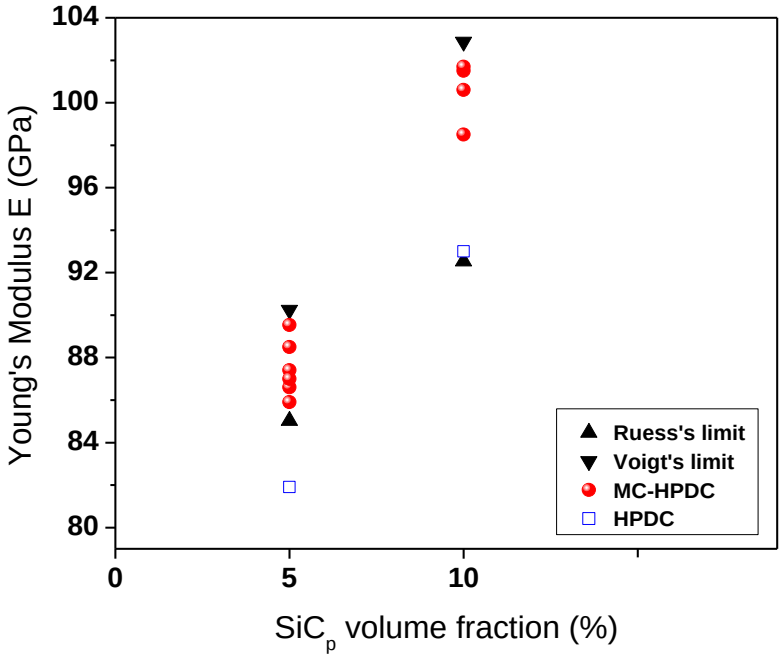

Figure 4.25 Hashin-Shtrikman bounds and measured values of the Young's modulus for LM24 – SiC PMMCs produced with the HPDC and MC-HPDC processes.

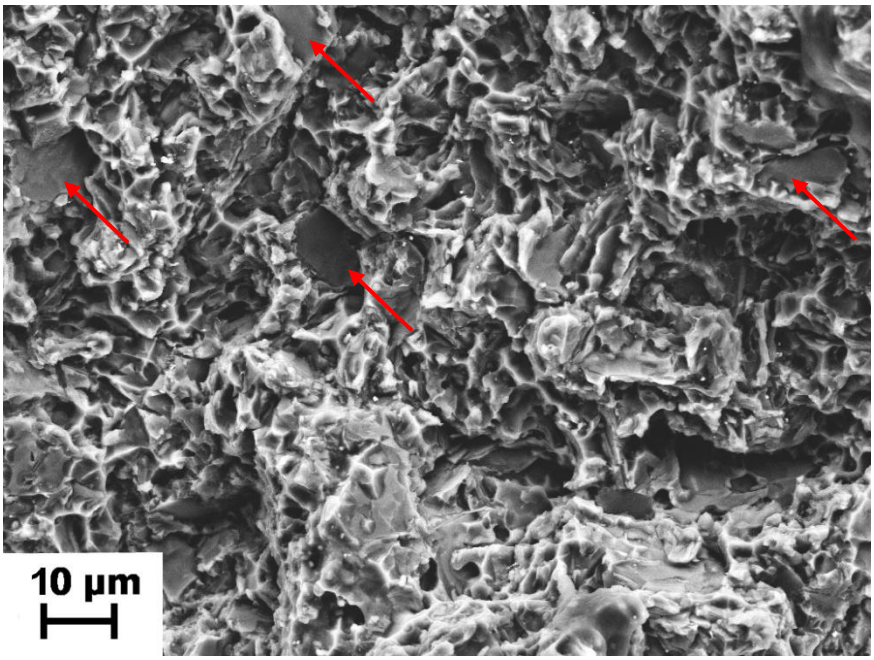

Figure 4.26 Fractograph of LM24- 5 % volume fraction SiC PMMC produced with the MC-HPDC process. Some of the intact SiC particles are indicated with arrows.

castings with a uniform distribution of the SiC particles in the aluminium matrix, confirmed by the Young's modulus values that fall within the Voigt's and Reuss' limits.

Figure 4.26 is a fractograph of the LM24 – 5 vol. % SiC_p MC-HPDC composite. The tensile fracture surfaces reveal the microstructural effects on the ductility and fracture properties of a composite. The fracture surface of the LM24 - 5 vol. % SiC_p MC-HPDC composite consisted of intact SiC_p particles, indicated in the micrograph by the red arrows, surrounded by ductile regions termed tear ridges. Examination of the tensile fracture surfaces revealed damage associated with ductile failure, with no evidence of void formation.

4.3.3 LM24 - Graphite composites

Previous work [Majumdar et al. 1984] suggested that graphite particles, being very weak compared to the aluminium matrix may be treated as non load-bearing constituents. The uniform distribution of the graphite particles in the matrix was expected to have an important effect on the mechanical properties of the

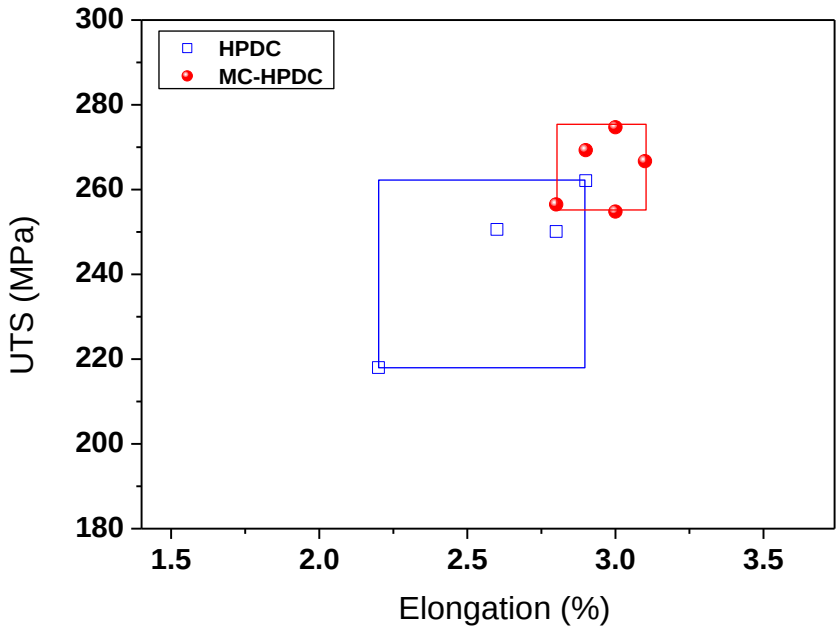

Figure 4.27 Comparison of mechanical properties of LM24 – 5 vol. % graphite composites produced with the HPDC and MC-HPDC processes.

composite material. The properties of LM24 – 5 vol. % graphite composites produced by conventional HPDC and MC-HPDC are compared in Figure 4.27. The MC-HPDC composites exhibited an increase in the tensile elongation together with an increase in the ultimate tensile strength of the material, which can be attributed to the improved dispersion of the graphite particles.

Several authors [Krishnan et al. 1981, Krishnan et al. 1983, Modi et al. 1992, Pillai et al. 1987, Pillai et al. 1995] have reported on mechanical properties of Al-graphite composites. However, the fact that each study used different experimental procedures does not allow a direct comparison of these properties. In an attempt to compare the mechanical properties of Al alloy-graphite composites, the tensile strength was normalised with respect to the base matrix as follows:

$$\sigma_n = \frac{\sigma_c}{\sigma_m} \tag{4.1}$$

where σ_n is the normalised UTS, σ_m is the UTS of the matrix and σ_C is the UTS of the composite. Table 4.2 lists the normalised UTS data from various previous

investigations. The homogeneous distribution of graphite particles in MC-HPDC processed composites resulted in a reasonably high UTS value, comparing well with the base alloy, which was in turn reflected on the high value of their normalised UTS.

4.3.4 The effect of composite microstructure on the mechanical properties

The fundamental links between microstructure, properties and processing conditions are well established for all materials and PMMCs could not be an exemption. The fracture of composite materials is mostly associated with particle clusters or agglomerates which act as cracks or de-cohesion sites, or both [Lloyd 1991]. The primary disadvantage of composites with clustered microstructures produced with the HPDC process is their brittle nature and they frequently suffer from low tensile ductility. Srivatsan and co-workers [Srivatsan et al. 2003] showed that in regions of pronounced particle clustering, the short interparticle distance facilitates the growth and association between neighbouring voids and microscopic cracks, which

Table 4.2 Normalised UTS data comparison for Al-based graphite PMMCs.

Matrix graphite composition (wt.%)	Normalised UTS (σ_c/σ_m)	Reference
LM13 – 3 graphite (die cast)	0.72	[Das et al. 1989]
LM30 – 3 graphite (die cast)	0.70	[Das et al. 1989]
Al-11.8Si-1Mg-3 graphite (as cast)	0.72	[Rohatgi and Surappa, 1984]
Al-12Si-1.5Mg-Cu-Ni-3 graphite (gravity die cast)	0.77	[Krishnan et al. 1983]
LM13-3 graphite (UPAL)	0.77	[Krishnan et al. 1981]
LM24 – 3.5 graphite (HPDC)	0.83	Present study
LM24 – 3.5 graphite (MC-HPDC)	0.90	Present study

result in the macroscopic failure and resultant low tensile ductility seen in conventional HPDC castings. Our study confirmed that the uniform dispersion of reinforcement particles will result in superior tensile properties as seen in Figures 4.22, 4.24 and 4.27. The hard, brittle and essentially deforming SiC particles resist the plastic flow of the aluminium alloy matrix and favour the formation of tear ridges, as seen in Figure 4.26. A uniform dispersion of the soft graphite particles, which are treated as non load-bearing constituents [Majumdar et al. 1984] also results in improved mechanical performance of Al-graphite composites, minimizing the reduction in tensile strength compared to the base metal. In accordance with previous studies [Asthana 1998(a)] the elastic modulus of discontinuously reinforced composites increases with increasing additions of the ceramic reinforcement, as seen in Figure 4.23 and 4.25.

Our study has demonstrated that the superior mechanical properties exhibited by the MC-HPDC samples when compared to conventional HPDC composites are attributed to the improved distribution of reinforcing particles and good interfacial integrity between the particles and the metallic matrix. A uniform distribution will minimise the presence of stress concentration sites and result in improved mechanical performance. The importance of the processing conditions in determining the final microstructure and uniform distribution of the reinforcement in the composites has also been demonstrated.

4.4 Concluding Remarks

The results from the implementation of intensive shearing for the production of high quality PMMCs with the MC-HPDC process were presented in this chapter and compared to PMMCs produced with conventional processing. The findings can be summarised as follows. The conventional stir casting process using mechanical stirring for the mixing of the reinforcement and the metal matrix and the HPDC process for casting produces highly agglomerated and non-uniform microstructures, in agreement to the findings of other researchers. However, the intensive shearing offered by the MCAST unit results in a uniform dispersion of the reinforcement particles in the LM25-SiC, LM24-SiC and LM24-C PMMC systems studied. The high shear stress produced by intensive shearing is adequate to overcome the tensile

strength of particle clusters and disperse them uniformly in the liquid metal matrix prior to casting.

Statistical analysis with the Quadrat method confirmed that the distribution of the reinforcement for PMMCs produced with the MC-HPDC could be described with a theoretical binomial or Poisson distribution, indicating the uniformity of the microstructure. By contrast, the distribution of the reinforcement in castings produced with the HPDC process could be described by a theoretical negative binomial distribution that has been found to describe clustered microstructures. Finally, the improvement of the microstructural uniformity was reflected in the mechanical properties of the MC-HPDC processed PMMCs. The tensile strength and elongation of the PMMCs produced with the MC-HPDC process was increased by 15-25 % compared to PMMCs produced with the conventional HPDC process, where particle clusters act as crack nucleation sites and deteriorate the mechanical performance of the composite.

CHAPTER 5

MAGNESIUM ALLOYS

RESULTS AND DISCUSSION

5.1 Introduction

The main objective of this chapter is to study the effect of intensive shearing on the solidification microstructure and mechanical properties of magnesium alloys. In general, heating, melting and melt handling of magnesium melts allow the chemical reaction with oxygen, even with the presence of a protective atmosphere. This chemical reaction results in the presence of solid oxide particle clusters and oxide films in the molten alloys, which are non-uniformly dispersed. Magnesium components cast with conventional processes usually exhibit a coarse and non-uniform microstructure, containing various casting defects and severe chemical segregation. Intensive shearing was implemented by means of the MCAST process on magnesium alloys of three different alloy series, namely AZ, AM and AJ series, and the resulting microstructures are presented in this chapter in section 5.2. In section 5.3 the AZ91D alloy was selected and studied in detail and its microstructure and mechanical properties were evaluated by producing cast components with the MC-HPDC process. In section 5.4, the potential of the MC-HPDC process as a physical route for the recycling of high grade magnesium alloy scrap is presented. Finally, in section 5.5 the discussion of the results is focused on the effects of intensive shearing on the refinement of the solidification microstructure and the subsequent improvement of the mechanical properties.

5.2 Microstructure of MCAST magnesium alloys

5.2.1 AZ91D magnesium alloy

Recent work in our research group was carried out to investigate the effect of intensive shearing on the grain size of AZ91D alloy [Xia et al. 2009]. The liquidus temperature of AZ91D magnesium alloy is 598 °C. Hence, to ensure that the molten metal was in a fully liquid state, the application of the MCAST process started at a

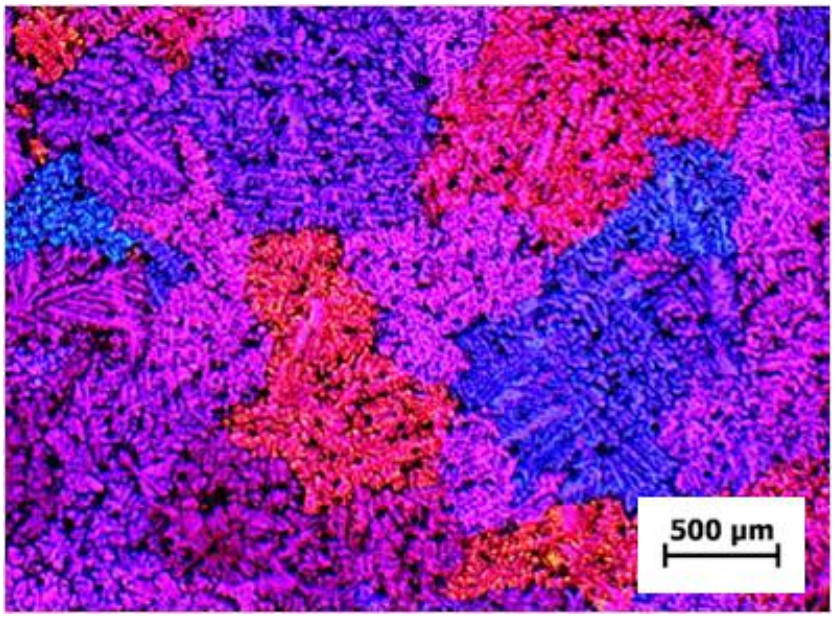

(a)

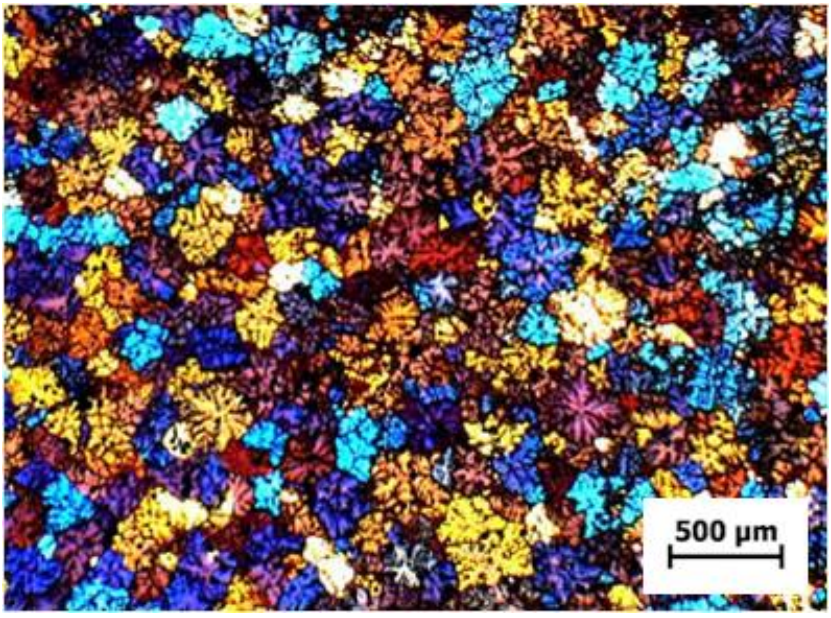

(b)

Figure 5.1 Microstructure of AZ91D alloy cast in a TP1 mould at 650 °C: (a) as cast; (b) MCAST [Xia et al. 2009]. The implementation of intensive shearing has clearly refined the grain structure.

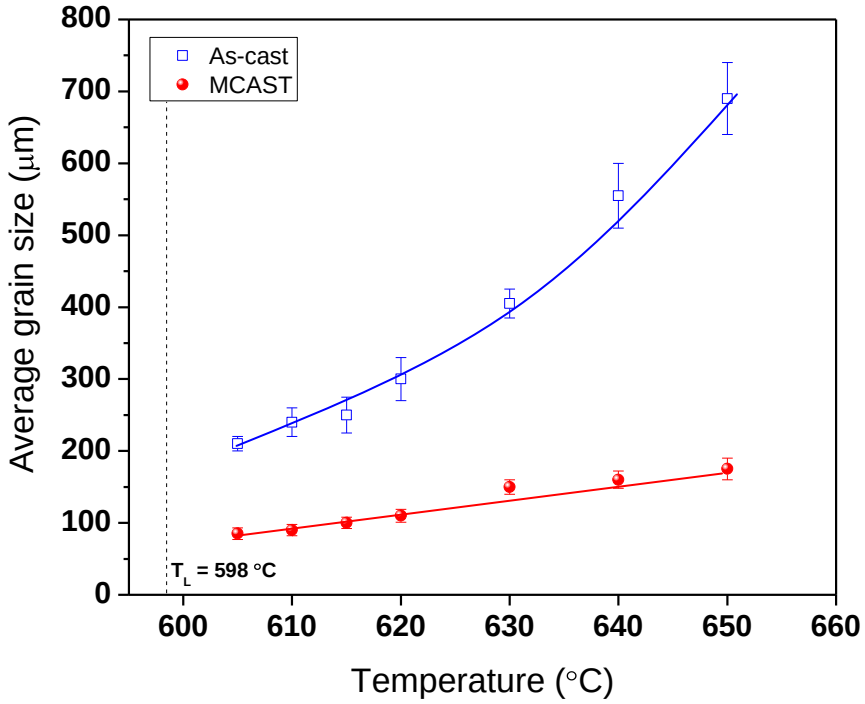

Figure 5.2 The effect of intensive shearing on the average grain size of AZ91D magnesium alloy, as a function of temperature [Xia et al. 2009]. The MCAST process refines the grain size and reduces its temperature dependence.

temperature of 605 °C. As the MCAST unit can reach a maximum temperature of 650 °C, the temperature range studied was between 605-650 °C. Figure 5.1 presents the microstructure of the AZ91D Mg alloy, with and without melt shearing, cast at 650 °C in the TP1 mould, showing the significant grain refinement provided by the intensive shearing. The mean grain size decreased from 690 μm to 175 μm at 650 °C. It was found that this grain refinement was effective over the whole casting temperature range studied for the AZ91D alloy, as presented in Figure 5.2. The influence of the melt superheat on the grain size was suppressed by the shearing effect, with the mean grain size varying from 85 μm to 175 μm when intensive shearing was imposed, compared to 210 μm to 690 μm without melt shearing.

5.2.2 AM60B magnesium alloy

AM60B, together with AZ91D, are the most widely used magnesium alloys in die-casting applications. Refinement of its microstructure would result in reduced

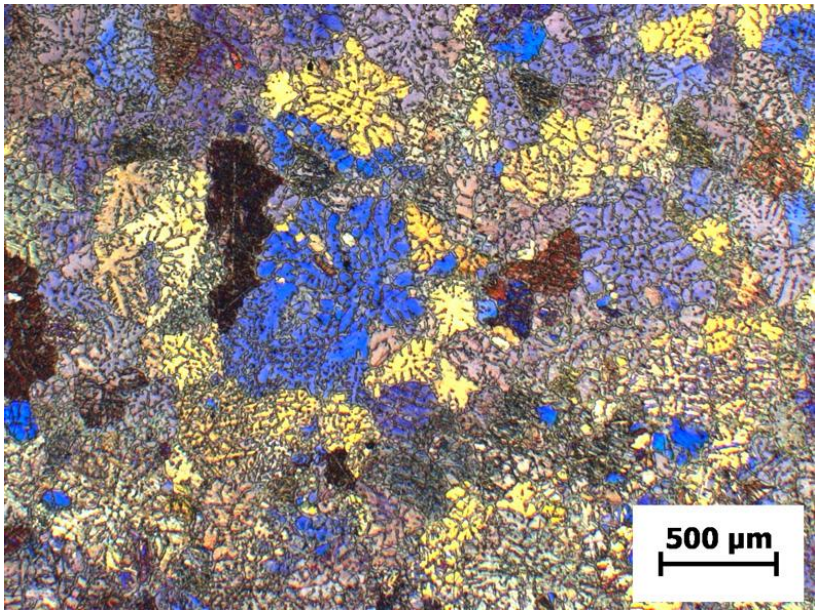

(a)

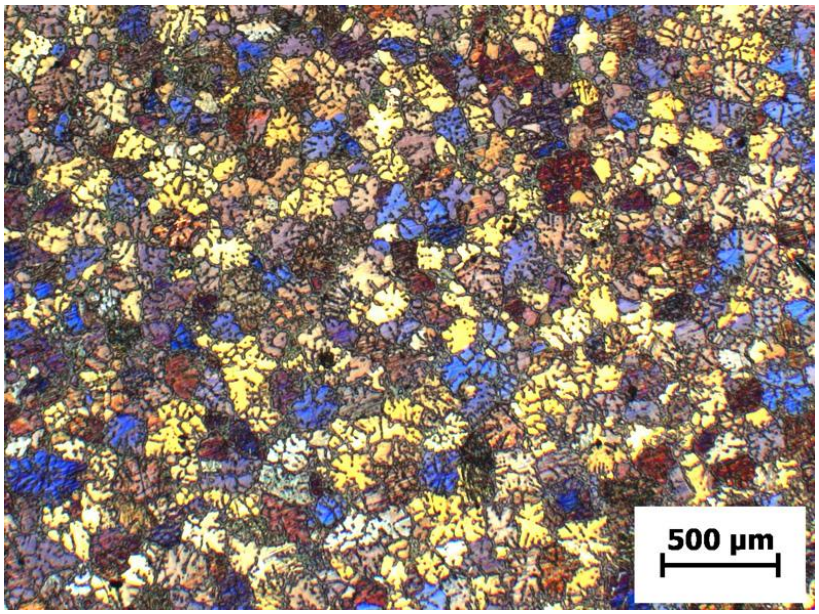

(b)

Figure 5.3 Microstructure of AM60B magnesium alloy cast in a TP1 mould at 650 °C: (a) as cast; (b) MCAST. The implementation of intensive shearing has clearly refined the grain structure.

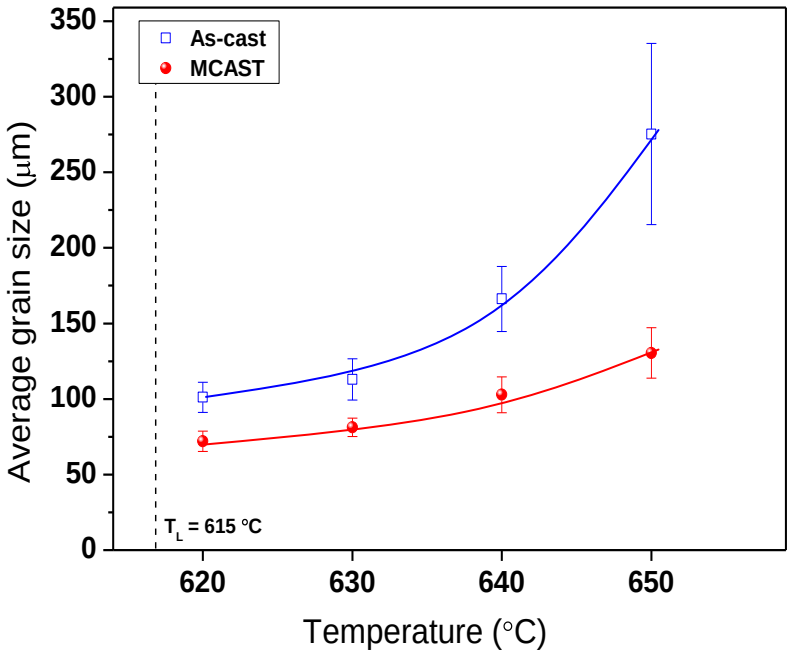

Figure 5.4 The effect of intensive shearing on the average grain size of AM60B magnesium alloy, as a function of temperature. The MCAST process refines the grain size and reduces its temperature dependence.

casting defects and more consistent, improved mechanical performance. AM60B alloy has a liquidus temperature of 615 °C and to ensure that intensive shearing was carried out at a fully liquid state, the temperature range for processing was selected between 620 °C and 650 °C. Figure 5.3 presents the microstructure of the AM60B magnesium alloy, with and without melt shearing, cast at 650 °C in the TP1 mould. Intensive shearing resulted in significant grain refinement and the average grain size decreased from 275 μm to 130 μm at 650 °C. The MCAST process lead to the formation of an equiaxed microstructure compared to the non-uniform coarse microstructure of the non-sheared alloy. Compared to the AZ91D alloy, at 650 °C the AM60B alloy is cast with a lower superheat hence the smaller grain sizes. Furthermore, the presence of manganese in small quantities has been shown to refine the microstructure [Cao et al. 2006]. The observed grain refinement was effective and intensive shearing reduced the effect of superheat. The average grain size as seen in Figure 5.4 varies from 70 μm to 130 μm for the MCAST process, compared to 100 μm to 275 μm without melt shearing.

5.2.3 AJ62 magnesium alloy

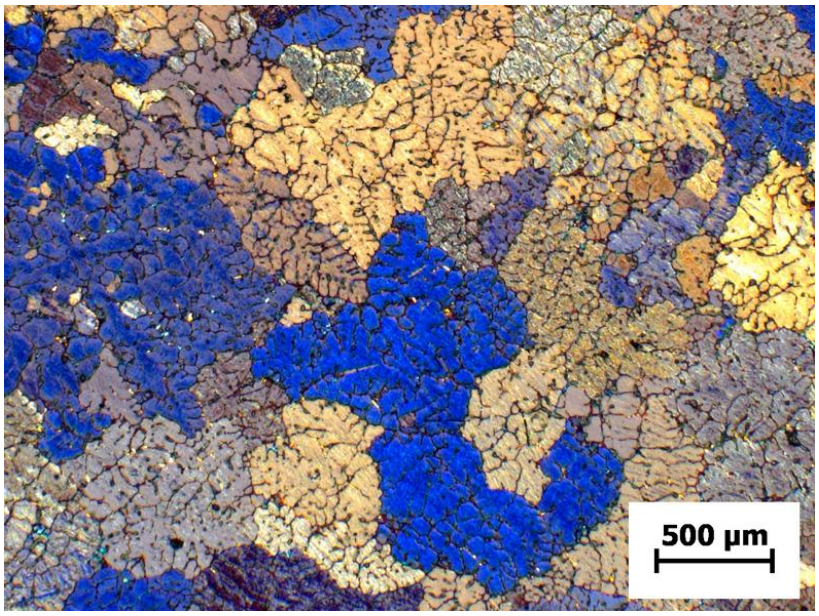

(a)

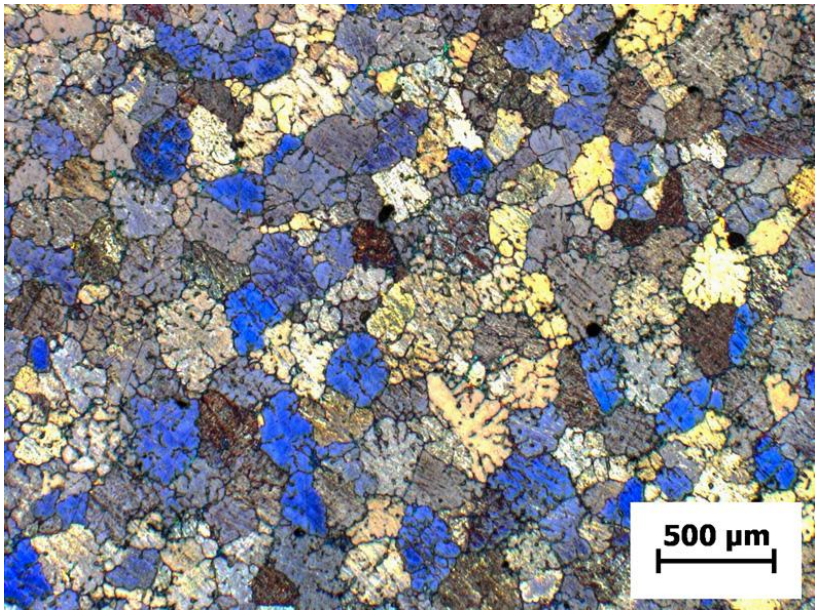

(b)

Figure 5.5 Microstructure of AJ62 magnesium alloy cast in a TP1 mould at 650 °C: (a) as cast; (b) MCAST. The implementation of intensive shearing has clearly refined the grain structure.

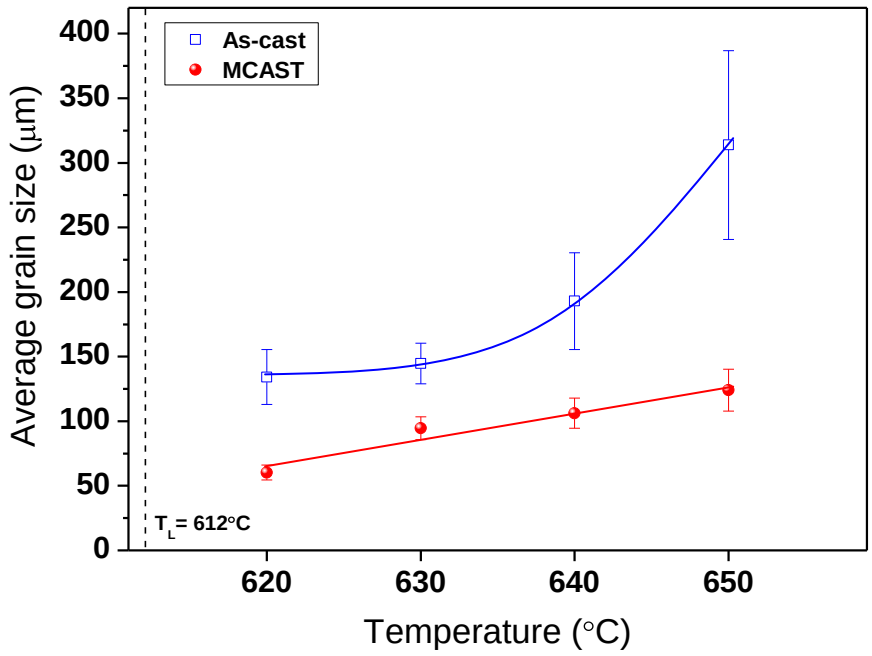

Figure 5.6 The effect of intensive shearing on the average grain size of AJ62 magnesium alloy, as a function of temperature. The MCAST process refines the grain size and reduces its temperature dependence.

Much attention has been paid to the research and development of cost competitive and high temperature creep resistant Mg based alloys that would enable the automotive industry to use more Mg alloy components in order to produce lightweight and fuel efficient vehicles. Among them, Mg-Al-Sr alloys have shown superior creep performance and tensile strength at temperatures as high as 175°C, with the particular AJ62 (Mg-6Al-2Sr) alloy giving an excellent combination of creep performance, tensile properties and castability [Luo and Pekguleryuz 1994, Pekguleryuz and Baril 2001]. The MCAST process was used to study the effect of intensive shearing on AJ62 magnesium alloy at a temperature range between 620 °C and 650 °C, as the liquidus temperature of the alloy is 612 °C. The microstructure of AJ62 alloy, with and without melt shearing, cast at 650 °C in the TP1 mould is presented in Figure 5.5, where the grain refinement of the solidification microstructure by intensive shearing is evident. The very large, coarse dendrites of the as cast microstructure are eliminated by the MCAST process and the mean grain size at 650 °C decreased from 315 μm to 125 μm. Similar to the results for AZ91D

alloy, this grain refinement was effective over the whole casting temperature range studied, as presented in Figure 5.6. The mean grain size varied from 60 μm to 125 μm over the temperature range when intensive shearing was imposed compared to 135 μm to 315 μm without melt shearing. In comparison to AZ91D alloy, there was less melt superheat for the temperature range studied which explains the smaller grain sizes measured. In addition to that, the presence of strontium is known to contribute to the grain refinement of Mg alloys [StJohn et al. 2005, Liu et al. 2008(a), Yang et al. 2008(b)]. Nevertheless, the difference between the non-sheared and sheared AJ62 alloy mean grain sizes clearly demonstrates the refining effect of intensive shearing.

5.3 Microstructure and mechanical properties of AZ91D MC-HPDC magnesium alloy

As described in section 2.2.2, the most commonly used fabrication process for magnesium components is high pressure die-casting (HPDC) and AZ91D is the Mg–Al based alloy mostly used. However, the AZ91D alloy has a wide solidification interval and is highly susceptible to casting defects. Current cast components usually exhibit a coarse and non-uniform microstructure, containing various casting defects and severe chemical segregation. The MC-HPDC process was used to produce AZ91D alloy castings and their microstructure and mechanical properties were studied and compared to castings produced with the conventional HPDC process.

5.3.1 Microstructure of HPDC and MC-HPDC processed AZ91D alloy

Figure 5.7 provides a comparison between the solidification microstructure of the AZ91D alloy prepared by the HPDC and MC-HPDC process, respectively. For the HPDC processed alloy in Figure 5.7(a), large and well developed dendrites are clearly visible, and segregation of the primary Mg phase has taken place, resulting in a non-uniform microstructure. Macro-pores were often observed in the centre of the sample. Two types of dendrites were found, distinguished by their dendrite arm spacing. During the HPDC process, the liquid stays for a few seconds in the shot

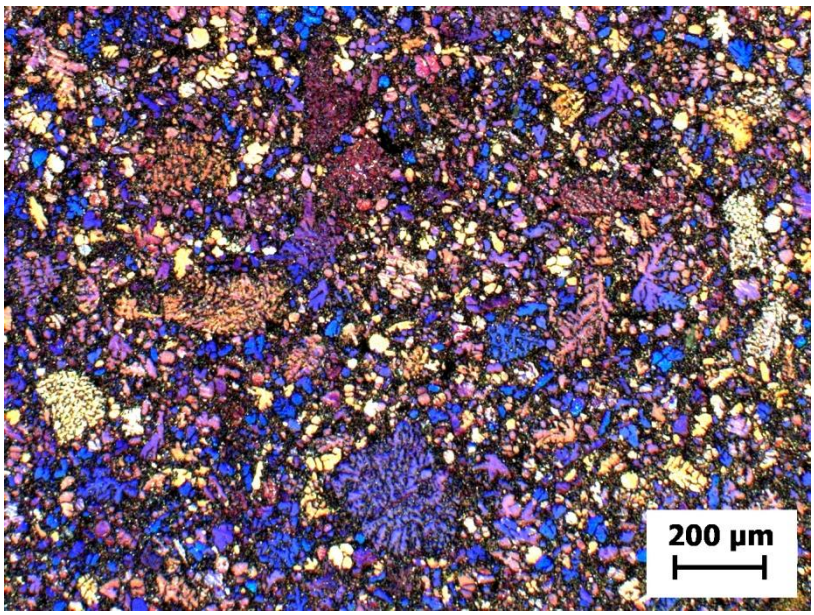

(a)

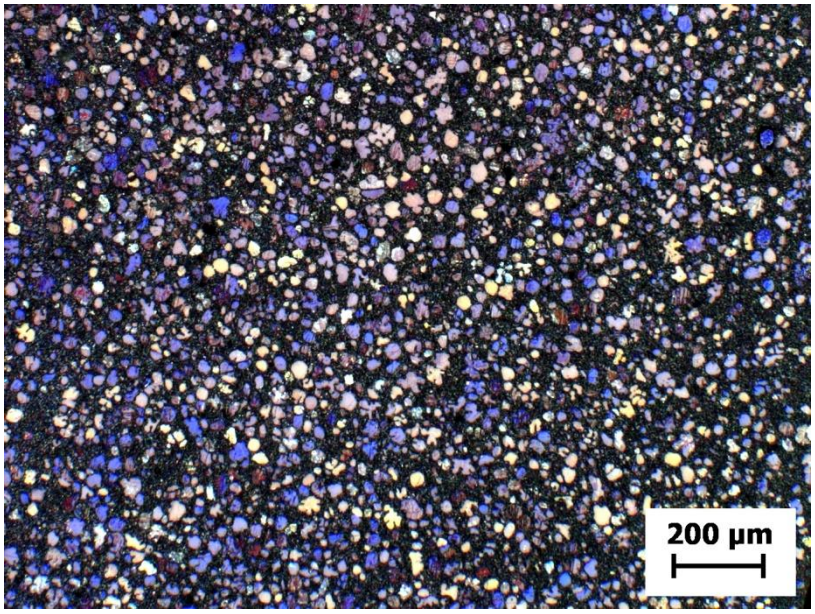

(b)

Figure 5.7 Polarised optical micrographs showing the detailed solidification microstructure of AZ91D alloy processed at 605 ºC by (a) the HPDC and (b) the MC-HPDC process, respectively. Notice the dendritic structure of the HPDC castings, which is completely eliminated after the implementation of intensive shearing and the MC-HPDC process.

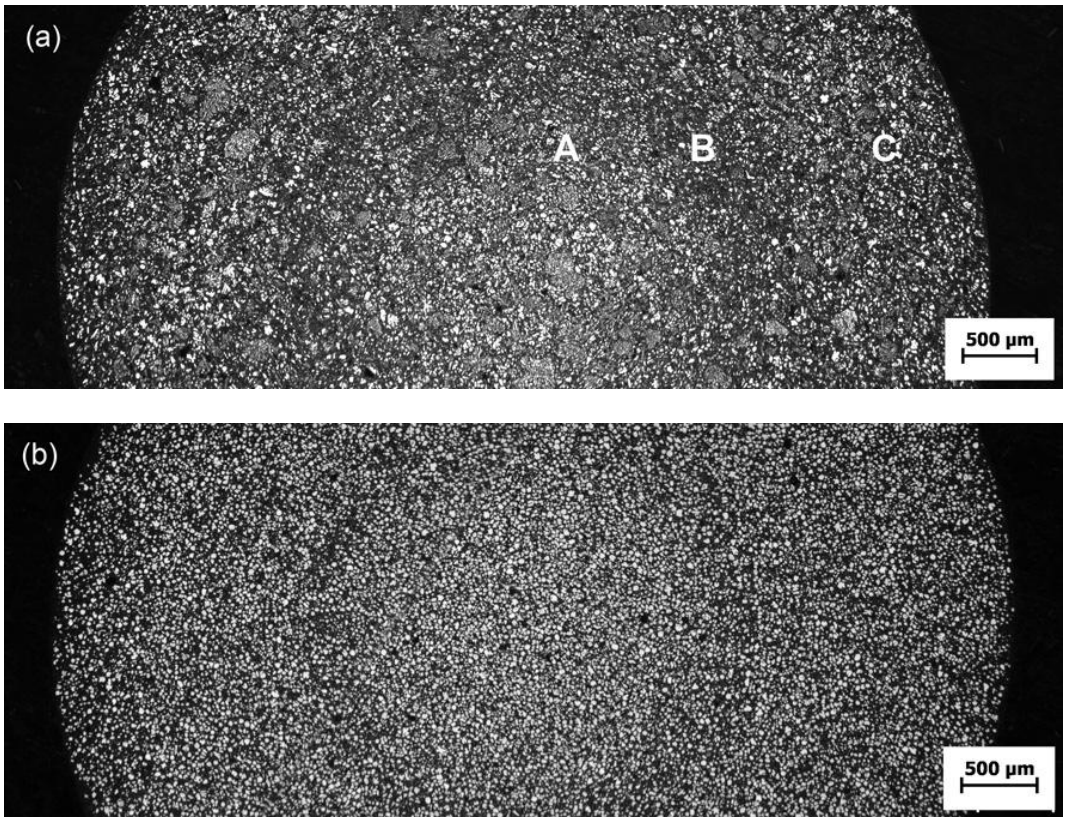

Figure 5.8 Cross-sectional micrographs of an AZ91D alloy cast component, 6.4 mm in diameter, (a) HPDC and (b) MC-HPDC processed at 615ºC. The three distinct regions in the microstructure of the HPDC processed alloy are indicated on the picture; A: central region, containing ESCs; B: defect band, enriched in solute and porosity; C: outer region, also known as 'skin'.

sleeve while pouring and then is injected into the die with the solidification being accomplished inside the die cavity.

Some of the dendrites that form in the shot sleeve are fragmented as they are pushed through the die gate and can be seen in the final microstructure in the form of dendrite fragments or shells. The well developed, coarse dendrites with the smaller arm spacing, seen in Figure 5.7(a), were formed in the die cavity of the HPDC unit. On the other hand, the AZ91D alloy prepared by the MC-HPDC process exhibited a significant improvement in both microstructural uniformity and refinement, as shown in Figure 5.7(b). The primary Mg phase was uniformly distributed across the whole sample, whilst no macro-porosity was observed. The dendritic structure seen in Figure 5.7(a) for the AZ91D alloy produced by HPDC is eliminated in the MC-

HPDC processed alloy, as Figure 5.7(b) shows. Furthermore, in the castings produced with the MC-HPDC process no dendrites as the result of the secondary solidification inside the die were found in the microstructure.

Cross-sectional micrographs of castings produced by HPDC and MC-HPDC processes, cast at 615 °C, are presented in Figure 5.8. The microstructure of a casting produced by HPDC is presented in Figure 5.8(a), where the presence of a defect band is evident. There are three distinct regions in the microstructure: (i) the central region, A, containing large and coarse dendrites and primary solid crystals that form in the cold shot sleeve, known as externally solidified crystals (ESCs), (ii) the defect band, B, enriched in solute and porosity and (iii) the outer region, C, also known as the 'skin', which has close to zero porosity. However, in the case of MC-HPDC AZ91D alloy processed at the same temperature, the formation of the defect band was suppressed as seen in Figure 5.8(b). The microstructure is fine and uniform in the whole cross section of the cast component and the different regions seen in Figure 5.8(a) cannot be distinguished.

To quantify and represent the changes in the defect band formation when intensive shearing is implemented on the liquid metal prior to casting, the volume fraction of the primary Mg particles for castings produced at different temperatures with both the HPDC and MC-HPDC processes was measured using an optical microscope equipped with image analysis software. For the purposes of this analysis, we considered as primary Mg-grains only those with an equivalent circle diameter $d_c \geq 10$ μm and the quantitative results are presented in Figure 5.9. Each point in the graph corresponds to the volume fraction of primary Mg-grains within an area of 400 μm in width and 1350 μm in height, when the diameter of the sample was 6400 μm. The HPDC processed castings showed severe segregation of the Mg phase ESCs at the centre of the sample. The results also confirmed the presence of the defect band located between the central ESCs region and the region that solidified on the die wall. For the intensively sheared sample, although the formation of the defect band was not completely eliminated, its formation was suppressed and the microstructure was more uniform, with a narrower distribution of the primary Mg-grains along the cross section.

Figure 5.10 presents characteristic optical micrographs of as-polished metallographic sections of AZ91D castings produced by HPDC and MC-HPDC

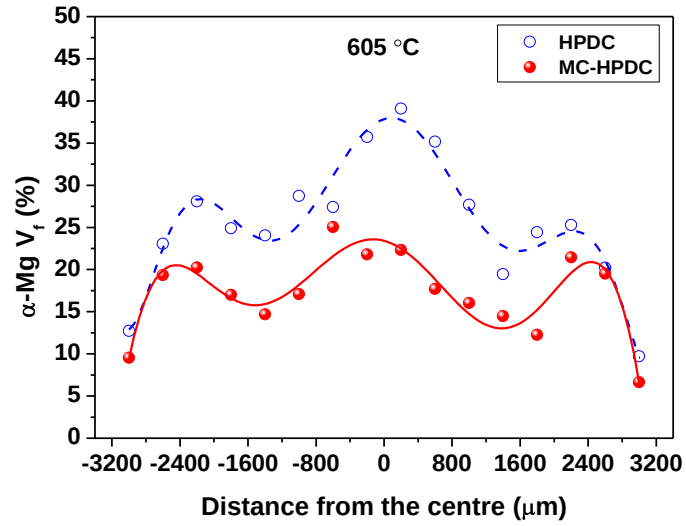

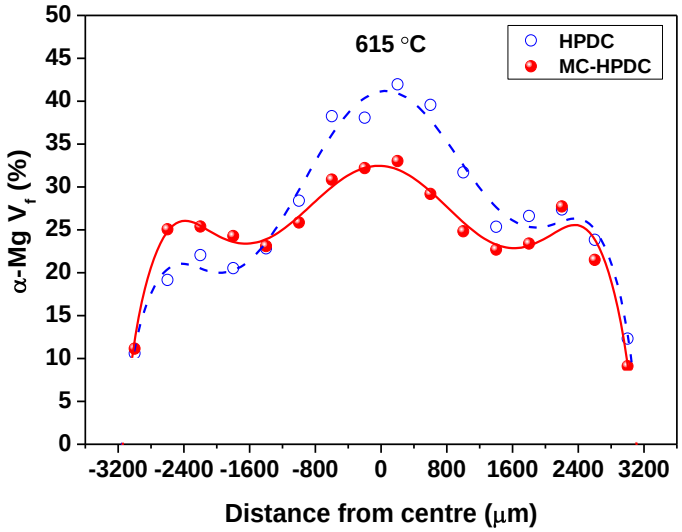

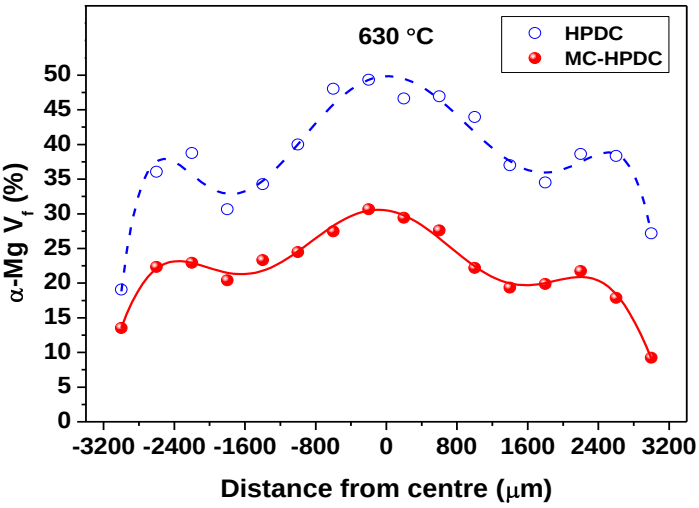

Figure 5.9 Variation of the primary Mg grains volume fraction as a function of the distance from the centre of the sample for AZ91D Mg-alloy prepared by the HPDC and MC-HPDC processes at different temperatures.

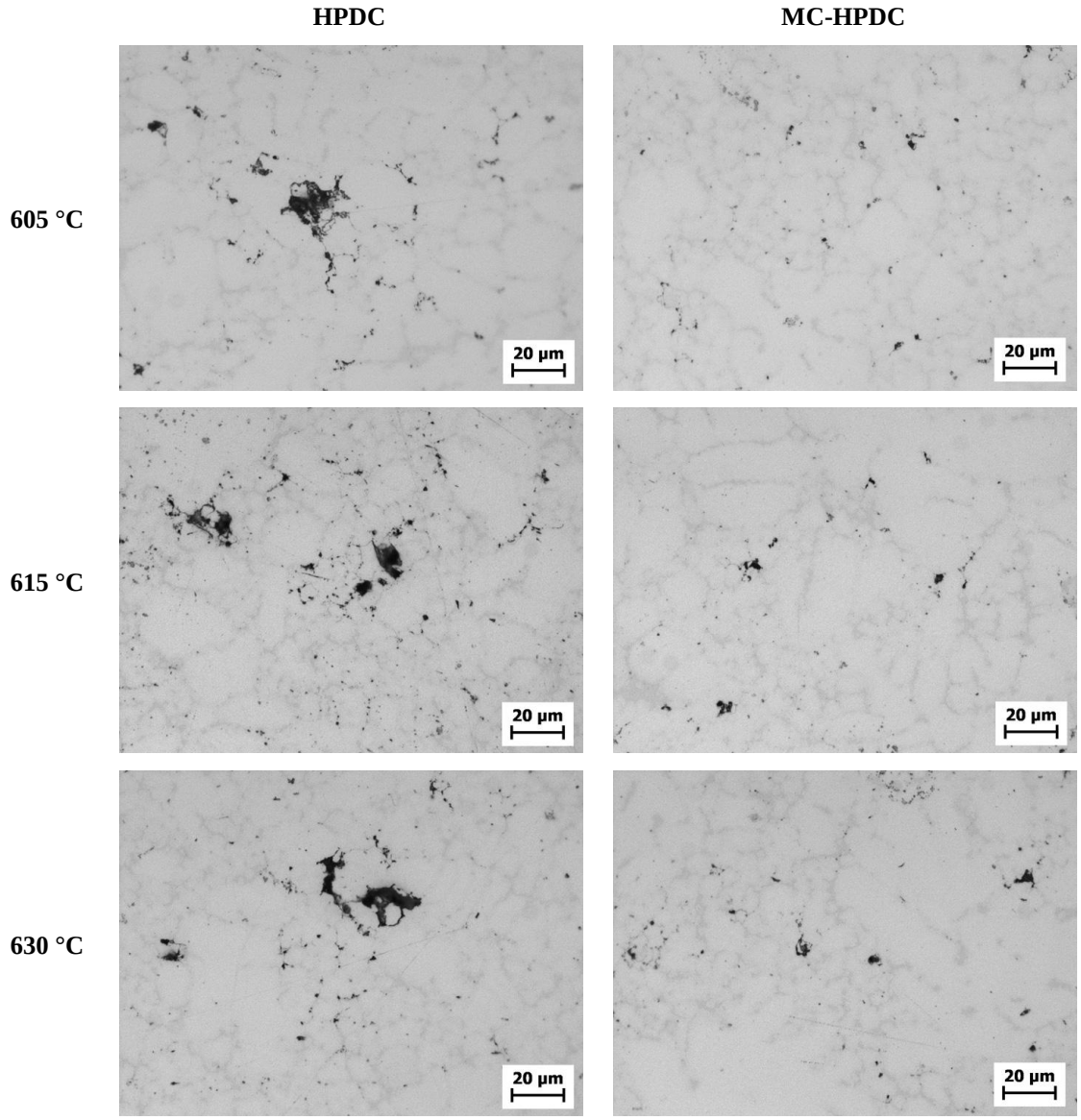

Figure 5.10 Porosity in AZ91D alloy castings produced at different temperatures by HPDC and MC-HPDC processes. The former is characterised by the presence of large, interconnected pores.

processes at different temperatures. The HPDC castings contained large pores (dark in contrast areas), clustered and commonly in some cases inter-connected. The implementation of intensive shearing however, prior to casting with the MC-HPDC process, significantly reduced the porosity levels. No large pores were found in the MC-HPDC castings, and any porosity present was fine in size, well dispersed and isolated. Image analysis was carried out to measure the area fraction of pores in

the microstructure in order to quantify the porosity. The results are presented in Figure 5.11 for both HPDC and MC-HPDC processes at different temperatures.

In all cases the porosity levels of the MC-HPDC castings were reduced, with the total porosity being 0.35–0.41 area % compared to 1.25 – 1.44 area % for the conventional HPDC components. To support these findings, the density of all the castings produced by HPDC and MC-HPDC processes was measured using a high precision Wallace X22B densimeter. The theoretical density was also calculated and the respective porosity levels were derived for the complete range of temperatures studied. The results of this analysis are presented in Table 5.1. In agreement with the porosity measurements using optical microscopy, the density measurements verified that the melt conditioned alloy shows significantly reduced porosity levels. For the AZ91D alloy components produced by the MC-HPDC process, porosity was negligible due to the microstructural refinement as a result of the unique solidification conditions after intensive shearing.

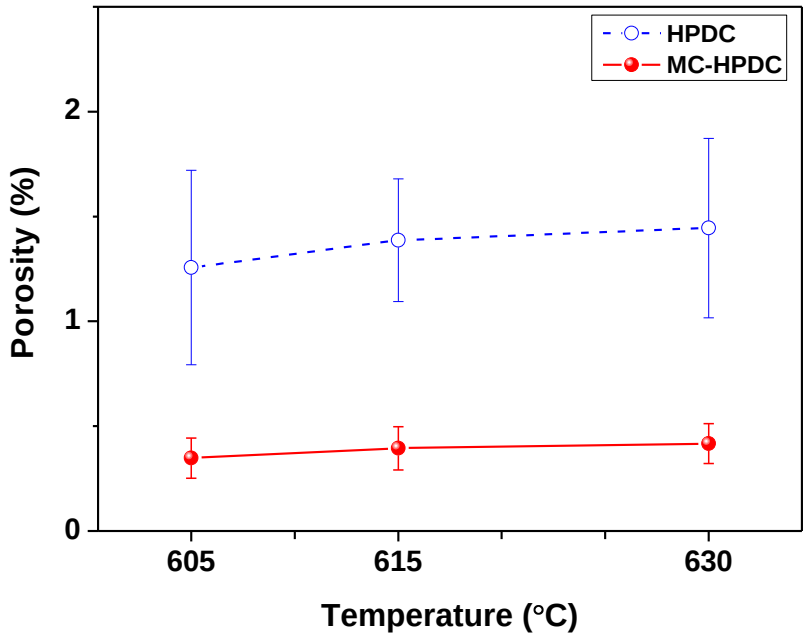

Figure 5.11 The levels of porosity in AZ91D alloy produced by HPDC and MC-HPDC processes. Intensive shearing of the melt with the MC-HPDC process significantly reduces the porosity in the castings.

Table 5.1 Average theoretical and measured density and porosity of HPDC and MC-HPDC processed AZ91D alloy.

	HPDC		MC-HPDC	
	Theoretical	Measured	Theoretical	Measured
Density (g/cm^3)	1.8	1.77	1.8	1.79
Porosity (%)	2.9	1.36	0.9	0.38

It is generally difficult to quantify the refinement in the high pressure die-cast structure by measuring an average grain size for the resultant microstructure of the AZ91D components. There are dendritic grains present, which form in the shot sleeve and are then transferred to the die, with the majority of them being fragmented. There are also grains that form inside the die cavity under a highly different cooling rate and at the same time a divorced eutectic phase is formed. The number of fine size dendritic fragments present in conventional HPDC microstructures is high and will give, in combination with the very fine structure that forms inside the die cavity, small average grain size measurements, without accounting for the presence of those well developed, coarse dendrites which greatly affect the mechanical properties of the components. Thus, it would be very beneficial to show that the implementation of intensive shearing eliminates the formation of such big dendrites, resulting in a much narrower size distribution of the Mg-grains.

Considering the equivalent circle grain diameter as the average grain size, we consider a group of primary Mg-grains within a grain size range of 10μm, for example, 10 μm ≤ d_c < 20μm. We have defined the relative area fraction A_{gi}, which is the area occupied by the primary Mg-grains within a certain group of grain sizes as a fraction of the total area occupied by the Mg-grains in the whole sample, according to the following equation:

$$A_{gi} = \frac{\text{area occupied by Mg–grains within group i}}{\text{total area occupied by Mg–grains in the whole sample}} \times 100\% \qquad (5.1)$$

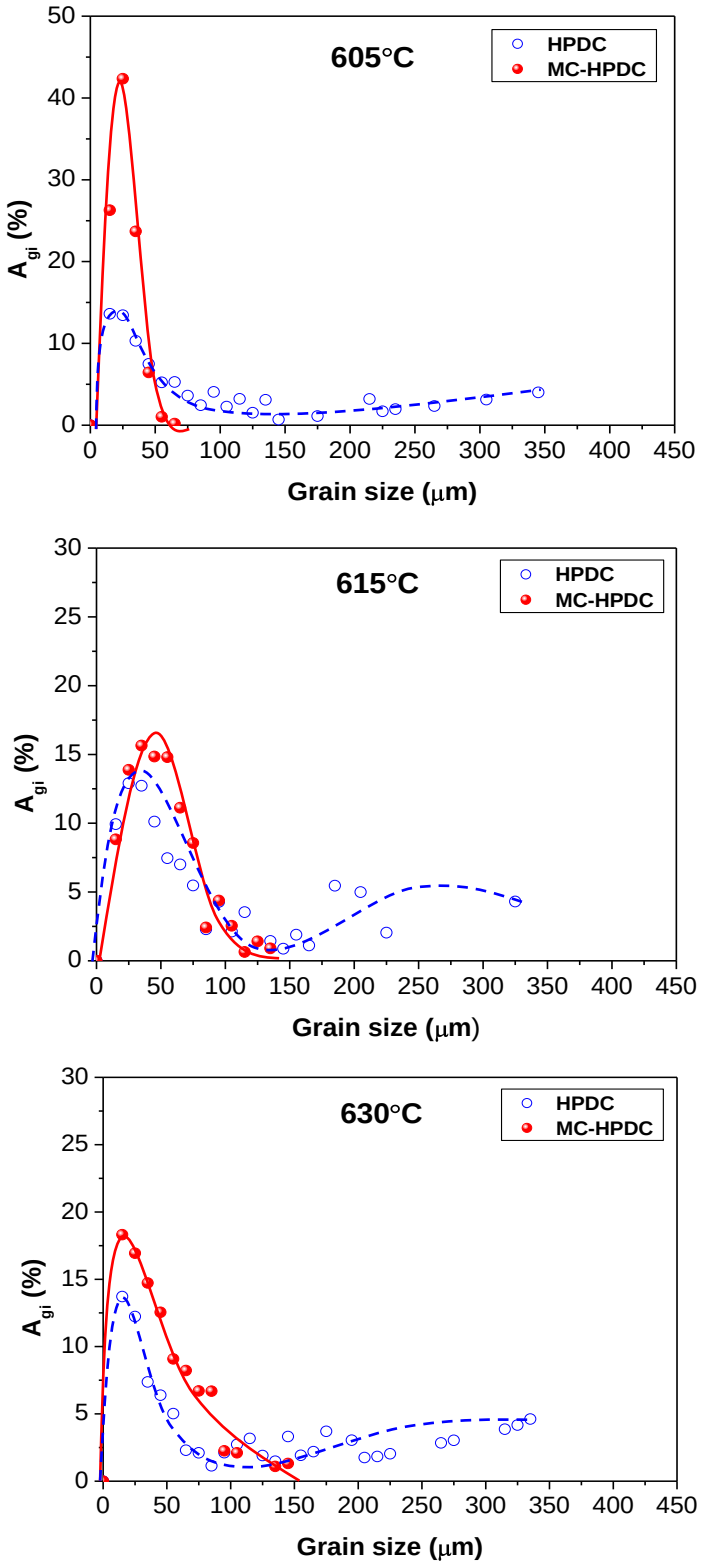

Figure 5.12 Relative area fraction of primary Mg grains depending on their grain size, for both HPDC and MC-HPDC processes at different temperatures. The MC-HPDC process leads to refinement of the grain structure, eliminating the formation of large and coarse dendrites.

To quantify the refinement of the microstructure caused by the implementation of intensive shearing on the liquid metal, we have plotted A_{gi} against the mean grain size value of each group of primary Mg-grains. The resultant plots can be seen in Figure 5.12 for different processing temperatures, where the points correspond to the measured values and the solid and dashed lines are guidelines for the distribution curves. The importance of the results obtained from this analysis is that the microstructural refinement by intensive shearing was effective over the whole casting temperature range studied for the AZ91D alloy. As the temperature increased, the microstructure of the MC-HPDC processed alloy remained fine and more uniform compared to the HPDC processed alloy. Without melt shearing, a significant part of the microstructure comprises of coarse dendrites that are known to be detrimental for the mechanical properties of cast components. However, with intensive melt shearing, the microstructure of AZ91D alloy was refined. The formation of coarse dendrites was eliminated and the grain size distribution in the microstructure was more uniform.

5.3.2 Mechanical properties of HPDC and MC-HPDC processed AZ91D alloy

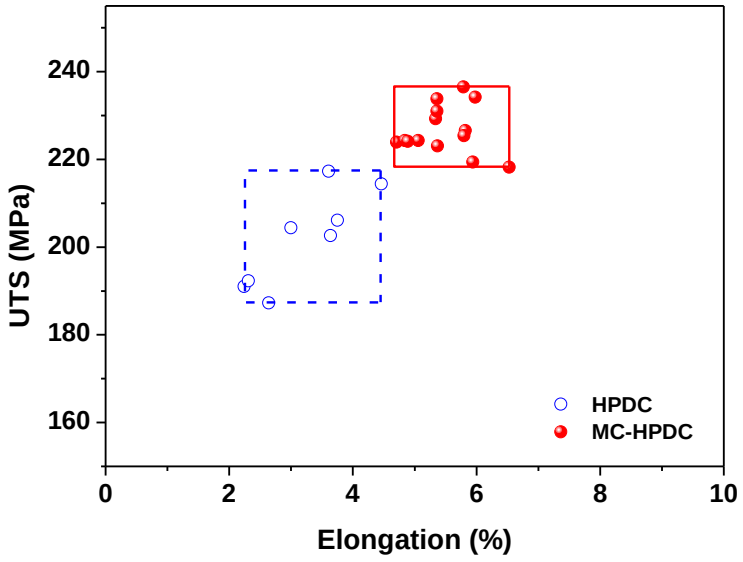

Figure 5.13 Comparison of the mechanical properties of AZ91D alloy produced by HPDC and MC-HPDC processes over the temperature range 605 – 630 ºC. The MC-HPDC process leads to a simultaneous increase in the strength and ductility of the castings.

As anticipated, a refined and more uniform microstructure, with reduced or eliminated casting defects would result in improved mechanical properties of the cast components. The finer grain structure of the alloy produced by the MC-HPDC was expected to increase its tensile strength compared to conventional HPDC, whilst the elimination of cast defects and the negligible porosity should improve the ductility. Figure 5.13 shows a plot of the ultimate tensile strength, *UTS* (MPa) of AZ91D alloy, as a function of the elongation, ε (%), over the whole temperature range covered in this study. The results confirmed that intensive shearing lead to a simultaneous increase in both the strength and the ductility of AZ91D alloy castings produced with the MC-HPDC process, compared to the HPDC process.

5.4 Recycling of high grade magnesium die-casting scrap

We discussed in section 2.2.4 that the increasing usage of magnesium alloys, driven by the quest for weight savings to improve fuel consumption and decrease emissions, will inevitably lead to a rapid increase in Mg-alloy scrap from both manufacturing sources (new scrap) and end-of-life vehicles (old scrap). Currently, chemical approaches are being followed in an attempt to recycle magnesium alloys [Javaid et al. 2006]. However, as these recycling technologies remain complex, energy demanding and low in productivity, they have not found increased applications. Finding a magnesium recycling technology which can effectively deal with the increased inclusions and impurity elements of magnesium scrap still remains a major technical, economical and environmental challenge. In this section, the potential of the MC-HPDC process as an effective magnesium recycling technology is investigated. The high grade die-casting scrap used in this study was a mixture of AM50A and AM60B alloy supplied by *Meridian Technologies.*

5.4.1 The effect of intensive shearing on inclusion and impurity elements

Heating, melting and melt handling of magnesium melts prior to casting allow the chemical reaction with oxygen, despite the presence of a protective atmosphere. This chemical reaction results in the presence of solid oxide particle clusters and oxide films which are non-uniformly dispersed. Recycling magnesium scrap involves further melt processing which will inevitably lead to an increase in the oxide

content. It is therefore of vital importance to deal with these inclusions effectively. However, it is usually very difficult to study inclusions and intermetallic particles in magnesium alloy melts or even in solidified samples because such particles are very fine in size and very scarce in population numbers. The Prefil® technique described in section 3.3.2 was used to collect the inclusions contained in molten magnesium scrap and investigate the effect of intensive shearing on their size and distribution.

5.4.1.1 Non sheared magnesium scrap

As received magnesium scrap was melted and transferred to the pre-heated crucible of the Prefil® unit at 630 °C for casting. Figure 5.14 shows SEM micrographs of the microstructure of the solidified metal adjacent to the filter. The large particles, light in contrast are the filter, separated from the rest of the microstructure by a dashed line. The dark area in contrast is the magnesium matrix whilst the light grey particles seen in the matrix are the well known Al_8Mn_5 intermetallic particles that form during solidification of manganese-containing magnesium alloys. A higher magnification micrograph revealed a large number of needle shaped and plate-like particles, apart from the common faceted Al_8Mn_5 intermetallics. To identify these particles, EDS analysis was carried out and the results can be seen in Table 5.2.

Table 5.2 EDS analysis results for the intermetallic particles found in the non-sheared AM series alloy scrap.

Element	**Needle and plate-like particles**		**Al_8Mn_5 particles**	
	Weight %	Atomic %	Weight %	Atomic %
Mg	8.45	12.92	-	-
Al	34.96	48.18	35.50	52.52
Si	0.92	1.22	0.88	1.25
Mn	55.67	37.68	63.62	46.23
Total	100.00	100.00	100.00	100.00

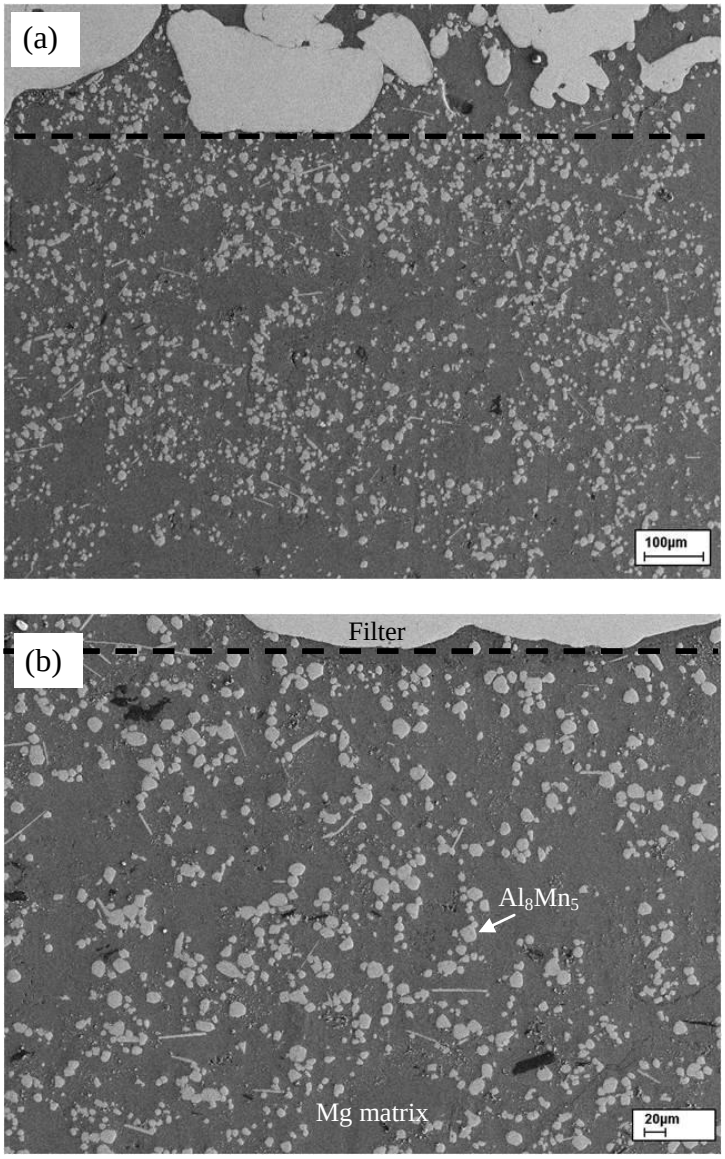

Figure 5.14 Al_8Mn_5 intermetallic particles in the non-sheared AM series alloy scrap collected with the Prefil® technique. The higher magnification microstructure (b) shows the needle shaped and plate-like particles.

Owing to the very fine size of the needle shaped particles, we believe that the increased Mg content seen in Table 5.2 for the needles and plate-like particles most probably originated from the surrounding magnesium matrix. Based on this assumption and the results of the EDS analysis, we have identified these needle shaped and plate-like particles as Al_8Mn_5 intermetallics. Image analysis carried out on the microstructures of the non-sheared magnesium scrap has calculated the average size of all the Al_8Mn_5 intermetallic particles to be equal to approximately 7.5 μm.

Figure 5.15 High magnification backscattered electron SEM micrograph showing the two different types of oxide inclusions in the non-sheared AM series alloy scrap: $MgAl_2O_4$ (spinel), indicated by circles and MgO, indicated by arrows.

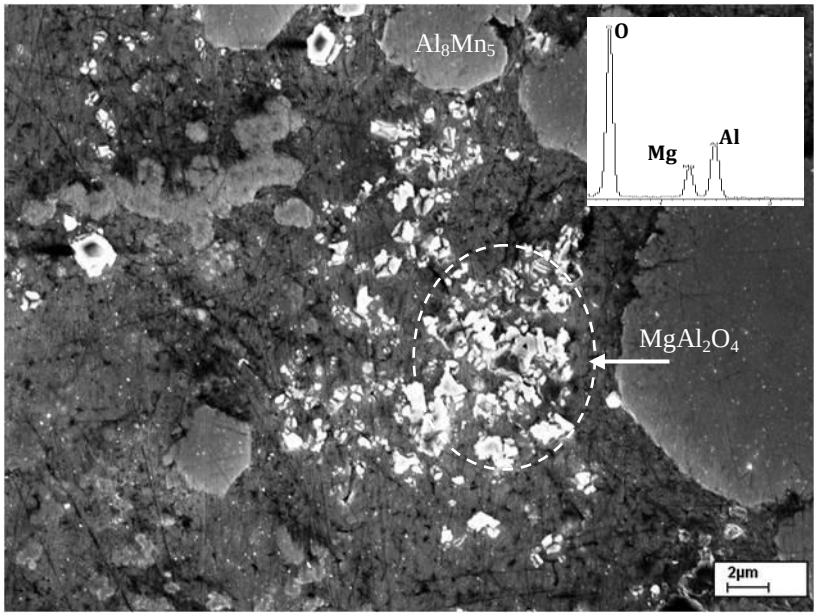

Figure 5.16 High magnification backscattered electron SEM micrograph showing the $MgAl_2O_4$ (spinel) particles, circled and indicated by the arrow, and inset the element peaks from the EDS analysis taken from the spinel particles.

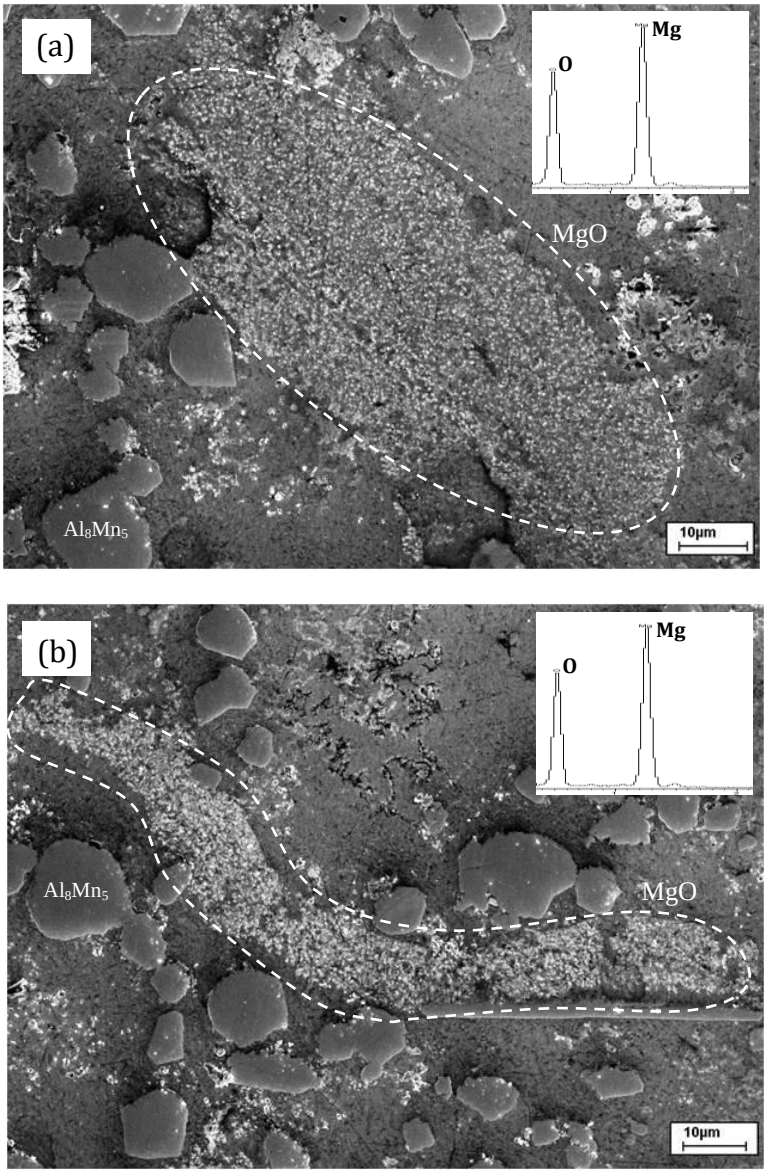

(b)

Figure 5.17 High magnification backscattered electron SEM micrograph showing (a) the large MgO particle clusters, enclosed by the dashed line, and (b) the ingot skins, also enclosed by the dashed line, with the element peaks from the EDS analysis taken from the MgO particles shown in the insets.

Examinations of the filtered non-sheared magnesium scrap using higher magnification backscattered electron SEM revealed more features of the microstructure, as seen in Figure 5.15. Non-sheared magnesium scrap contained a very large number of two different oxide inclusions. Figure 5.16 shows the first type of oxide which was $MgAl_2O_4$ particles, also known as spinel, with the individual

particles having sharp, faceted edges and an average size of approximately 1.5 μm. The second type of oxide, seen in detail in Figure 5.17, was MgO which was found to have two different morphologies. The first morphology type of MgO can be described as oxide particle clusters, seen in Figure 5.17(a), which were developed during melt handling and pouring. They consisted of extremely fine MgO particles (100–200 nm) dispersed in the alpha-Mg matrix. The second MgO morphology type can be described as ingot skin, seen in Figure 5.17(b), which was carried in from the solid ingots. They are usually straight segments with a thickness of 10–15 μm and a length that can extend to more than 100 μm. These oxide skins also consisted of MgO particles dispersed in an alpha-Mg matrix.

5.4.1.2 Sheared magnesium scrap

To investigate the effect of intensive shearing on the intermetallic particles and the oxide found in magnesium scrap, the alloy melt was intensively sheared in the MCAST unit at 630 °C and 500 rpm for 45 s and then transferred to the pre-heated crucible of the Prefil® unit for casting. It was found that intensive shearing of the magnesium alloy scrap prior to solidification changed the morphology of the intermetallic particles, as no needle shaped Al_8Mn_5 particles were found in the microstructure, confirmed by the microstructure presented in Figure 5.18.

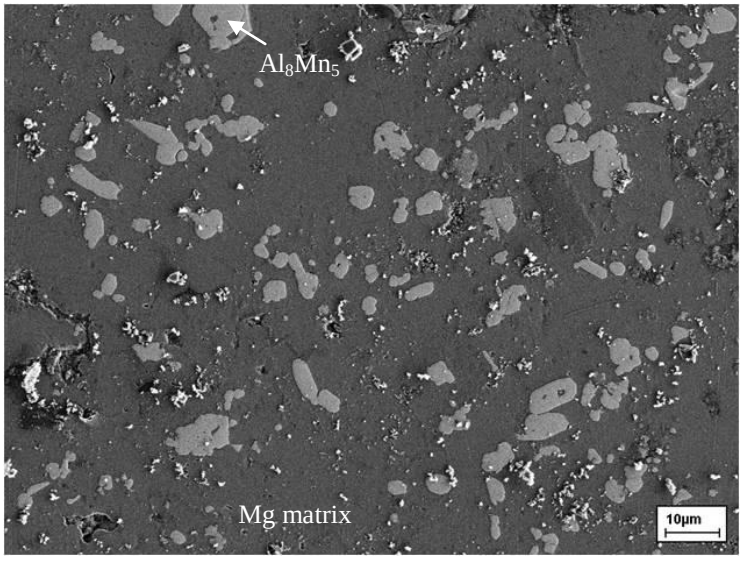

Figure 5.18 Al_8Mn_5 intermetallic particles in the sheared AM series alloy scrap collected with the Prefil® technique.

Also, intensive shearing resulted in the formation of Al_8Mn_5 particles with a finer size of approximately 3.5 μm compared to 7.5 μm of the non-sheared alloy, and a narrower size distribution, as seen in Figure 5.19.

Figure 5.20 provides SEM examinations of the oxides in the sheared magnesium scrap samples, which revealed that similar to the non-sheared alloy, two oxide types were present in the microstructure. $MgAl_2O_4$ particles were found in the microstructure, having the same size and morphology as in the non-sheared samples. They were individual particles having sharp, faceted edges and an average size of approximately 1.5 μm, as seen in Figure 5.21. The second type of oxide found in the sheared magnesium scrap alloy was MgO, which can be seen in closer detail in Figure 5.22. In the sheared sample, both the MgO particle clusters and the ingot skin were eliminated from the microstructure. SEM examination of the sheared sample at high magnifications showed that both the young oxide films and the oxide skins were broken up and dispersed as extremely fine individual particles with a size of 100–200 nm, as presented in Figure 5.23.

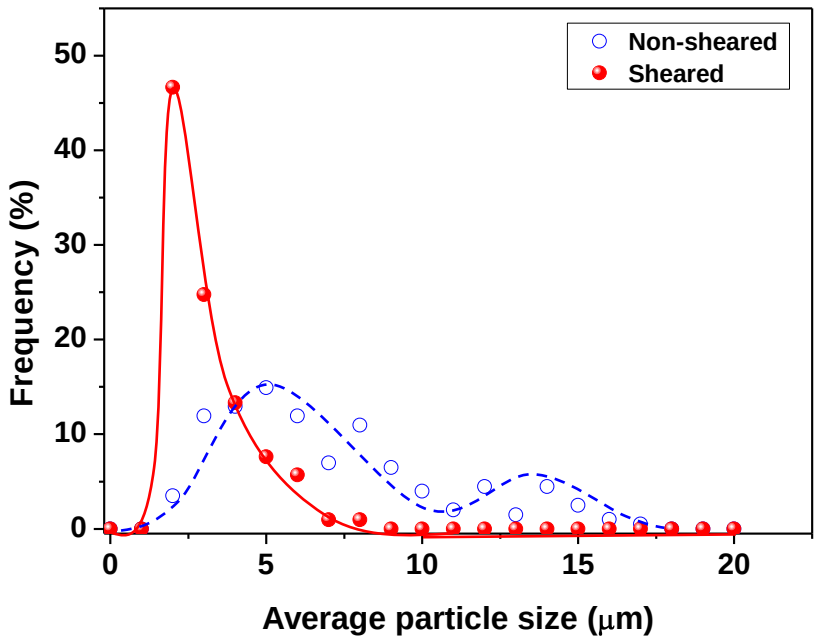

Figure 5.19 The Al_8Mn_5 intermetallic particle size distributions of the non-sheared and sheared AM series alloy scrap.

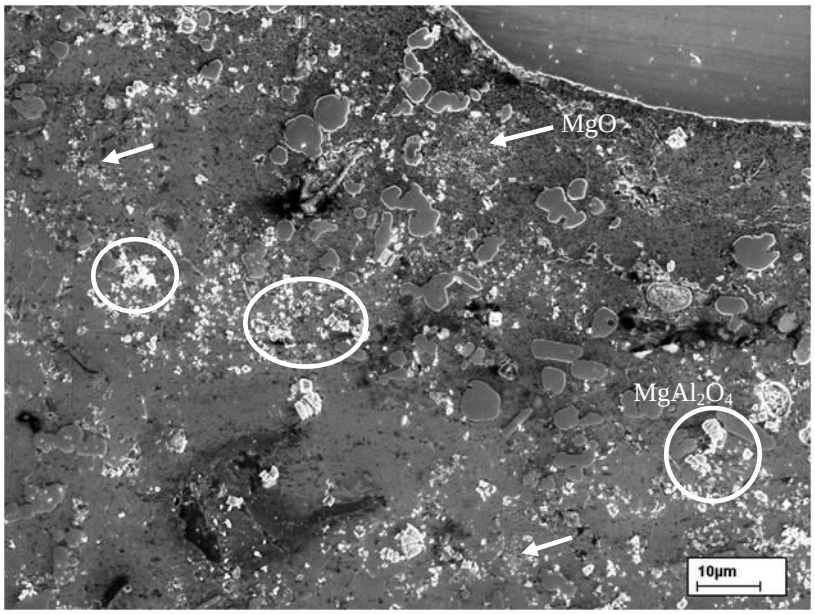

Figure 5.20 High magnification backscattered electron SEM micrograph showing the two different types of oxide inclusions in the sheared AM series alloy scrap: $MgAl_2O_4$ (spinel), indicated by circles and MgO, indicated by arrows.

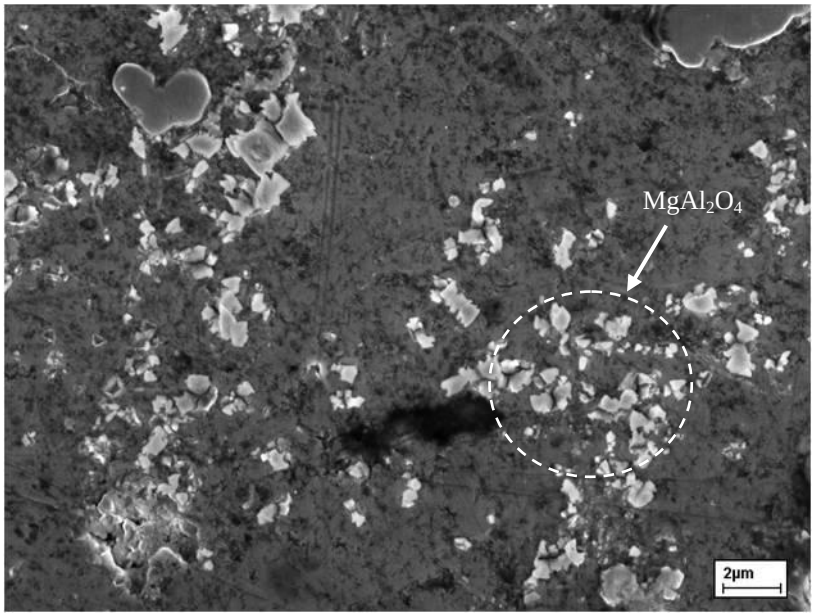

Figure 5.21 High magnification backscattered electron SEM micrograph showing the $MgAl_2O_4$ (spinel) particles, circled by the dashed line and indicated by the arrow.

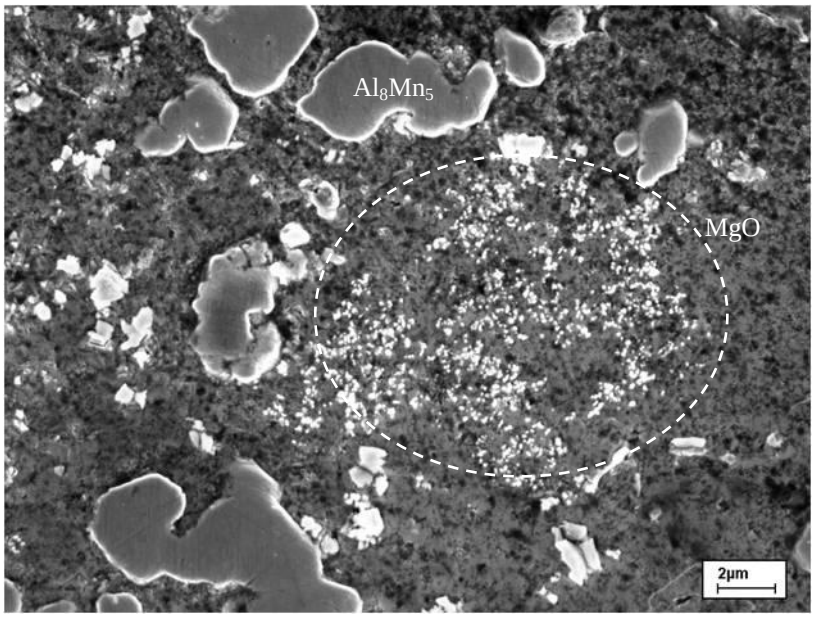

Figure 5.22 Backscattered electron SEM micrograph, showing the MgO particles, enclosed by the dashed line, present in the sheared AM series alloy scrap.

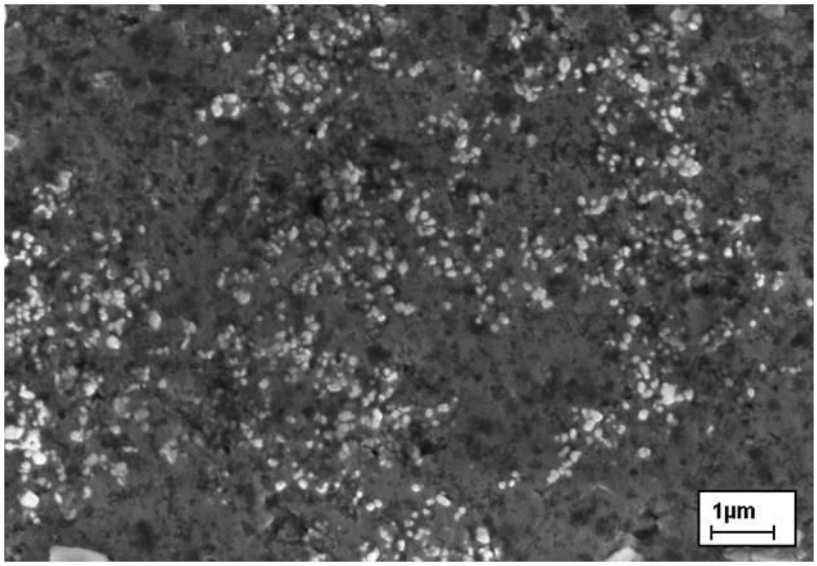

Figure 5.23 High magnification backscattered electron SEM micrograph of the MgO particles in the sheared AM series alloy scrap, revealing the very fine size dispersion.

5.4.2 Optimization of the MC-HPDC process for the recycling of AM series Mg scrap alloys

The results from the investigation of the effect of melt shearing on the intermetallic particles and oxide inclusions have indicated that intensive shearing could be utilised to effectively recycle high grade magnesium scrap alloy. The MC-HPDC process was used to produce castings in order to examine their microstructure and evaluate their mechanical properties. The initial studies revealed interesting phenomena which suggested that it was important to optimise the processing parameters of the MC-HPDC process before conclusions on its effectiveness as a recycling technology could be drawn.

5.4.2.1 Phenomena

Mechanical testing of standard tensile test components cast with the MC-HPDC process produced highly scattered and inconsistent results. Minor changes in the processing parameters resulted in a large variation of the mechanical properties of the components. Even samples cast under identical parameters exhibited inconsistent mechanical behaviour, with their properties varying from sample to sample. Table 5.3 summarises the processing conditions that were used to cast a series of tensile test samples. The two main processing conditions that were altered at this stage of the investigation were the temperature at which the magnesium scrap melt was

Table 5.3 The processing conditions used in the initial trials of the MC-HPDC process for AM series alloy scrap castings.

Sample ID	Shearing Temperature (ºC)	Die Temperature (ºC)
1 – 8	630	250
9 – 38	630	220
39 – 45	630	200
46 – 57	630	180
58 – 65	650	220
66 – 123	615	235

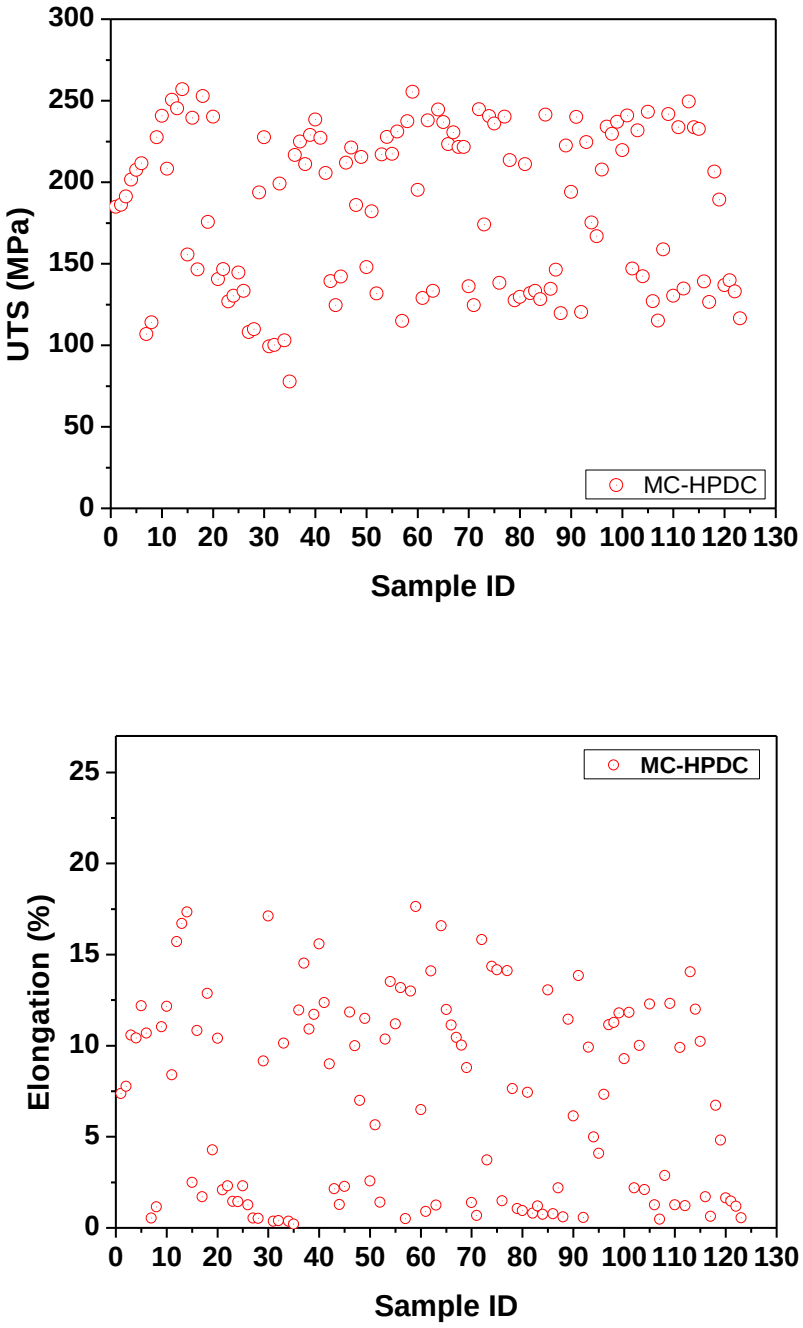

Figure 5.24 The variation of mechanical properties of MC-HPDC recycled AM series scrap. Initial results suggested that the process required optimisation.

sheared prior to casting and the die temperature of the die-casting machine. The phenomena observed with the large variation of the mechanical properties are presented in Figure 5.24.

5.4.2.2 Origin of the observed phenomena and probable mechanism

The origin of the large variations in the mechanical properties of cast components was identified after careful examinations of their macro- and microstructures. Visual inspection of the cast samples both prior to and after the mechanical testing to failure revealed a connection between the sample surface and the result of the tests. Samples that exhibited unexpected mechanical performance and failed prematurely always followed the same trend. Failure was located outside the gauge length of the tensile sample and always occurred at the shoulder of the sample. These observations, in conjunction with the well known link between structure and mechanical properties, lead us to believe that the observed phenomena originated from the structure of the tensile samples at the shoulder area. Inspection of the castings prior to mechanical testing identified the presence of dark lines in contrast, as presented in Figure 5.25, on the surface of the majority of the samples that would fail unexpectedly. Metallographic sections of samples where these dark lines were found revealed the presence of cracks in the microstructure, starting from the surface and extending well into the sample body. A characteristic micrograph is presented in Figure 5.26(a). Optical microscopy examinations at higher magnification, as seen in Figure 5.26(b), exposed the detailed structure of these shoulder cracks, which consisted of porosity and solidified eutectic liquid.

Although the connection between the processing parameters and the microstructure and mechanical properties of the final components produced by high pressure die-casting is well established, there is a combination of several parameters that can affect the final result. These are summaried in Figure 5.27 [Avedasian and Baker 1999]. Investigation of the origin of the phenomena observed with the MC-HPDC processing of magnesium alloy scrap concluded that it was cracks located at the tensile test sample shoulders, consisting of porosity and solidified eutectic liquid, that were responsible for the inconsistent mechanical behaviour of the castings.

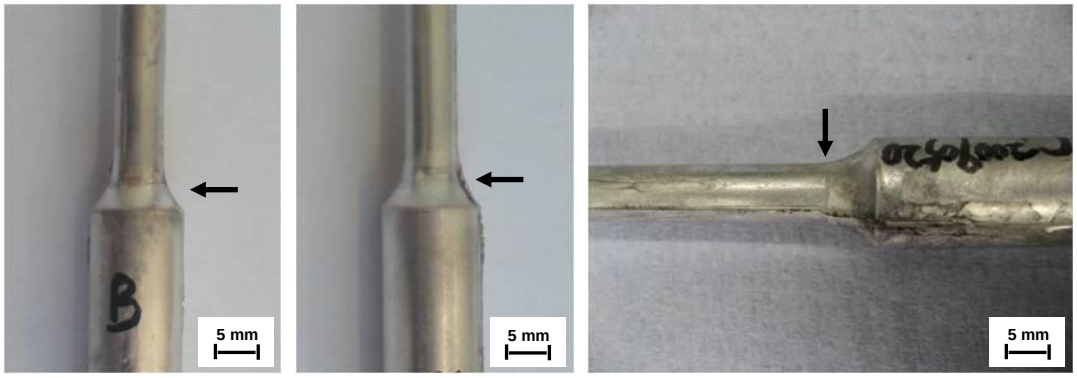

Figure 5.25 Visual examination revealed the presence of dark line on the sample surface, suggesting the existence of shoulder cracks.

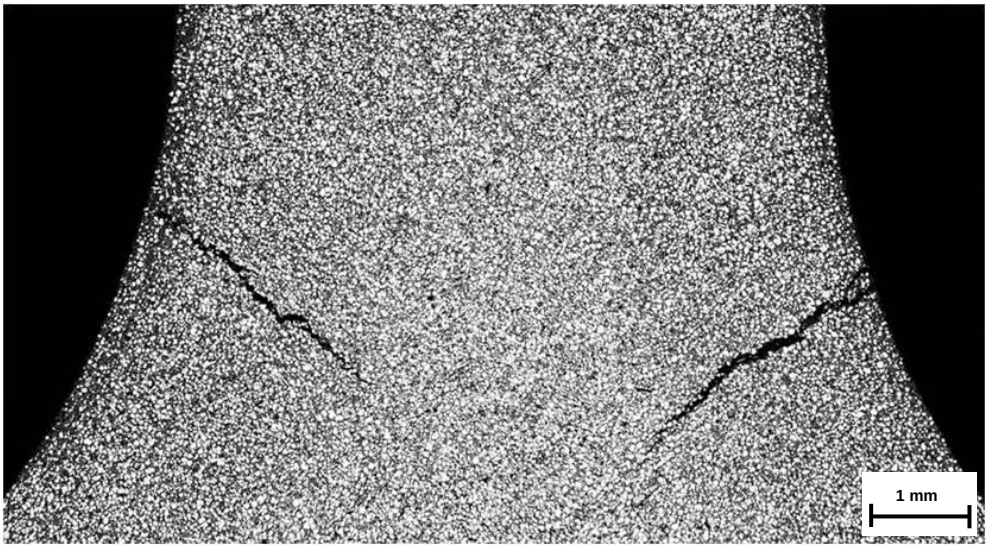

(a)

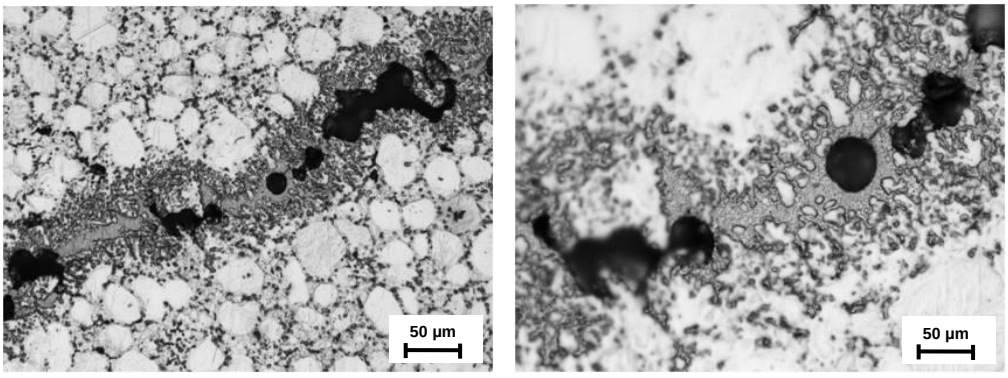

(b)

Figure 5.26 (a) Shoulder crack - The major defect of MC-HPDC recycled AM series scrap tensile samples prior to optimization; (b) The detailed structure of a shoulder crack.

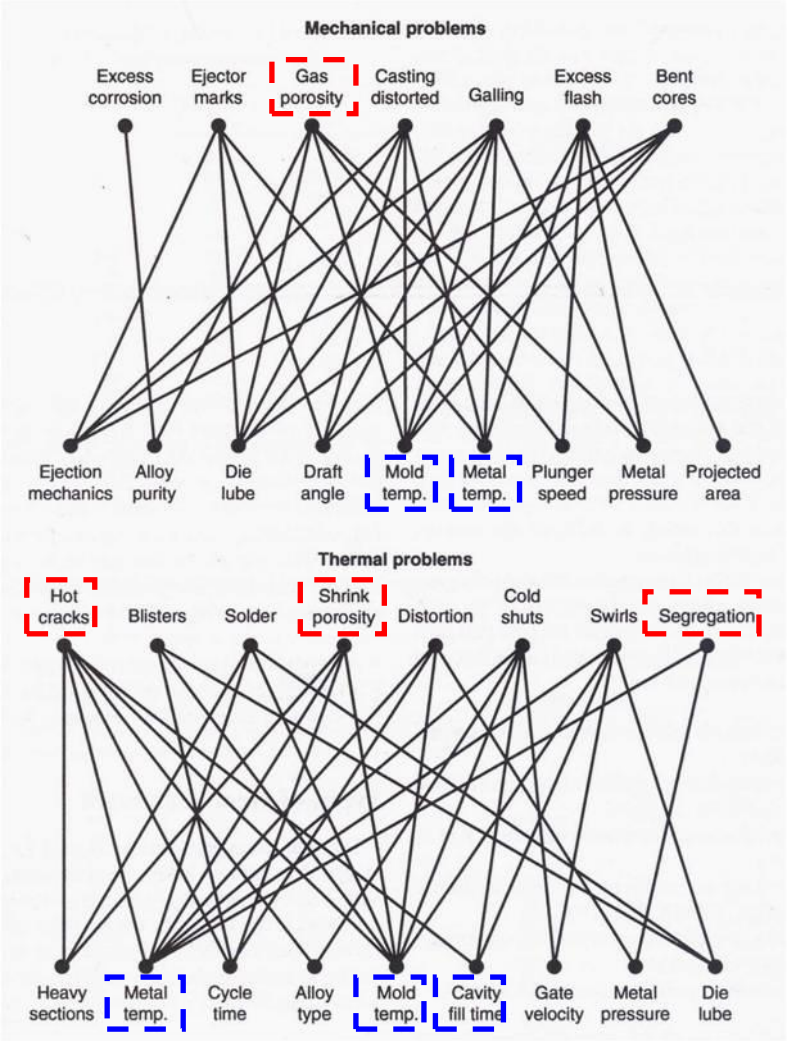

Figure 5.27 Relationships between Mg die-casting defects and casting parameters [Avedasian and Baker 1999].

Hence, according to Figure 5.27, the mechanical and thermal problems that had to be controlled in order to optimise the MC-HPDC process were *gas porosity, hot cracks, shrinkage porosity and chemical* segregation. The die-casting parameters that could be varied and manipulated in order to eliminate these defects were identified as **mould (or die) temperature, metal temperature** and **cavity fill time**. The die temperature was controlled directly from the die-casting machine control panel and the metal temperature could be altered by varying the shearing temperature of the magnesium scrap alloy melt in the MCAST unit. Finally, to control the cavity fill time it was determined that the die-casting parameter that had to be altered was the position where the intensifying pressure is applied during the

casting cycle. The effect of each of the processing parameters on the casting defects is presented in the following section.

5.4.2.3 Optimization of processing parameters

The first parameter under investigation for the optimization of the MC-HPDC process for magnesium scrap was the position of the plunger at which the intensifying pressure was applied, termed here *intensifier position*. A lower intensifier position value indicates that the pressure was applied earlier in the casting cycle resulting in faster filling of the die cavity. The ratio of castings that exhibited the shoulder cracks to the overall number of castings is defined as *defective rate*. The defective rate percentage of the MC-HPDC magnesium scrap alloy castings is plotted in Figure 5.28 as a function of the intensifier position. At higher intensifier position values, when the die filling time was longer, the defective rate of the castings was very high. At 215 mm the defective rate was as high as 75 %, which meant that on average, less than three out of ten castings were crack free and performed well in the tensile tests. When the intensifier position was reduced to 200 mm, the defective rate dropped to 56 % which was still quite high.

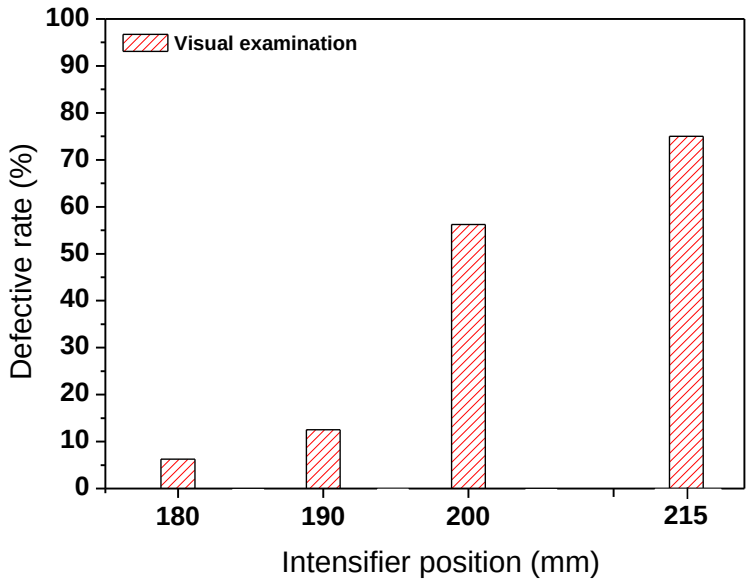

Figure 5.28 The casting defective rate determined by visual examination, as a function of the intensifier position. The die temperature ranged between 160 and 240 °C and the processing temperature ranged between T_L -5 and T_L+15 °C.

However, when the intensifier position was reduced to 190 mm and 180 mm, the defective rate was only 12.5 % and 6.25 % respectively. It was obvious that in order to produce sound castings with no shoulder cracks, the die filling time had to be short. Thus, the intensifier position value was fixed at 180 mm and the optimization of the MC-HPDC process continued with the investigation of the other two casting parameters.

The second parameter that was studied in order to optimise the MC-HPDC process and reduce the occurrence of shoulder cracks was the die temperature of the die-casting unit. It was found that as the die temperature was decreased, the quality of the samples improved. There was a lower limit to which the temperature of the die could be reduced, before the shoulder crack phenomena re-appeared. The effect of the die temperature on the probability of finding a shoulder crack in the castings is presented in Figure 5.29. The defective rate of the castings as a percentage is plotted against the die temperature. A very useful observation was that in some cases, although visual examination suggested the absence of shoulder cracks, the samples would break at the shoulder location indicating that there was a casting defect associated with those samples, which visual examination did not reveal.

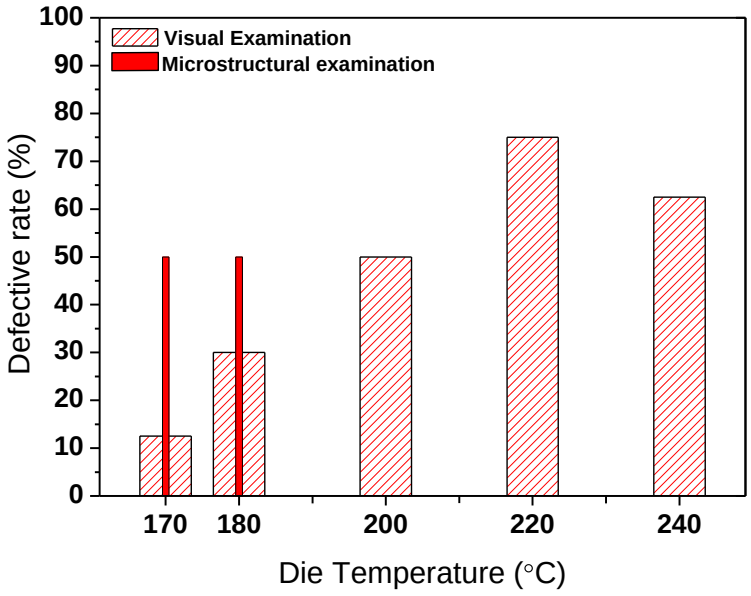

Figure 5.29 The casting defective rate determined by visual and microstructural examination, as a function of the die temperature. The intensifier position was 180 mm and the processing temperature ranged between T_L -5 and T_L+15 °C.

This lead to the conclusion that although the visual examination gave a satisfactory indication for the probability of a shoulder crack in relation to the die temperature, as the die temperature decreased this indication was less accurate and microstructural examination of the samples was necessary. As the die temperature decreased the shoulder cracks did not initiate as close to the sample surface, and were not visible under visual examination. However, the castings exhibited a clear trend to improved performance with decreasing die temperature.

The optimised die temperature for the MC-HPDC process was selected to be 180 °C, as this was the temperature that consistently produced the highest quality of castings. The final parameter to be optimised therefore was the melt temperature, determined by the shearing temperature in the MCAST unit prior to casting. Since the liquidus temperature of the AM series alloy scrap was found to range between 620 and 625 °C, the shearing temperature was determined in relation to the liquidus. The shearing temperatures studied were equal to T_L - 5 °C, T_L + 5 °C and T_L + 15 °C. The results of the optimization process are presented in Figure 5.30, where the sample defective rate percentage is plotted as a function of the shearing temperature.

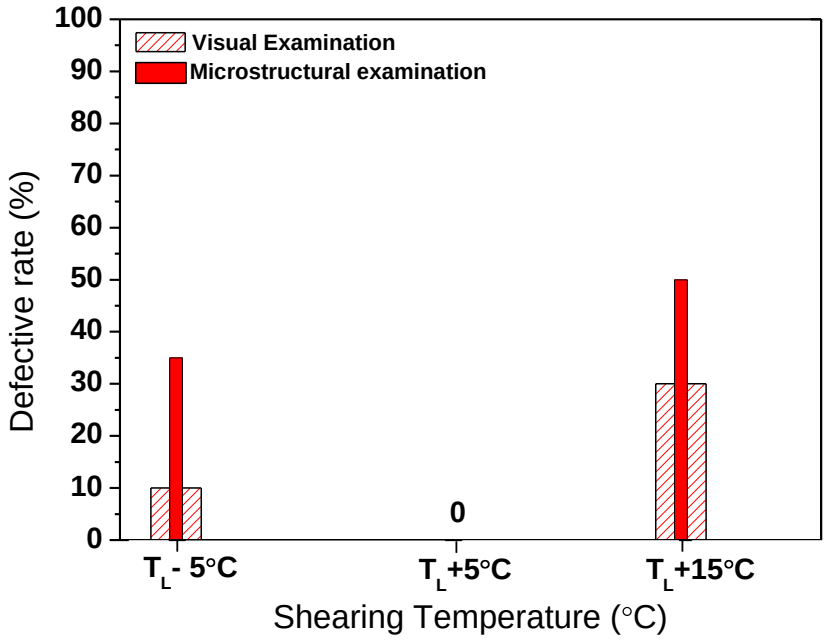

Figure 5.30 The casting defective rate determined by visual and microstructural examination, as a function of the processing temperature. The intensifier position was fixed at 180 mm and the die temperature at 180 °C.

Table 5.4 Optimised parameters for the MC-HPDC process of high grade magnesium scrap.

Shearing time	Shearing temperature	Die temperature	Intensifier position
45 s	T_L + 5 °C	180 °C	180 mm

It was found that when the melt was sheared with a higher superheat (+15 °C), the defective rate was about 30 % based on visual inspection of the samples and increased to 50 % when the samples were sectioned and their microstructure was examined. When the melt was sheared at a temperature close to, but below the liquidus temperature (-5 °C), the defective rate decreased to 10 % with visual examination but was still as high as 35 % when the microstructure was examined. However, when the shearing temperature was just above the liquidus of the alloy (+5 °C), no defective samples were found either by visual or microstructural examination.

In summary, the parameters of the MC-HPDC process of magnesium alloy scrap were optimised in order to eliminate the occurrence of cracks located at the shoulder of the tensile test sample castings. The optimised parameters are given in Table 5.4. It was found that the parameters that were related with the appearance of such cracks were the position at which the intensifying pressure was applied, the die temperature of the die-casting unit and the shearing temperature of the melt. Figure 5.31 shows a direct comparison of the microstructure of castings produced by the conventional HPDC process and the optimised MC-HPDC process for the AM-series alloy high grade magnesium scrap, at the same temperature T_L + 5 °C.

For the HPDC processed scrap in Figure 5.31(a), the resultant microstructure was dendritic and non-uniform. The two types of dendrites that can be seen in the microstructure formed at different stages of the HPDC process. As the liquid stays for a few seconds in the shot sleeve during pouring and is then injected into the die, dendrites form. When the melt is pushed through the die gate, the high shear rate experienced by these dendrites leads to their fragmentation and they can be seen in the final microstructure in the form of dendrite fragments or shells. The well developed, coarse dendrites with the smaller arm spacing were formed in the die cavity of the HPDC unit. On the other hand, the AM-series alloy scrap prepared by

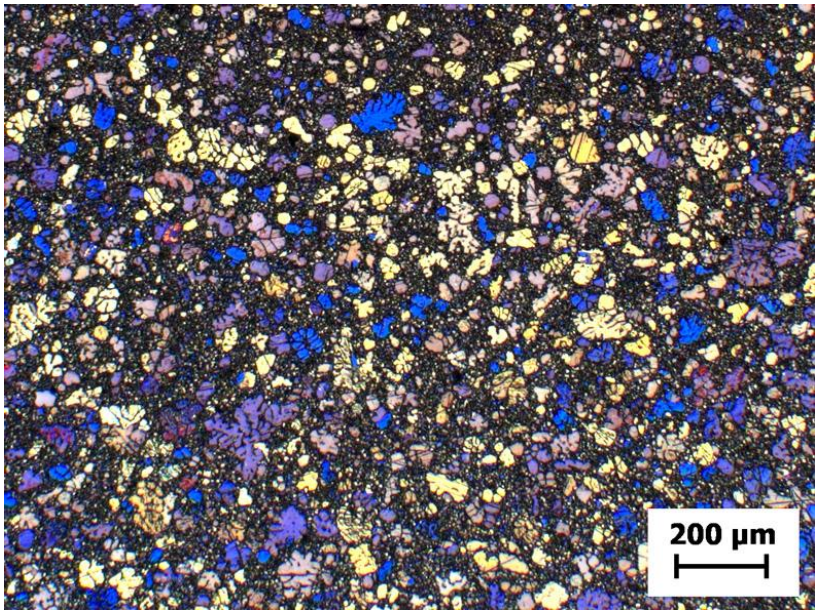

(a)

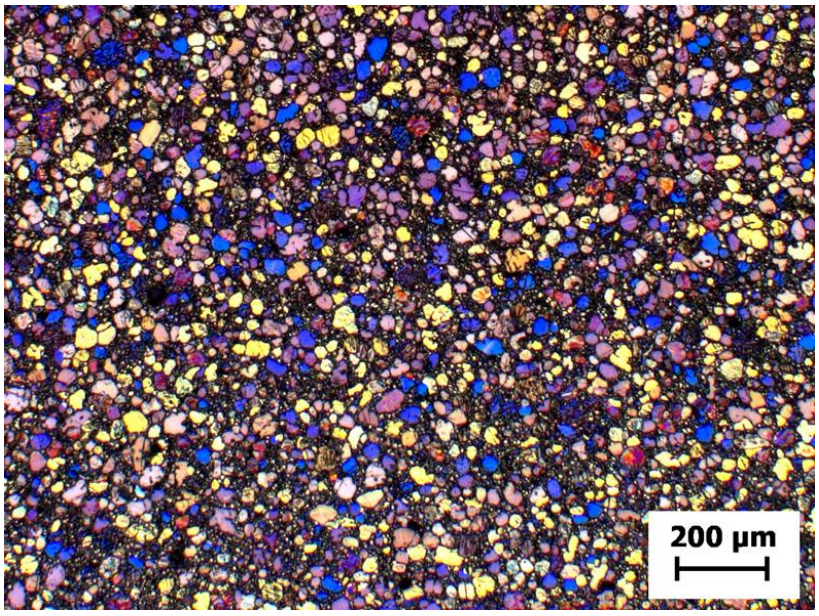

(b)

Figure 5.31 Polarised optical micrographs showing the detailed solidification microstructures of AM-series recycled alloy scrap processed at T_L + 5 °C by (a) the HPDC and (b) the MC-HPDC process, respectively.

the MC-HPDC process exhibited a significant improvement in both microstructural uniformity and refinement, as shown in Figure 5.31(b). As a result of the intensive shearing of the melt prior to casting, the dendritic structure produced by the HPDC process is eliminated in the MC-HPDC processed alloy. The primary magnesium particles had a fine spherical morphology. No dendrite fragments or dendrites as the result of the secondary solidification inside the die were found in the microstructure.

The optimization of the processing parameters for the MC-HPDC process was confirmed not only by the very low defective rates of the castings produced, seen in Figure 5.30, or the refined and uniform microstructure seen in Figure 5.31(b). The optimization of the process was also reflected in the uniformity of the mechanical properties of the samples that were subjected to tensile tests. Figure 5.32 shows the UTS and elongation of a series of castings produced with the MC-HPDC process after the processing parameters were optimised. In comparison to Figure 5.24, the properties exhibit a high level of consistency. No failures of the tensile test components were observed at unexpectedly low strengths or elongations. Failure was always located at the middle of the gauge length confirming the elimination of the shoulder crack defect.

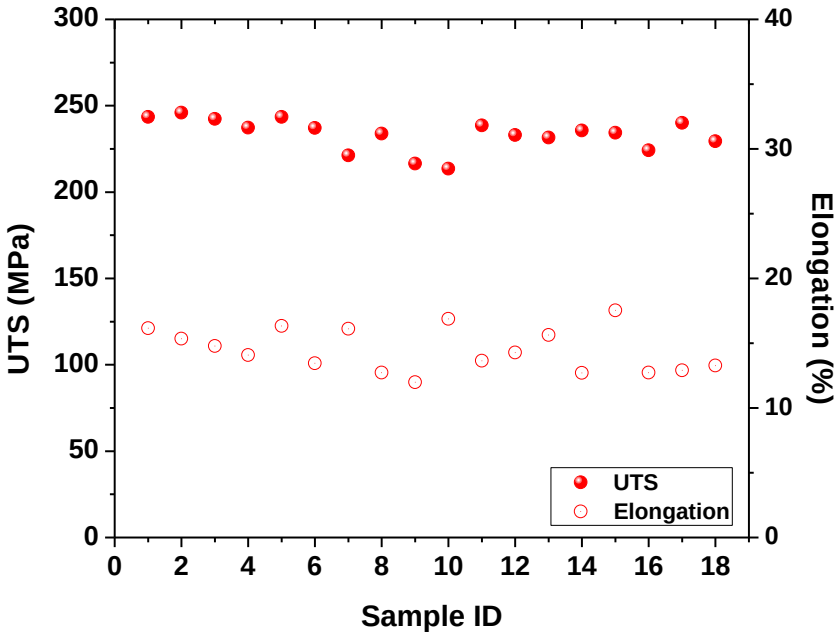

Figure 5.32 Consistency of the mechanical properties after the process optimization, showing the reliability and reproducibility of the MC-HPDC process.

5.5 Solidification behaviour of magnesium alloys under intensive shearing

The basis for understanding the solidification behaviour of commercial AZ and AM series alloys is the phase equilibria and thermodynamics of the quaternary Mg – Al – Mn – Zn system. These have been recently assessed in detail [Ohno et al. 2006(a), Ohno et al. 2006(b)] and the suggested solidification path starts upon cooling with the precipitation of intermetallic Al_8Mn_5 particles, followed by the formation of primary α-Mg grains and finishes with the binary eutectic reaction between α-Mg and the β-$Mg_{17}Al_{12}$ phase. This solidification path can be described in terms of heterogeneous nucleation by solid particles present in the liquid metal.

5.5.1 Heterogeneous nucleation in cast magnesium alloys

The experimental results in Section 5.4.1 have shown that magnesium melts contain a significant amount of oxide particles in the form of $MgAl_2O_4$ and MgO, as seen in Figures 5.15 and 5.20. After intensive shearing, no changes in the size or morphology of the former are observed, however, the morphology and size of MgO is altered. As seen in Figures 5.22 and 5.23, MgO films and lumps are broken down and the MgO particles have a fine size and are well dispersed compared to the non-sheared sample. Another important observation from the experimental results is that intensive shearing of the melt prior to casting leads to the formation of refined Al_8Mn_5 intermetallics with a narrower size distribution as seen in Figure 5.19. The above suggest that MgO particles can act as potent nucleation sites for the Al_8Mn_5 intermetallics. Recent work by Fan et al. [Fan et al. 2009(b)] has confirmed this by means of crystallographic analysis. Based on the crystal structure and lattice parameters of MgO, which has an FCC crystal structure with lattice parameter a = 0.42112 nm, and Al_8Mn_5, which has a rhombohedral crystal structure and lattice parameters a = 1.2645 nm and c = 1.5855 nm, they have calculated that the atomic misfit along the closely packed directions $[1\ 1\ 0]_{MgO}$ and $[1\ -2\ 1\ 0]_{Al8Mn5}$ is 5.80 %, which is within the required limits [Zhang et al. 2005] for a particle to act as a nucleation site. Hence, it can positively be concluded that the solidification path of magnesium alloys could start with heterogeneous nucleation of Al_8Mn_5 on MgO particles.

Next in the solidification sequence of magnesium alloys is the nucleation of the primary α-Mg phase. The two solid phases that now pre-exist in the melt are oxides and Al_8Mn_5 intermetallic particles. The latter have been studied in detail and there is considerable debate as to whether they can act as potent nucleation sites for primary magnesium. Several researchers [Tamura et al. 2003, Kim et al. 2007(a), Kim et al. 2007(b)] have observed Al_8Mn_5 particles in the microstructure of solidified Mg-Al cast alloys, often located in the centre of α-Mg grains, and suggested that these particles served as nucleation sites. This however should not be taken as convincing evidence for heterogeneous nucleation on the observed particles, as solid particles located at the solid/liquid interface have been shown to be engulfed inside the grains without having contributed to a nucleation process [Schaffer et al. 2007]. Recently Kim et al. [Kim et al. 2010] have investigated the potential of Al_8Mn_5 particles to act as nucleation sites for α-Mg and found strong and coherent bonding between the two phases. The work by Cao et al. [Cao et al. 2006] on the other hand suggested that it is a high temperature ε-AlMn phase and not Al_8Mn_5 particles that effectively nucleate α-Mg grains and promote grain refinement of Mg-Al alloys. In addition to that, the crystallographic analysis by Zhang et al. [Zhang et al. 2005] revealed a poor matching between Al_8Mn_5 and α-Mg, concluding that it is highly unlikely that Al_8Mn_5 can serve as a potent nucleation site for primary magnesium grains. Finally, recent high resolution transmission electron microscopy (HRTEM) work carried out by Wang et al. [Wang et al. 2010] observed no well-defined orientation relationship between Al_8Mn_5 intermetallic particles and α-Mg, concluding that they are unlikely to be effective for heterogeneous nucleation.

Research on the potency of MgO particles to act as nucleation substrates for α-Mg has recently attracted more interest. An orientation relationship between the two phases was found during a high resolution transmission electron microscopy (HRTEM) investigation of magnesium nanonparticles produced by gas-phase synthesis [Kooi et al. 2006]. Based on the edge-to-edge matching model developed by Zhang et al. [Zhang et al. 2005], Kim et al. [Kim et al. 2010] calculated the interplanar spacing mismatch between matching planes of MgO and α-Mg and concluded that MgO particles can effectively act as potent nucleants. The detailed HRTEM study by Fan et al. [Fan et al. 2009(b)] also provided convincing experimental evidence for the orientation relationship between MgO particles and α-

Mg. The results indicated that the interatomic spacing misfit along the closely packed directions $[1\ \bar{2}\ 1\ 0]_{Mg}$ and $[0\ 1\ \bar{1}]_{MgO}$ was 5.46 % and their interface was semi-coherent. The above studies are all in agreement and provide strong evidence that MgO particles could potentially act as nucleation substrates for α-Mg in the solidification path of magnesium alloys based on the Mg-Al-Mn-Zn system.

5.5.2 Microstructural refinement of MC-HPDC magnesium alloys

Based on the discussion on heterogenous nucleation presented above, the solidification path of magnesium alloys starts with the nucleation of Al_8Mn_5 on MgO particles. There is no conclusive evidence to date that these Al_8Mn_5 participate in the nucleation process of primary magnesium. However, the remaining MgO take part in the solidification process by triggering the nucleation of primary α-Mg grains. Therefore, it can be said that magnesium melts contain the required potent nucleating particles which, under the right conditions, can contribute to the grain refinement of the solidified microstructure.

For effective heterogeneous nucleation and subsequent grain refinement of a given alloy composition to take place, the number and size distribution of the potent nucleating particles are critical [Quested and Greer 2004]. According to the free growth theory developed by Greer et al. [Greer et al. 2000], the undercooling ΔT_{fg} required for achieving the state of free growth is given by:

$$\Delta T_{fg} = 4\gamma_{sl} / \Delta S_v d_{pi} \qquad (5.1)$$

where ΔS_v is the volumetric entropy of fusion and d_{pi} is the diameter of the potent inoculant particles. It is obvious from Equation (5.1) that the undercooling for free growth is inversely proportional to the inoculant particle size, where the larger particles are more potent for heterogeneous nucleation and are activated first. Under typical solidification conditions, only a small fraction of the particles become active before recalesence occurs. In order to promote the efficiency of inoculation, more particles need to contribute to heterogeneous nucleation; hence a narrow size distribution is desirable.

The experimental results in Section 5.4.1 showed that without melt shearing, MgO exists in magnesium melts in the form of coarse oxide particle clusters and oxide skins. Although they all consist of fine MgO particles, each oxide cluster or skin

segment participates in the nucleation process as a single entity. This will considerably reduce the number of potential active nucleating particles in the alloy melt, giving rise to a coarse grain structure in the as-cast samples. On the contrary, the experimental results show that intensive melt shearing has broken down the MgO clusters and skins and dispersed individual MgO particles with a fine size. The narrow particle distribution of the MgO particles achieved after intensive melt shearing will significantly increase the number of active nucleating particles, resulting in a much finer magnesium grain size after solidification. In summary, MgO is a poor grain refiner for the non-sheared Mg–Al alloy melts due to its morphology of coarse particle clusters and skins and insufficient numbers. However, with the implementation of intensive shearing, MgO particles become an effective grain refiner.

5.5.3 Effect of intensive shearing on the defect band formation

Figure 5.8(a) presented a cross-section of an AZ91D casting produced by conventional HPDC and the solidification microstructure was highly inhomogeneous. Solidification of the liquid metal in the HPDC process starts when the shot sleeve is filled. The ESCs that form in the shot sleeve are transported to the die where solidification takes place for the remaining liquid. Their volume concentration, governed by the temperature of the melt in the shot sleeve, can be influenced by several parameters, such as liquid metal superheat, heat transfer coefficient, surface properties of the shot sleeve and alloy composition [Dahle and StJohn 1999, Dahle et al. 2001(b)]. ESCs remain in the final cast product and are concentrated in the centre of the casting. The remaining liquid metal is entrapped between the ESCs in the central region and as it solidifies, there is not sufficient feeding to compensate for shrinkage. Porosity is commonly found in the centre of HPDC castings and it is directly related to insufficient feeding during the last stages of solidification.

Several researchers have identified a very common defect in HPDC Mg-alloy components that is the formation of segregation and/or porosity bands, commonly referred to as ‘defect’ bands, that follow contours parallel to the casting surface [Dahle and StJohn 1999, Dahle et al. 2001(a), Dahle et al. 2001(b), Gourlay et al. 2007]. Such a defect band was observed in the microstructure of the castings of

AZ91D alloy produced by conventional HPDC, without the implementation of intensive shearing. Dahle and StJohn [Dahle and StJohn 1999] suggest that the formation of defect bands should be attributed to the formation of a shear plane between areas of different solid fractions that exist in the melt as it solidifies in the die. A region of lower solid fraction exists between the central ESCs region and the solidifying layer in contact with the die wall, and the shear stress deformation caused by the solidifying fluid flow is concentrated there.

Gourlay *et al.* [Gourlay et al. 2004] proposed a mechanism for the defect band formation based on the response to shear stress of the different areas in the solid faction gradient that exists as we move away from the central ESCs region. As the solid fraction increases, a dendrite network begins to form and the shear strength increases rapidly. When these dendrites interlock, interdendritic flow of the remaining liquid will start, as a response to the shear stress. A further increase of the solid fraction as we move towards the die wall will result in a denser dendritic network with smaller and more tortuous interdendritic paths. These compact dendrites are very likely to be interlocked and their shear strength varies depending on the degree of locking. Slip will occur at the weakest regions allowing additional interdendritic flow and the increased concentration of liquid will decrease the local shear strength. Additional slip will occur with more interdendritic flow resulting in the formation of segregated liquid bands. However, if the mechanism for the defect band formation is activated in the final stages of solidification, insufficient interdendritic flow can lead to the formation of porosity bands.

The results presented in Figure 5.9 can now be explained in respect to the proposed mechanism for the band formation. In the conventional HPDC process, there is a higher concentration of ESCs in the central region as seen by the peaks in the primary grain distribution curves. This leads to a steeper solid fraction gradient between the liquid adjacent to the central ESCs region and the layer solidifying at the die wall. The defect band formed is very distinct, as seen in Figure 5.8(a), and has resulted from the interdendritic flow when slip occurs at the interlocked network of dendrites during solidification. The tortuous interdendritic paths and the compact interlocking of the dendrites when the solid fraction increases also accounts for the insufficient feeding of the interdendritic regions and the increased porosity of the HPDC castings, as seen in Figures 5.10 and 5.11. On the other hand, castings

produced with the MC-HPDC process have more uniform temperature and composition fields during solidification. The effective nucleation promoted by intensive shearing results in the formation of considerably less and more uniformly distributed ESCs which will flow suspended in the liquid metal. The small size, uniformity and spherical morphology of these ESCs allow for increased and less restricted inter-particle flow, resulting in more uniform solidification microstructures with considerably reduced amounts of porosity.

5.5.4 Elimination of hot cracking phenomena in recycled AM series alloy scrap

Hot cracking, also known as hot tearing or solidification cracking, is a major defect in alloy castings and has been comprehensively reviewed by Eskin et al. [Eskin et al. 2004]. Hot cracks nucleate and grow in the late stages of solidification, close to the solidus temperature when the metal is in a mushy zone with 85-95 % solid fraction. At that stage, the growing dendritic grains in the conventional HPDC process start to interlock and liquid is isolated resulting in pore and crack formation with further contraction of the solidifying metal [Eskin et al. 2004].

Cao and Kou [Cao and Kou 2006] studied the hot cracking phenomena in binary Mg-Al castings containing 0.25 to 8 wt. % aluminium. They concluded that with increasing aluminium content the tendency for hot crack formation is increased at lower solid fractions. If we try to translate this in terms of the die-casting cycle in the MC-HPDC process, the nucleation and growth of hot cracks in the casting will start more rapidly once the molten metal is injected into the die. Hence the intensifying pressure needs to be applied earlier to ensure fast and adequate feeding of the regions between the grains and prevent the hot cracking phenomena. The experimental results presented in Figure 5.28 are in agreement with these findings. The defective rate of the MC-HPDC castings of AM series magnesium alloy scrap decreased with decreasing intensifier position values. The faster the melt was injected into the die and the shorter the casting cycle was, the less susceptible the castings were to hot cracking.

The hot crack formation has been discussed at a theoretical level by Fredriksson and co-workers [Fredriksson et al. 2005]. They have studied and analyzed theoretical models according to which lattice defects or vacancies form during solidification

and these can promote the nucleation and growth of cracks. According to their proposed theory, at higher cooling rates the fine grain structure means that the area fraction for vacancy condensation is larger. The more condensed the vacancies are, the more probable it is that the lattice vacancies will cluster and form dislocations which will decrease the vacancy supersaturation. As the vacancy supersaturation is decreased, a level can be reached where nucleation and growth of hot cracks can no longer exist. This theory is consistent with the results from the optimization process followed for the recycling of AM series alloy scrap with the MC-HPDC process. The defective rate of the castings plotted as a function of the die temperature in Figure 5.29 is decreased when the die temperature decreases and higher cooling rates are achieved.

The two theories presented above can also be combined to describe the reduced tendency for hot cracking that the MC-HPDC castings of AM series magnesium alloy scrap exhibited at temperatures above but close to the liquidus temperature. As presented in section 5.2, intensive shearing in a fully liquid state but very close to the liquidus temperature of magnesium alloys results in a very fine grain size microstructure. The results presented in Figure 5.4 show that intensive shearing close to the liquidus temperature produced the smaller grain size for the AM60B alloy. Moreover, as seen in Figure 5.12, the fine grain size produced with the MC-HPDC process is very uniform in the microstructure of the castings. This is also confirmed by the micrograph of the MC-HPDC AM-series alloy scrap seen in Figure 5.31(b). The fine grain structure produced by intensive shearing at a temperature equal to T_L + 5 °C will decrease the supersaturation of vacancies in the lattice and reduce the hot cracking susceptibility. In addition to that, the near spherical and uniform grain structure will prevent grain interlocking and allow easier feeding of the regions between the solidifying grains at any time during the casting cycle. This is experimentally confirmed by the defective rate presented in Figure 5.30 as a function of the processing temperature.

5.5.5 Mechanical properties of MC-HPDC processed magnesium alloys

The qualitative and quantitative analysis in section 5.3 for the microstructure of the AZ91D alloy castings produced with the MC-HPDC process revealed reduced porosity levels, limited defect band formation and a significant refinement of the

grain structure both in terms of size and uniform distribution compared to the castings produced with the conventional HPDC process. As expected, the MC-HPDC processed AZ91D alloy tensile specimens exhibited improved mechanical properties, possessing a good combination of tensile strength and elongation, as presented in Figure 5.13.

The presence of porosity in Mg castings and its effect on the mechanical properties has been investigated by several researchers [Balasundaram and Gokhale 2001, Mayer et al. 2003, Weiler et al. 2005]. Pores present in the microstructure are known to favour crack initiation and propagation and are detrimental to the mechanical performance of the castings. With the conventional HPDC process, the resultant dendritic structure inevitably leads to liquid entrapment between the growing and interlocking dendritic arms. The entrapped remaining liquid solidifies last without adequate melt compensation which results in increased porosity in the final cast structure, as presented in Figure 5.11. The unique solidification behaviour of the intensively sheared melt in the MC-HPDC process, as discussed in the previous sections, gives rise to a uniform temperature and composition field which promote the growth of equiaxed grains and prevent liquid entrapment. The porosity of the solidified melt is significantly reduced and the grain structure is finer compared to the conventional HPDC process.

The Hall-Petch equation [Hall 1951, Petch 1953], given as equation 2.12 in section 2.2.3 of the present work, correlates the strength of an alloy to the grain size and predicts improved mechanical properties for alloys with fine grain sizes. The relationship between grain size and strength given by the Hall-Petch equation has been confirmed for numerous metals and recent work by Ono et al. [Ono et al. 2004] confirmed the validity of applying this relationship to polycrystalline magnesium. Hence, it can be used to justify the improved mechanical properties of castings produced with the MC-HPDC process, showing a simultaneous increase in both strength and elongation. This improvement in the mechanical properties of MC-HPDC processed magnesium alloys, originating from the unique solidification conditions after the implementation of intensive shearing resulting in microstructures with fine grain sizes, reduced casting defects and well dispersed inclusions, suggests that the MC-HPDC process can be used as a physical approach for the recycling of high grade magnesium die-casting scrap. The results presented

in Table 5.5 confirm that MC-HPDC recycled AM series Mg scrap castings possess mechanical properties that compare well with fresh AM50A and AM60B alloy castings.

Table 5.5 Tensile strength and elongation of AM series Mg-alloy scrap recycled with the MC-HPDC process and properties of fresh AM50A and AM60B alloy castings reported in the literature, compared to the recycled AM-series alloy scrap recycled in this study.

Alloy	Processing	UTS (MPa)	Elongation (%)	Reference
AM50A	HPDC	210	8.5	[Aune and Westengen 1992]
		210	10	[Avedasian and Baker 1999]
		225.5±33.5	6.9±2.1	[Song et al. 2008]
		241±7	12.9±2.1	[Ji et al. 2005]
AM60B	HPDC	225	8	[Avedasian and Baker 1999]
		214±43.3	7.5±4.2	[Lee 2007(a)]
		205.8±40.4	9.2±5.5	[Lee 2007(c)]
AM series scrap	HPDC	230.9±17.2	12.4±3.4	Current study
	MC-HPDC	231.5±11.1	14.1±1.9	Current study

5.6 Concluding remarks

In the present chapter the experimental results from the implementation of intensive shearing at temperatures very close to or above the liquidus temperature of magnesium alloys are presented and the solidification behaviour and mechanical properties of these alloys are discussed. The findings of this work can be summarised as follows. Implementation of intensive shearing, prior to casting of different alloys belonging in the Mg-Al alloy family, results in significant grain refinement and a reduced temperature dependence of the grain size. In particular experiments were carried out by casting in the standardised TP1® mould with or without the implementation of intensive shearing with the MCAST process. The grain size of alloys AZ91D, AM60B and AJ62 was significantly decreased after intensive melt shearing with the MCAST process.

The MC-HPDC process was employed to produce cast tensile test specimens which were used to evaluate the microstructure in both a quantitative and qualitative manner, and also determine the mechanical properties of the most commonly used cast magnesium alloy, AZ91D. Compared to castings produced with the conventional HPDC process, the MC-HPDC AZ91D alloy castings have a significantly refined microstructure. The formation of the well known defect band has been suppressed; the grain size in the castings is fine and more uniform, with a narrower size distribution and the porosity levels in the castings are considerably reduced. As expected, the microstructural refinement was then reflected in the mechanical performance, with the MC-HPDC castings exhibiting a very good combination of tensile strength and elongation.

Finally, the potential of the MC-HPDC process to be utilised as a recycling process for high grade magnesium alloy scrap was investigated. AM series magnesium alloy die-casting scrap was used to produce tensile test cast specimens with the MC-HPDC process. Intensive shearing was found to significantly alter the size and morphology of solid particle inclusions present in the molten metal. Initial specimen casting trials with the MC-HPDC process were characterised by a high occurrence of shoulder cracks. A successful optimization process was followed and the final castings produced exhibited consistent properties. The MC-HPDC process was shown to have excellent potential as a physical recycling technology for high grade Mg-alloy scrap.

CHAPTER 6

CONCLUSIONS

The major objective of the research work presented in this thesis was to develop a solidification processing technology suitable for the production of cast Mg-alloys and Al-based PMMCs, that would help overcome all the difficulties presented by conventionally used processes. The proposed approach involved the application of high shear forces capable of dispersing solid particles and inclusions present in the molten metal, which would create solidification microstructures with increased homogeneity in structure and chemical composition. From this point of view it was of major importance to investigate the solidification behaviour under intensive melt shearing provided by the MCAST process.

6.1 Metal Matrix Composites (MMCs)

The MC-HPDC process was introduced as an alternative processing technology for the production of high quality Al-based PMMCs. Intensive shearing was found to alter the distribution of the reinforcement particles in the aluminium matrix and subsequently improve the mechanical properties. The main conclusions of this work can be summarised as follows:

- PMMC reinforcement additions have an extensive clustering tendency when a conventional stir casting process is followed. This was confirmed by the microstructures of LM25 – 5 vol. % SiC, LM24 – 5 vol. % SiC, LM24 – 10 vol. % SiC and LM24 – 5 vol. % C composites presented in Section 4.1.1. Particle agglomerates were present in the microstructure and were preferentially located at the grain boundaries or the interdendritic regions.
- The implementation of intensive shearing in the MC-HPDC process resulted in a more homogeneous dispersion of the reinforcement in LM25 – SiC, LM24 – SiC and LM24 – C composites. Statistical analysis by means of the Quadrat method revealed the improvement in the reinforcement dispersion, as the N_q distribution of MC-HPDC processed PMMCs resembled the Poisson and binomial model distribution curves. In contrast, the N_q particle

distribution for the conventionally processed PMMCs was close to the negative binomial curve, confirming the clustering of the reinforcement.

- Implementation of intensive shearing offers a significant improvement in the distribution of the reinforcement, however increasing the shearing time over 120 s only offers a marginal improvement. The skewness value, which describes the asymmetry of the N_q distribution, was 0.821 for conventionally processed LM25 – SiC PMMCs, which then reduced to 0.353 for 60 s of intensive shearing with the MC-HPDC process, 0.234 for 120 s of shearing and 0.199 after intensive shearing for 180 s indicating an improvement in the distribution.
- Improvement of the reinforcement distribution was offered by an increase in the shearing speed. The skewness value of the N_q distribution was 2.208 for conventionally processed LM24 – 5 vol. % SiC, which dropped to 1.286, 1.201 and 1.089 with intensive shearing at 400, 600 and 800 rpm respectively. Similar results were reported for LM24 – 10 vol. % SiC PMMCs.
- Reduction of the shearing temperature improved the reinforcement distribution uniformity. The lowest skewness value of the N_q distribution for LM24 – 5 vol. % SiC composites was 0.765 when processed at 600 ºC (which was the lowest temperature studied) after intensive shearing at 800 rpm for 180 seconds.
- The improvement in the uniformity of the reinforcement distribution offered by the MC-HPDC process resulted in improved mechanical properties. This was reflected in the Vickers hardness of LM25 – 5 vol. % SiC composites, which increased from 73.6 for the conventionally processed to 79.1 for the MC-HPDC processed castings. In addition, a simultaneous increase was observed in UTS and elongation, by a magnitude of 15 % for LM25 – 5 vol. % SiC composites and 25 % for LM24 – 10 vol. % SiC PMMCs. Finally, the average normalised UTS value of MC-HPDC processed LM24 – 5 vol. % C composites was 0.91, which was higher compared with the normalised UTS data of other Al-based MMCs reported in the literature.
- The MC-HPDC process produces PMMC castings with uniform distribution of the reinforcement particles in the aluminium matrix. This was confirmed

by the Young's modulus values of LM25 – 5 vol. % SiC, LM24 – 5 vol. % SiC and LM24 – 10 vol. % SiC, which fall within the Hashin-Shtrikman bounds for isotropic composites.

6.2 Magnesium alloys

Intensive shearing with the MCAST process was also employed prior to casting a series of different Mg-alloys. The MC-HPDC was used to produce high quality AZ91D alloy castings and was also investigated as a physical recycling technology for Mg-alloys, using a mixture of AM series Mg-alloy scrap. The main conclusions drawn from this work are summarised as follows:

- Implementation of intensive shearing prior to casting resulted in significant grain refinement of the microstructure and reduced dependence of the grain size on the casting temperature. The grain size of AZ91D alloy cast in the TP1® mould was found to vary from 85 μm to 175 μm over a temperature range of 605 to 650 °C when intensive shearing was imposed, compared to 210 μm to 690 μm without melt shearing. Similar results were reported for AM60B and AJ62 alloys.
- The MC-HPDC process produced AZ91D alloy castings with a significantly refined microstructure and more uniform distribution of the grain structure. Optical microscopy revealed the elimination of large, well developed dendrites present in the microstructure of castings produced with the conventional HPDC process. In addition, analysis of the relative area fraction A_{gi} revealed a narrower size distribution of the primary magnesium grains with the MC-HPDC process.
- The MC-HPDC process can reduce casting defects such as porosity and the formation of defect bands. Quantitative analysis of the volume fraction of the primary magnesium grains as a function of the distance from the centre of the casting confirmed the suppression of the defect band in AZ91D castings, when compared to castings produced with the conventional HPDC process. Moreover, the MC-HPDC castings showed reduced levels of porosity, 0.35–0.41 area % compared to 1.25 – 1.44 area % for the conventional HPDC components.

- The microstructural refinement and elimination of casting defects for AZ91D alloy was subsequently reflected in the mechanical performance, with the MC-HPDC castings exhibiting a very good combination of tensile strength and elongation.
- Two main types of inclusions were found in the AM series Mg-alloy scrap melt, namely Al_8Mn_5 intermetallic particles and Mg-based oxides, and intensive shearing was found to significantly alter the size and morphology of both.
- The initial specimen casting trials for the AM series Mg-alloy scrap with the MC-HPDC process were characterised by a high occurrence of shoulder cracks and a successful optimization process was followed by altering the die-casting conditions. Intensive shearing should take place at 5 °C above the melt liquidus temperature, the die temperature should be kept to 180 °C and short die filling times should be used by reducing the intensifier position to 180 mm in order to produce defect free castings that exhibit consistent properties.
- The MC-HPDC process was shown to have excellent potential as a physical recycling technology for high grade Mg-alloy scrap, producing castings with tensile properties – UTS and elongation – comparable to the properties reported in the literature for fresh AM50A and AM60B alloy castings.

CHAPTER 7

RECOMMENDATIONS FOR FUTURE WORK

The work presented in this thesis has investigated the solidification behaviour of Al-based PMMCs and cast Mg alloys under intensive melt shearing. The results have provided a useful insight into the excellent potential of the MC-HPDC process to find increased applications for the production of high quality cast products. However, further experiments should be carried out in order to investigate further the beneficial impact of intensive shearing on the materials studied, as well as other PMMCs and cast alloys.

The quality of the microstructures in PMMC production is affected by the characteristics of the fluid flow in the mixing process used and fluid dynamic simulations for both the conventional stir casting process and the MCAST process could prove to be very useful. Understanding the complex fluid flow characteristics inside the MCAST unit could help optimise the MC-HPDC process for the production of PMMCs. Furthermore, the improvements offered by the MC-HPDC process in the production of Al-SiC and Al-C should be investigated in terms of not only their tensile properties, but also their wear resistance and fatigue behaviour. Addition of the reinforcement particles could be increased to levels of 20-30 vol. % and the effect of intensive shearing on their uniform dispersion should be examined The production of castings from other Al-based PMMCs could also be studied, such as Al-Al_2O_3 and Al-Aerogel, as well as Mg-based PMMCs such as Mg-SiC and Mg-Mg_2Si. The size of the reinforcement particles could be varied and the MC-HPDC process could be used to investigate the possibility of producing nano-particle reinforced MMCs. Finally, the intensive shearing offered by the MCAST process could be combined with an extrusion process to produce near net shape composites with improved mechanical properties.

Further work would also be required in the investigation of the fatigue performance of Mg-alloy castings produced with the MC-HPDC process. The refined and uniform microstructure of Mg alloy castings after intensive melt shearing should result in improved fatigue properties. In addition to that, the uniformity offered by

the MC-HPDC process should increase the corrosion resistance of Mg-alloys and future work could be carried to confirm this and understand the mechanisms for improved corrosion resistance. Moreover, the initial results with the high temperature AJ62 alloy confirm that the MC-HPDC process refines the microstructure and indicate that the mechanical performance should be improved. The high temperature properties of this alloy, as well as other creep resistance alloys prepared with the MC-HPDC process, should be investigated. Finally, this work has confirmed the excellent potential of the MC-HPCD process for physical recycling of Mg alloy scrap. The optimization of the process carried out in this study has eliminated the formation of shoulder cracks and exhibited good reliability and reproducibility for the production of castings with mechanical properties comparable to commercially available fresh alloys. However, the process could be optimised further to reduce casting defects such as the porosity and further improve the mechanical properties of sheared castings.

References

[Abramov 1994] Abramov OV (1994). *Ultrasound in Liquid and Solid Metals*, Boca Raton, FL: CRC Press.

[Akhalaghi et al. 2004] Akhalaghi F, Lajevardi A, Maghanaki HM (2004), 'Effects of casting temperature on the microstructure and wear resistance of compocast A356/SiC_p composites: a comparison between SS and SL routes'. *Journal of Materials Processing Technology,* 155–156 pp. 1874–1880.

[Aniban et al. 2002] Aniban N, Pillai RM, Pai BC (2002), 'An analysis of impeller parameters for aluminium metal matrix composites synthesis'. *Materials Design,* 23 pp. 553-556.

[Antrekowitsch et al. 2002] Antrekowitsch H, Hanko G, Ebner P (2002), 'Recycling of different types of magnesium scrap'. In: Kaplan, H.I. (Ed.), *Magnesium Technology 2002,* pp. 43–49.

[Asthana 1998(a)] Asthana R (1998), 'Processing effects on the engineering properties of cast metal matrix composites'. *Advanced Performance Materials*, 5 pp. 213-255.

[Asthana 1998(b)] Asthana R (1998): 'Reinforced cast metals -Part II Evolution of the interface'. *Journal of Materials Science*, 33 pp. 1959-1980.

[Aune and Westengen 1992] Aune T, Westengen H (1992), 'Mechanical properties of pressure die cast Mg-alloys'. In: Mordike BL, Hechmann F (Eds.) *Magnesium alloys and their applications*, pp. 221-228

[Avedasian and Baker 1999] Avedasian MM, Baker H (1999). *ASM Specialty Handbook®* - *Magnesium and Magnesium Alloys*, Materials Park, OH: ASM International.

[Balasundaram and Gokhale 2001] Balasundaram A, Gokhale AM (2001), 'Quantative characterization of spatial arrangement of shrinkage and gas (air) pores in cast magnesium alloys'. *Materials Characterization,* 46 pp. 419–426.

[Bamberger 2001] Bamberger M (2001), 'Structural refinement of cast magnesium alloys'. *Materials Science and Technology,* 17 pp. 15-24.

[Bamberger and Dehm 2008] Bamberger M, Dehm G (2008), 'Trends in the development of new Mg alloys'. *Annual Review of Materials Research*, 38 pp. 505-533.

[Baril et al. 2003] Baril E, Labelle P, Pekguleryuz MO (2003), 'Elevated temperatureMg-Al-Sr: creep resistance mechanical properties and microstructure'. *JOM*, 55 pp. 34-39.

[Bartos et al. 2007] Bartos S, Laush C, Scharfenberg J, Kantamaneni R (2007), 'Reducing greenhouse gas emissions from magnesium diecasting'. *Journal of Cleaner Production*, 15 pp. 979-987.

[Beck et al. 1991] Beck W, Forschner P, Junghanns R, Klatt D, Philipp G, Sauter F, et al. (1991), *Handbook of Mixing Technology*. Schopfheim: EKATO Ruhr- und Mischtechnik GmbH.

[Bezdek and Wendling 2005] Bezdek RH, Wendling RM (2005). 'Fuel efficiency and the economy'. *American Scientist*, 93 pp. 132-139.

[Bhaduri et al. 1996] Bhaduri A, Gopinathan V, Ramakrishnan P, Miodownik AP (1996), 'Processing and properties of SiC particulate reinforced A1-6.2Zn-2.5Mg-I.7Cu alloy (7010) matrix composites prepared by mechanical alloying'. *Materials Science and Engineering A*, 221 pp. 94-101.

[Bindumadhavan et al. 2001] Bindumadhavan PN, Chia TK, Chandrasekaran M, Wah HK, Lam LN, Prabhakar O (2001), 'Effect of particle-porosity clusters on tribological behaviour of cast aluminium alloy A356–SiC_p metal matrix composites'. *Materials Science and Engineering A*, 315 pp. 217–226.

[Boselli et al. 1998] Boselli J, Pitcher PD, Gregson PJ, Sinclair I (1998), 'Quantitative assessment of particle distribution effects on short crack growth in SiC_p reinforced Al-alloys'. *Scripta Materialia*, 38(5) pp. 839-844.

[Brandes 1983] Brandes EA (1983). *Smithells Metals Reference Book*, 6th edition, London, UK: Butterworths.

[Brungs 1997] Brungs D (1997), 'Light weight design with light metal castings'. *Materials & Design*, 18(6) pp. 285-291.

[Cahn et al. 2005] Cahn RW, Haasen P, Kramer EJ (Eds.) (2005). *Materials Science and Technology: A Comprehensive Treatment*, Weinheim: Wiley-VCH.

[Cao and Kou 2006] Cao G, Kou S (2006), 'Hot cracking of binary Mg-Al alloy castings'. *Materials Science and Engineering A*, 417 pp. 230-238.

[Cao et al. 2004] Cao P, Qian M, StJohn DH (2004), 'Effect of iron on grain refinement of high-purity Mg-Al alloys'. *Scripta Materialia*, 51(2) pp. 125-129.

[Cao et al. 2006] Cao P, Qian M, StJohn DH (2006), 'Effect of manganese on grain refinement of Mg-Al based alloys'. *Scripta Materialia*, 54 pp. 1853-1858.

[Cao et al. 2007] Cao P, Qian M, StJohn DH (2007), ' Mechanism for grain refinement of magnesium alloys by superheating'. *Scripta Materialia*, 56 pp. 633-636.

[Chawla 1998] Chawla KK (1998). *Composite Materials*, 2nd edition. New York: Springer.

[Chawla and Chawla 2006] Chawla N, Chawla KK (2006), 'Metal matrix composites in ground transportation'. *JOM*, 58(11) pp. 67-70.

[Chernyshova and Kobeleva 1985] Chernyshova TA, Kobeleva LI (1985), 'Products of interaction in the Al-Si alloy-carbon fiber system'. *Journal of Materials Science*, 20, 10 pp. 3524-3528.

[Clyne 1997] Clyne TW (1997), 'The effect of interfacial characteristics on the mechanical performance of particulate, fibrous and layered metal matrix composites - a review of some recent work'. *Key Engineering Materials*, 127-131 pp. 81-98.

[Clyne and Mason 1987] Clyne TW, Mason JF (1987), 'The squeeze infiltration process for fabrication of metal-matrix composites'. *Metallurgical Transactions A*, 18 pp. 1519-1530.

[Clyne and Withers 1993] Clyne TW, Withers PJ (1993). *An introduction to metal matrix composites*, 1st edition. Cambridge: Cambridge University Press.

[Clyne et al. 1985] Clyne TW, Bader MG, Cappleman GR, Hubert PA (1985), 'The use of a δ-alumina fibre for metal-matrix composites'. *Journal of Materials Science*, 20 pp. 85-96.

[Cole 2007] Cole GS (2007), 'Summary of Magnesium vision 2020: a North Americal automotive strategic vision for magnesium'. In: Beals, S., Luo, A.A., Neelameggham, N.R., Pekguleryuz, M.O. (Eds.), *Magnesium Technology 2007*, pp. 35-40.

[Curtis and McIntosh 1950] Curtis JT, McIntosh RP (1950), 'The interrelations of certain analytic and synthetic phytosociological characters'. *Ecology*, 31 pp. 434-455.

[Dahle and StJohn 1999] Dahle AK, StJohn DH (1999), 'Rheological behaviour of the mushy zone and its effect on the formation of casting defects during solidification'. *Acta Materialia*, 47 pp. 31-41.

[Dahle et al. 2001(a)] Dahle AK, Lee YC, Nave MD, Schaffer PL, StJohn DH (2001), 'Development of the as-cast microstructure in magnesium–aluminium alloys'. *Journal of Light Metals*, 1 pp. 61-72.

[Dahle et al. 2001(b)] Dahle AK, Sannes S, StJohn DH, Westengen H (2001), 'Formation of defect bands in high pressure die cast magnesium alloys'. *Journal of Light Metals*, 1 pp. 99–103.

[Das et al. 1989] Das S, Prasad V, Ramachandran TR (1989), 'Microstructure and wear of cast (Al-Si alloy)-graphite composites'. *Wear,* 133 pp. 173-187.

[Dasgupta and Meenai 2005] Dasgupta R, Meenai H (2005), 'SiC particulate dispersed composites of an Al–Zn–Mg–Cu alloy: Property comparison with parent alloy'. *Materials Characterization*, 54 pp. 438– 445.

[Delannay et al. 1987] Delannay F, Froyen L, Deruyttere A (1987), 'The wetting of solids by molten metals and its relation to the preparation of metal-matrix composites'. *Journal of Materials Science*, 22 pp. 1-16.

[Deng and Chawla 2006] Deng X, Chawla N (2006), 'Modeling the effect of particle clustering on the mechanical behaviour of SiC particle reinforced Al matrix composites'. *Journal of Materials Science*, 41 pp. 5731-5734.

[Dieringa et al. 2007] Dieringa H, Bohlen J, Hort N, Letzig D, Kainer KU (2007). 'Advances in manufacturing processes for magnesium alloys'. In: Beals S, Luo AA, Neelameggham NR, Pekguleryuz MO (Eds.), *Magnesium Technology 2007*, pp. 3-8.

[Du et al 2008] Du J, Yang J, Kuwabara M, Li W, Peng J (2008), 'Improvement in grain refining efficiency for M-Al alloy modified by the combination of carbon and calcium'. *Journal of Alloys and Compounds*, 470(1-2) pp. 134-140.

[Dupré 1869] Dupre A (1869). *Theorie Mecanique de la Chaleur*. Paris: Gauthier-Villars.

[Easton et al. 2006] Easton MA, Schiffl A, Yao JY, Kaufmann H (2006), 'Grain refinement of Mg-Al(-Mn) alloys by SiC additions'. *Scripta Materialia*, 55 pp. 379-382.

[El-Kaddah and Chang 1991] El-Kaddah NK, Chang E (1991), 'On the dispersion of SiC-Al slurries in rotating flows'. *Materials Science and Engineering A*, 144 pp. 221-227.

[Eliezer et al. 1998] Eliezer D, Aghion E, (Sam) Froes FH (1998), 'Magnesium science, technology and applications'. *Advanced Performance Materials,* 5 pp. 201-212.

[Emley 1966] Emley EF (1966). *Principles of Magnesium Technology*, Oxford, UK: Pergamon Press.

[Eskin et al. 2004] Eskin DG, Suyitno, Katgerman L (2004), 'Mechanical properties in the semisolid state and hot tearing of aluminium alloys'. *Progress in Materials Science*, 49 pp. 629-711.

[Eustathopoulos et al. 1974] Eustathopoulos N, Joud JC, Desre P, Hicter JM (1974), 'The wetting of carbon by aluminum and aluminum alloys'. *Journal of Materials Science,* 9 pp. 1233-1242.

[Falk and Langer 1998] Falk ML, Langer JS (1998), 'Dynamics of viscoplastic deformation in amorphous solids'. *Physical Reviews E,* 57 pp. 7192–7205.

[Fan 2002] Fan Z (2002), 'Semisolid metal processing'. *International Materials Reviews*, 47 pp. 49-85.

[Fan 2005] Fan Z (2005), 'Development of the rheo-diecasting process for magnesium alloys'. *Materials Science and Engineering A*, 413-414 pp. 72-78

[Fan and Liu 2005] Fan Z, Liu G (2005), 'Solidification behaviour of AZ91D under intensive forced convection in the RDC process'. *Acta Materialia*, 53 pp. 4345-4357.

[Fan et al. 1999] Fan Z, Bevis MJ, Ji S (1999), PCT Patent WO 01/21343 A1.

[Fan et al. 2001] Fan Z, Ji S, Zhang J (2001), 'Processing of immiscible metallic alloys by rheomixing process'. *Materials Science and Technology,* 17 pp. 837-842.

[Fan et al. 2005] Fan Z, Fang X, Ji S (2005), 'Microstructure and mechanical properties of rheo-diecast (RDC) aluminium alloys'. *Materials Science and Engineering A,* 412 pp. 298-306

[Fan et al. 2009(a)] Fan Z, Xia M, Zhang H, Liu G, Patel JB, Bian Z, Bayandorian I, Wang Y, Li HT, Scamans GM (2009), 'Melt conditioning by advanced shear technology (MCAST) for refining solidification microstructures'. *International Journal of Cast Metal Research,* 22, pp. 103-107.

[Fan et al. 2009(b)] Fan Z, Wang Y, Xia M, Arumuganathar S (2009), 'Enhanced heterogeneous nucleation in AZ91D alloy by intensive melt shearing'. *Acta Materialia*, 57(16) pp. 4891-4901.

[Fang et al. 2007] Fang, X., Shao, G., Liu, Y.Q., Fan, Z. (2007), 'Effects of intensive forced melt convection on the mechanical properties of Fe containing Al–Si based alloys'. *Materials Science and Engineering A*, 445–446 pp. 65–72.

[Farbenindustrie 1931] Farbenindustrie IG (1931). British Patent GB359,425.

[Farbenindustrie 1942] Farbenindustrie IG (1942). Belgian Patent 444757.

[Fechner et al. 2007] Fechner D, Hort N, Blawert C, Kainer KU (2007), ' Development of a magnesium recycling alloy based on the AM alloy system'. In: Beals S, Luo AA, Neelameggham NR, Pekguleryuz MO (Eds.), *Magnesium Technology 2007*, pp. 287-291.

[Fredriksson et al. 2005] Fredriksson H, Haddad-Sabzevar M, Hansson K, Kron J (2005), 'Theory of hot crack formation'. *Materials Science and Technology*, 21 pp. 521-529.

[Ganguly and Poole 2002] Ganguly P, Poole WJ (2002), 'Characterisation of reinforcement distribution inhomogeneity in metal matrix composites'. *Materials Science and Engineering A*, 332 pp. 301-310.

[Gourlay et al. 2004] Gourlay CM, Laukli HI, Dahle AK (2004), 'Segregation band formation in Al-Si die castings'. *Metalurgical and Materials Transaction A*, 35 pp. 2881-2891.

[Gourlay et al. 2007] Gourlay CM, Laukli HI, Dahle AK (2007), 'Defect Band Characteristics in Mg-Al and Al-Si High-Pressure Die Castings'. *Metalurgical and Materials Transaction A*, 38 pp. 1833–1844.

[Greer et al. 2000] Greer AL, Bunn AM, Tronche A, Evans PV, Bristow DJ (2000), 'Modeling of inoculation of metallic melts: application to grain refinement of aluminium by Al-Ti-B'. *Acta Materialia*, 48 pp. 2823–2835.

[Guang et al. 2009] Guang H, Xiangfa L, Haimin D (2009), 'Grain refinement of Mg–Al based alloys by a new Al–C master alloy'. *Journal of Alloys and Compounds*, 467 pp. 202-207.

[Gupta et al. 1996] Gupta M, Lai MO, Soo CY (1996), 'Effects of type of processing on the microstructure features and mechanical properties of Al–Cu/SiC metal matrix composites'. *Materials Science and Engineering A*, 210 pp. 114–122.

[Hall 1951] Hall EO (1951), 'The deformation and ageing of mild steel: III Discussion of results'. *Proceeding of the Physical Society B*, 64(9) pp. 747-753.

[Hansen et al. 1998] Hansen S, Khakhar DV, Ottino M (1998), 'Dispersion of solids in nonhomogeneous viscous flows'. *Chemical Engineering Science*, 53(10) pp. 1803-1817.

[Harnby et al. 1997] Harnby N, Edwards MF, Nienow AW (1997). *Mixing in the process industries*, 2nd edition. Oxford, UK: Butterworth-Heinemann.

[Hashim et al. 1999] Hashim J, Looney L, Hashmi MSJ (1999). 'Metal Matrix Composites: Production by the Stir casting method'. *Journal of Materials Processing Technology*, 92-93 pp. 1-7.

[Hashim et al. 2002(a)] Hashim J, Looney L, Hashmi MSJ (2002), 'Particle distribution in cast metal matrix composites Part-I'. *Journal of Materials Processing Technology*, 123 pp. 251-257.

[Hashim et al. 2002(b)] Hashim J, Looney L, Hashmi MSJ (2002), 'Particle distribution in cast metal matrix composites Part-II'. *Journal of Materials Processing Technology*, 123 pp. 258-263.

[Hong et al. 2003] Hong SJ, Kim HM, Huh D, Chun BS, Suryanarayana C (2003), 'Effect of clustering on the mechanical properties of SiC particulate-reinforced aluminium alloy 2024 metal matrix composites'. *Materials Science and Engineering A*, 347(1-2) pp. 198-204.

[Housecroft and Sharpe 2007] Housecroft CE, Sharpe AG (2007). *Inorganic Chemistry: Solutions manual*, 3rd edition, Harlow, UK: Pearson Prentice Hall.

[Hull and Clyne 1996] Hull D, Clyne TW (1996). *An introduction to composite materials*, 2nd edition, Cambridge, UK: Cambridge University Press.

[Hunt Jr 2009] Hunt Jr WH (2009), 'Metal Matrix Composites: Applications'. In. Buschow KHJ, Cahn R, Flemings MC, Ilschner B, Kramer EJ, Mahajan S, Veyssiere P (Eds.), *Encyclopedia of Materials: Science and Technology*, pp. 5442-5446.

[Ibrahim et al. 1991] Ibrahim IA, Mohamed FA, Lavernia EJ (1991), 'Particulate reinforced metal matrix composites – A review'. *Journal of Materials Science,* 26 pp. 1137- 1156.

[Janssen 1978] Janssen LPBM (1978). *Twin screw extrusion*, Netherlands: Elsevier Scientific Publishing Company.

[Javaid et al. 2006] Javaid A, Essadiqi E, Bell S, Davis B (2006), 'Literature review on magnesium recycling'. In: Luo AA, Neelameggham NR, Beals RS (Eds.), *Magnesium Technology 2006*, pp. 7–12.

[Ji et al. 2001] Ji S, Fan Z, Bevis MJ (2001), 'Semi-solid processing of engineering alloys by a twin screw rheomoulding process'. *Materials Science and Engineering A*, 299, 120 pp. 210–217.

[Ji et al. 2005] Ji S, Zhen Z, Fan Z (2005), 'Effects of rheodiecasting process on the microstructure and mechanical properties of am50 magnesium alloy '. *Materials Science and Technology*, 21, pp. 1019-1024.

[Jia 2000] Jia DC (2000), 'Influence of SiC particulate size on the microstructural evolution and mechanical properties of Al–6Ti–6Nb matrix composites'. *Materials Science and Engineering A*, 289 pp. 83–90.

[Kainer and Von Buch 2003] Kainer KU, Von Buch F (2003), 'The current state of technology and potential for further development of magnesium applications'. In: Kainer KU (Ed.) (2003). *Magnesium Alloys and Technology*, Weineim, Germany: Wiley-VCH.

[Karnezis et al. 1998] Karnezis PA, Durrant G, Cantor B (1998), 'Characterization of reinforcement distribution in cast Al-alloys/SiC_p composites'. *Materials Characterization*, 40 pp. 97-109.

[Kaczmar et al. 2000] Kaczmar JW, Pietrzak K, Wlosinski W (2000), 'The production and application of metal matrix composite materias'. *Journal of Materials Processing Technology*, 106 pp. 58-67.

[Kelly 1989] Kelly A (1989). *Concise Encyclopedia of Composite Materials*, Oxfrod, UK: Pergamon Press.

[Kendall 1988] Kendall K (1998), 'Agglomerate strength'. *Powder Metall*urgy, 31(1) pp. 28-31.

[Kennedy and Wyatt 2000] Kennedy AR, Wyatt SM (2000), 'Effect of processing on the mechanical properties and interfacial strength of aluminium TiC MMCs'. *Composites Science and Technology*, 60(2) pp. 307-314.

[Kim et al. 2007(a)] Kim YM, Yim CD, You BS (2007), Grain refining mechanism in Mg-Al base alloys with carbon addition'. *Scripta Materialia*, 57 pp. 691-694.

[Kim et al. 2007(b)] Kim YM, Yim CD, Kim YH, You BS (2007), 'The role of carbon for grain refinement in Mg-Al base alloys'. In: Beals, R.S., Luo, A.A., Neelameggham, N.R., Pekguleryuz, M.O. (Eds.), *Magnesium Technology 2007*, pp. 121-126.

[Kim et al. 2010] Kim YM, Wang L, You BS (2010), 'Grain refinement of Mg-Al cast alloy by the addition of manganese carbonate'. *Journal of alloys and compounds*, 490 pp. 695-699

[Kirkwood 1994] Kirkwood DH (1994), 'Semisolid metal processing'. *International Materials Reviews*, 39(5) pp. 173-189.

[Kooi et al. 2006] Kooi BJ, Palasantzas G, De Hosson JThM (2006), 'Gas-phase synthesis of magnesium nanonparticles: A high-resolution transmission electron microscopy study'. *Applied Physics Letters*, 89 pp. 161914/1-3.

[Krishnan et al. 1981] Krishnan BP, Surappa MK, Rohatgi PK (1981), 'The UPAL process: A direct method of preparing cast aluminum alloy-graphite particle composites'. *Journal of Materials Science*, 16(5) pp. 1209-1216.

[Krishnan et al. 1983] Krishnan BP, Raman N, Narayanaswamy K, Rohatgi PK (1983), 'Performance of aluminum alloy graphite bearings in a diesel engine'. *Tribology International*, 16(5) pp. 239-244.

[Kurzydlowski and Ralph 1995] Kurzydlowski KJ, Ralph B (1995). *The quantitative description of the microstructures of materials*, 1st edition, Florida: CRC Press.

[Lacey 1943] Lacey PMC (1943), 'The mixing of solid particles'. *Transactions of the Institution of Chemical Engineers*, 21 pp. 53-59.

[Lacey 1954] Lacey PMC (1954), 'Developments in the theory of particulate mixing'. *Journal of Applied Chemistry*, 4 pp. 257-268.

[Landry et al. 1998] Landry K, Kalogeropoulou S, Eustathopoulos N (1998), 'Wettability of carbon by aluminum and aluminum alloys'. *Materials Science and Engineering A*, 254 pp. 99-111.

[Laurent et al. 1987] Laurent V, Chatain D, Eustathopoulos N (1987), 'Wettability of SiC by aluminum and Al-Si alloys'. *Journal of Materials Science*, 22 pp. 244-250.

[Lee 2007(a)] Lee CD (2007), 'Dependence of tensile properties of AM60 magnesium alloy on microporsity and grain size'. *Materials Science and Engineering A*, 454-455, pp. 575-580.

[Lee 2007(b)] Lee CD (2007), 'Effect of grain size on the tensile properties of magnesium alloy'. *Materials Science and Engineering A*, 459 pp. 355-360.

[Lee 2007(c)] Lee CD (2007), 'Tensile properties of high-pressure die-cast AM60 and AZ91 magnesium alloys on microporosity variation', *Journal of Materials Science*, 42 pp. 10032–10039.

[Lee et al. 1993] Lee YJ, Feke DL, Manas-Zloczower I (1993), 'Dispersion of titanium dioxide agglomerates in viscous media'. *Chemical Engineering Science*, 48(19) pp. 3363–3372.

[Lee et al. 1998] Lee JC, Byun JY, Park SB, Lee HI (1988), 'Prediction of Si contents to suppress the formation of Al_4C_3 in the SiC_p/Al composite'. *Acta Materialia*, 46 pp. 1771–1780.

[Lee et al. 2000] Lee YC, Dahle AK, StJohn DH (2000), 'The Role of Solute in Grain Refinement of Magnesium'. *Metallurgical and Materials Transactions A*, 31 pp. 2895-2906.

[Lin et al. 1998] Lin CB, Ma CL, Chung YW (1998), 'Microstructure of A380-SiCp composites for die casting'. *Journal of Materials Processing Technology*, 48 pp. 236-246.

[Lin et al. 1999] Lin CB, Wu CL, Chiang CH (1999), 'Analysis of mold flow and microstructures of die casting in Al alloy/SiCp composites'. *Journal of Materials Science*, 34 pp. 2229-2240.

[Ling et al. 1995] Ling CP, Bush MB, Perera DS (1995), 'The Effect of Fabrication Techniques on the Properties of A1-SiC Composites'. *Journal of Materials Processing Technology*, 48 pp. 325-331

[Liu et al. 2008(a)] Liu SF, Liu LY, Kang LG, 'Refinement role of electoemagnetic stirring and strontium in AZ91 magnesium alloy'. *Journal of Alloys and Compounds*, 450 pp. 546-550.

[Liu et al. 2008(b)] Liu X, Osawa Y, Takamori S, Mukai T (2008), 'Microstructure and mechanical properties of AZ91 alloy produced with ultrasonic vibration'. *Materials Science and Engineering A*, 487 pp. 120-123.

[Liu et al. 2008(c)] Liu G, Wang Y, Fan Z (2008), 'A physical approach to the direct recycling of Mg-alloy scrap by the rheo-diecasting process'. *Materials Science and Engineering A*, 472 pp. 251–257

[Llorca and Gonzalez 1998] Llorca, J., Gonzalez, C. (1998), 'Microstructural factors controlling the strength and ductility of particle-reinforced metal-matrix composites'. *Journal of the Mechanics and Physics of Solids*, 46 pp. 1-28.

[Lloyd 1991] Lloyd DJ (1991), 'Aspects of fracture in particulate reinforced metal matrix composites'. *Acta Metallurgica et Materialia,* 39(1) pp. 59-71.

[Lloyd 1994] Lloyd DJ (1994), 'Particle reinforced aluminum and magnesium matrix composites'. *International Materials Reviews* 39(1) pp. 1-23.

[Lu et al. 2006] Lu L, Dahle AK, StJohn DH (2006), 'Heterogeneous nucleation of Mg-Al alloys'. *Scripta Materialia,* 54 pp. 2197-2201.

[Luo 2002] Luo AA (2002), 'Magnesium: Current and Potential Automotive Applications'. *JOM,* 56(2) pp. 42-48.

[Luo and Pekguleryuz 1994] Luo A, Pekguleryuz MO (1994). 'Cast magnesium alloys for elevated temperature applications'. *Journal of materials science,* 29 pp. 5259 – 5271.

[Ma et al. 1994] Ma ZY, Ning XG, Lu YX, Li JH, Bi J, Zhang YZ (1994), 'Microstructure and properties of Sic whisker reinforced Al-8.5Fe- 1.3V- 1.7Si alloy composite'. *Materials Letters,* 21 pp. 69-72.

[Mabuchi et al. 2000] Mabuchi M, Yamada Y, Shimojima K, Wen CE, Chino Y, Nakamura M (2000), 'The Grain Size Dependence of Strength in the Extruded AZ91 Mg Alloy'. In: Kainer, K.U. (Ed.). *Magnesium alloys and their applications*. Weinheim: Wiley-VCH.

[Mada and Ajersch 1996(a)] Mada M, Ajersch F (1996), 'Rheological model of semi-solid A356-SiC composite alloys. Part-I: Dissociation of agglomerate structure during shear'. *Materials Science and Engineering A,* 212 pp. 157-170.

[Mada and Ajersch 1996(b)] Mada M, Ajersch F (1996), 'Rheological model of semi-solid A356-SiC composite alloys. Part-II: Reconstitution of agglomerate structure at rest'. *Materials Science and Engineering A,* 212 pp. 171-177.

[Majumdar et al. 1984] Majumdar BS, Yegneswaran AH, Rohatgi PK (1984), 'Strength and fracture behaviour of metal matrix particulate composites'. *Materials Science and Engineering,* 68 pp. 85-96.

[Matthews and Rawlings 1994] Matthews FL, Rawlings RD (1994). *Composite Materials: Engineering and Science,* 1st edition. Oxford, UK: Chapman & Hall.

[Mayer et al. 2003] Mayer H, Papakyriacou M, Zettl B, Stanzl-Tschegg SE, 'Influence of porosity on the fatigue limit of die cast magnesium and aluminium alloys'. *International Journal of Fatigue,* 25 pp. 245–256.

[Mayr 2006] Mayr SG (2006), 'Activation energy of shear transformation zones – a key for understanding rheology of glasses and liquids'. *Physical Review Letters*, 97 p. 195501.

[Metcalfe 1974] Metcalfe AG (1974). *Composite materials, Volume 1: Interfaces in Metal Matrix Composites*, 1st edition. London, UK: Academic Press.

[Miracle 2005] Miracle DB (2005), 'Metal matrix composites – From science to technological significance'. *Composites Science and Technology*, 65 pp. 2526-2540.

[Modi et al. 1992] Modi OP Yegneswaran AH, Asthana R, Rohatgi PK (1992), 'Thermomechanical processing of aluminum-based particulate composites'. *Journal of Materials Science*, 23(1) pp. 83-92.

[Mondolfo 1976] Mondolfo LF (1976). *Aluminum alloys: Structure and properties*. London: Butterworths.

[Mordike and Ebert 2001] Mordike BL, Ebert T (2001), 'Magnesium: Properties – applications – potential'. *Materials Science & Engineering A*, 302 pp. 37-45.

[Murphy et al. 1998] Murphy AM, Howard SJ, Clyne TW (1998), 'Characterisation of severity of particle clustering and its effect on fracture of particulate MMCs'. *Materials Science and Technology*, 14 pp. 959-968.

[Nagarajan et al. 1999] Nagarajan S, Dutta B, Surappa MK (1999), 'The effect of SiC particles on the size and morphology of eutectic silicon in cast A356/SiC_p composites'. *Composites Science and Technology*, 59 pp. 897–902.

[Nagata 1975] Nagata S (1975). *Mixing principles and applications*. New York: Wiley.

[Naher et al. 2003] Naher S, Brabazon D, Looney L (2003), 'Simulation of the stir casting process'. *Journal of Materials Processing Technology*, 143–144 pp. 567–571.

[Naher et al. 2005] Naher S, Brabazon D, Looney L (2005), ' Development and assessment of a new quick quench stir caster design for the production of metal matrix composites', *Journal of Materials Processing Technology,* 166 (3) pp. 430–439.

[Naher et al. 2007] Naher S, Brabazon D, Looney L (2007), 'Computational and experimental analysis of particulate distribution during Al–SiC MMC fabrication'. *Composites Part A*, 38 pp. 719–729.

[Nair et al. 1985] Nair SV, Tien JK, Bates RC (1985), 'SiC-reinforced aluminium metal matrix composites', *International Metals Reviews*, 30 pp. 275-290.

[Narendranath et al. 1986] Narendranath CS, Rohatgi PK, Yegneswaran AH (1986), 'Observation of graphite structure under optical and scanning electron microscopes'. *Journal of Materials Science Letters*, 5(6) pp. 592-594.

[Ogel and Gurbuz 2001] Ogel B, Gurbuz R (2001), 'Microstructural characterization and tensile properties of hot pressed Al–SiC composites prepared from pure Al and Cu powders'. *Materials Science and Engineering A*, 301 pp. 213–220.

[Oh et al. 1989] Oh SY, Cornie JA, Russell KC (1989), 'Wetting of ceramic particulates with liquid aluminum alloys: Part I. Experimental techniques'. *Metallurgical Transactions A*, 20 pp. 527-532.

[Ohno et al. 2006(a)] Ohno M, Mirkovic D, Schmid-Fetzer R (2006), 'Phase equilibria and solidification of Mg-rich Mg-Al-Zn alloys'. *Materials Science and Engineering A*, 421(1-2) pp. 328-337.

[Ohno et al. 2006(b)] Ohno M, Mirkovic D, Schmid-Fetzer R (2006), 'Liquidus and solidus temperatures of Mg-rich Mg-Al-Mn-Zn alloys'. Acta Materialia, 54 pp. 3883-3891.

[Ono et al. 2004] Ono N, Nowak R, Miura S (2004), 'Effect of deformation temperature on Hall-Petch relationship registered for polycrystalline magnesium'. *Materials Letters*, 58 pp. 39-43.

[Ourdjini et al. 2001] Ourdjini A, Chew KC, Khoo BT (2001), 'Settling of silicon carbide particles in cast metal matrix composites'. *Journal of Materials Processing Technology*, 116 pp. 72-76.

[Pai et al. 1995] Pai BC, Ramani G, Pillai RM, Satyanarayana KG (1995). 'Role of magnesium in cast aluminium alloy matrix composites'. *Journal of Materials Science*, 30(8) pp. 1903-1911.

[Pekguleryuz and Baril 2001] Pekguleryuz MO, Baril E (2001), 'Development of creep resistant Mg-Al-Sr alloys'. In: Hryn J (Ed.) (2001). *Magnesium Technology*. New Orleans, TMS 2001.

[Petch 1953] Petch NJ (1953), ' The cleavage strength of polycrystals'. *Journal of the Iron and Steel Institute*, 174 pp. 25-28.

[Pierrat and Caram 1997] Pierrat P, Caram HS (1997), 'Tensile strength of wet granular materials'. *Powder Technology*, 91 pp. 83-93.

[Pillai et al. 1987] Pillai UTS, Pandey RK, Rohatgi PK (1987), 'Effect of volume fraction and size of graphite particulates on fracture behaviour of Al-graphite composites'. *Engineering Fracture Mechanics*, 28(4) pp. 461-477.

[Pillai et al. 1995] Pillai UTS, Pai BC, Satyanarayana KG, Damodaran AD (1995), 'Fracture behaviour of pressure die-cast aluminum-graphite composites'. *Journal of Materials Science*, 30(6) pp. 1455-1461.

[Polmear 1995] Polmear IJ (1995). *Light alloys: Metallurgy of the light metals.* 3rd edition, Oxford: Butterworth-Heinmann.

[Powell et al. 2001] Powell BR, Rezhets V, Luo AA (2001), US Patent No. 6,264,763.

[Qian and Cao 2005] Qian M, Cao P (2005), 'Discussions on grain refinement of magnesium alloys by carbon inoculation'. *Scripta Materialia*, 52 pp. 415-419.

[Qian and Das 2006] Qian M, Das A (2006), 'Grain refinement of magnesium alloys by zirconium: Formation of equiaxed grains'. *Scripta Materialia*, 54 pp. 881-886.

[Quaak and Kool 1994] Quaak CJ, Kool WH (1994), 'Properties of semisolid aluminum matrix composites'. *Materials Science and Engineering A*, 188 pp. 277-282.

[Quaak et al. 1994] Quaak CJ, Horsten MG, Kool WH (1994), 'Rheological behaviour of partially solidified matrix composites'. *Materials Science and Engineering A*, 183 pp. 247-256.

[Quested and Greer 2004] Quested TE, Greer AL (2004), 'The effect of the size distribution of inoculant particles on as-cast grain size in aluminium alloys'. *Acta Materialia*, 52 pp. 3859-3868.

[Rajan et al. 1998] Rajan TPD, Pillai RM, Pai BC (1998), 'Reinforcement coatings and interfaces in aluminium metal matrix composites'. *Journal of Materials Science*, 33(14) pp. 3491-3503.

[Ramirez et al. 2008] Ramirez A, Qian M, Davis B, Wilks T, StJohn DH (2008), 'Potency of high-intensity ultrasonic treatment for grain refinement of magnesium alloys'. *Scripta Materialia*, 59 pp. 19-22

[Rana et al. 1989] Rana F, Dhindaw BK, Stefanescu DM (1989), 'Optimisation of SiC particles dispersion in aluminium metal matrix composites'. *AFS Transactions*, 1989 pp. 255-264.

[Rauwendaal 1994] Rauwendaal C (1994). *Polymer extrusion,* 3rd revised edition. New York: Hanser Publisher.

[Ravi et al. 2007] Ravi KR, Sreekumar VM, Pillai RM, Mahato C, Amaranathan KR, Arul Kumar R, Pai BC (2007), 'Optimization of mixing parameters through a water model for metal matrix composites synthesis'. *Materials Design*, 28 pp. 871-881.

[Ravi et al. 2008] Ravi KR, Pillai RM, Amaranathen KR, Pai BC, Chakraborty M (2008), 'Fluidity of aluminium alloys and composites: A review'. *Journal of Alloys and Compounds*, 456(1-2) pp. 201-210.

[Rawal 2001] Rawal S (2001), 'Metal-matrix composites for space applications'. *JOM*, 53 pp. 14-17.

[Ray 1993] Ray S (1993), 'Review - Synthesis of cast metal matrix particulate composites'. *Journal of Materials Science*, 28 pp. 5397-5413.

[Revzin et al. 1996] Revzin B, Fuks D, Pelleg J (1996), 'Influence of alloying on the solubility of carbon fibers in aluminium-based composites: non-empirical approach'. *Composites Science and Technology*, 56 pp. 3-10.

[Richardson and Zaki 1954] Richardson JF, Zaki WN (1954), 'Sedimentation and fluidisation. Part 1'. *Transactions of the Institution of Chemical Engineers*, 32 pp. 35-53.

[Ricketts et al. 2003] Richetts N, Cashion S, Bailey R (2003). 'Industrial trials with the AM-cover gas system for magnesium melt protection'. In: Dahle A (Ed.). *Proceedings of the 1st International Light Metals Technology Conference*, Brisbane, Australia.

[Rogers 1974] Rogers A (1974). *Statistical analysis of spatial dispersions: the quadrat method*, London, UK: Pion.

[Rohatgi 1993] Rohatgi PK (1993), 'Metal-matrix composites'. *Defence Science Journal*, 43(4) pp. 323-349.

[Rohatgi 2001] Rohatgi PK (2001), 'Cast metal matrix composites: Past, present and future'. *AFS Transactions*, 109, 01-133 pp. 1-25

[Rohatgi and Surappa, 1984] Rohatgi PK, Surappa MK (1984), 'Deformation of graphite during hot extrusion of cast aluminum-silicon-graphite particle composites'. *Materials Science and Engineering*, 62 pp. 159-162.

[Rohatgi et al. 1986] Rohatgi PK, Asthana R, Das S (1986), 'Solidification, structure and properties of metal-ceramic particle composites'. *International Metals Review*, 31(3) pp. 115-139.

[Rohatgi et al. 1993] Rohatgi PK, Ray S, Asthana R, Narendranath CS (1993). 'Interfaces in cast metal-matrix composites'. *Materials Science and Engineering A*, 162 pp. 163-174.

[Rohatgi et al. 1998] Rohatgi PK, Sobczak J, Asthana R, Kim JK (1998), 'Inhomogeneities in silicon carbide distribution in stirred liquids—a water model study for synthesis of composites'. *Materials Science and Engineering A*, 252 pp. 98-108.

[Rohatgi et al. 2005] Rohatgi PK, Thakkar RB, Kim JK, Daoud A (2005), 'Scatter and statistical analysis of tensile properties of cast SiC reinforced A359 alloys'. *Materials Science and Engineering A*, 398 pp. 1-14.

[Rumpf 1962] Rumpf H (1962). *The strength of granules and agglomerates,* In Knepper, W.A., editor. *Agglomeration*. New York: Interscience Publishers.

[Schaffer et al. 2007] Schaffer PL, Miller DN, Dahle AK (2007), 'Crystallography of engulfed and pushed TiB_2 particles in aluminium'. *Scripta Materialia*, 57 pp. 1129-1132.

[Scharf 2003] Scharf C (2003), ' Recycling of Magnsium alloys'. In: Kainer, K.U. (Ed.), *Magnesium alloys and technologies'*. Weinheim: Wiley – VCH.

[Scharf et al. 2004] Scharf C, Blawert C, Ditze A (2004), 'Application of remelted post consumer scrap for structural magnesium parts'. In: Kainer KU (Ed.). *Magnesium*, Weinheim:Wiley-VCH.

[Schuh and Lund 2003] Schuh CA, Lund AC (2003), 'Atomistic basis for the plastic yield criterion of metallic glass'. *Nature Materials*, 2 pp. 449–52.

[Schwartz 1984] Schwartz MM (1984). *Composite Materials Handbook*, USA: McGraw-Hill Book Company.

[Segurado et al. 2003] Segurado J, Gonzalez C, Llorca J (2003), 'A numerical investigation of the effect of particle clustering on the mechanical properties of composites'. *Acta Materialia*, 51 pp. 2355-2369.

[Sevik and Kurnaz 2006] Sevik H, Kurnaz S (2006), 'Properties of alumina particulate reinforced aluminum alloy produced by pressure die casting'. *Materials Design*, 27 pp. 676-683.

[Song 2009] Song M (2009), 'Effects of volume fraction of SiC particles on mechanical properties of SiC/Al composites'. *Transactions of the Nonferrous Metals Society of China*, 19 pp. 1400-1404.

[Song et al. 2008] Song J, Xiong SM, Li M (2008), 'The correlation between microstructure and mechanical properties of high pressure die-cast AM50 alloy'. *Journal of Alloys and Compounds*, 477 pp. 863-869.

[Srivatsan et al. 2003] Srivatsan TS, Al-Hajri M, Smith C, Petraroli M (2003), 'The tensile and fracture behaviour of 2029 aluminum alloy metal matrix composite'. *Materials Science and Engineering A*, 346 pp. 91-100.

[Staiger et al. 2006] Staiger MP, Pietak AM, Huadmai J, Dias G (2006), 'Magnesium and its alloys as orthopedic biomaterials: A review'. *Biomaterials*, 27 pp. 1728-1734.

[Stefanescu et al. 1988] Stefanescu DM, Dhindaw BK, Kacar SA, Moitra A (1988), 'Behaviour of ceramic particles at the solid-liquid metal interface in metal matrix composites'. *Metallurgical Transactions A*, 19 pp. 2847-2855.

[Stefanescu et al. 1990] Stefanescu DM, Moitra A, Kacar AS, Dhindaw BK (1990), 'The influence of buoyant forces and volume fraction of particles on the particle pushing/entrapment transition during directional solidification of Al/SiC and Al/graphite composites'. *Metallurgical and Materials Transactions A*, 21 pp. 231-239.

[StJohn et al. 2005] StJohn DH, Ma Qian, Easton MA, Cao P, Hildebrand ZM (2005), 'Grain Refinement of Magnesium Alloys'. *Metallurgical and Materials Transactions A*, 36 pp. 1669-1679.

[Street 1977] Street AC (1977), *The Diecasting Book*, 1st edition. Redhill, England: Portcullis Press Ltd.

[Surappa and Rohatgi 1981] Surappa MK, Rohatgi PK (1981), 'Heat diffusivity criterion for the entrapment of particles by moving solid-liquid interface'. *Journal of Materials Science Letters*, 16(2) pp. 562-564.

[Tamura et al. 2003] Tamura Y, Yagi J, Haitani T, Motegi T, Kono N, Tamehiro H, Saito H (2003), 'Observation of manganese-bearing particles in molten AZ91 magnesium alloy by rapid solidification'. *Materials Transactions*, 44 pp. 552-557.

[Taya and Arsenault 1989] Taya M, Arsenault RJ (1989), *Metal matrix composites: Thermomechanical behaviour*, 1st edition. Oxford, UK: Pergamon Press.

[Tham et al. 2001] Tham LM, Gupta M, Cheng L (2001), 'Effect of limited matrix–reinforcement interfacial reaction on enhancing the mechanical properties of aluminium–silicon carbide composites'. *Acta Materialia*, 49 pp. 3243-3253.

[The Aluminium Association 1990] The Aluminum Association (1990). *Standard Test Procedure for aluminium alloy grain refiners: TP-1*. Washington DC, USA.

[Tomas 2007] Tomas J (2007), 'Adhesion of ultrafine particles - A micromechanical approach'. *Chemical Engineering Science*, 62 pp. 1997-2010.

[USGS 2008] United States Geological Survey (USGS) (2008). *2007 Minerals Yearbook, Volume I – Metals & Minerals.* Washington: United States Government Printing Office.

[Uhlmann et al. 1964] Uhlmann R, Chalmers B, Jackson KA (1964), 'Interaction between particles and a solid–liquid interface'. *Journal of Applied Physics*, 35 pp. 2986-2993.

[Villars and Calvert 1991] Villars P, Calvert LD (Eds) (1991). *Pearson's Handbook of crystallographic data for intermetallic phases*, 2nd edition. Materials Park, Ohio: ASM International.

[Wang et al. 2010] Wang Y, Xia M, Fan Z, Zhou X, Thompson GE (2010), 'The effect of Al_8Mn_5 intermetallic particles on grain size of as-cast Mg-Al-Zn AZ91D alloy'. *Intermetallics*, 18 pp. 1683-1689.

[Watson et al. 2005] Watson IG, Forster MF, Lee PD, Dashwood RJ, Hamilton RW, Chirazi A (2005), 'Investigation of the clustering behaviour of titanium diboride particles in aluminum'. *Composites: Part A*, 36 pp. 1177-1187.

[Watt 1997] Watt IM (1997), *The principles and practice of electron microscopy*, 2nd edition. Cambridge, England: Cambridge University Press.

[Weiler et al. 2005] Weiler JP, Wood JT, Klassen RJ, Maire E, Berkmortel R, Wang G, (2005), 'Relationship between internal porosity and fracture strength of die-cast magnesium AM60B alloy'. *Materials Science and Engineering A*, 395 pp. 315–322.

[White 1990] White JL (1990). *Twin screw extrusion: Technology and principles*, Munich, Germany: Hanser Publisher.

[Xia et al. 2009] Xia M, Wang Y, Li H, Arumuganathar S, Zuo Y, Scamans GM, Fan Z (2009), 'Refinement of Solidification Microstructure by MCAST Process'. In: Nyberg EA, Agnew SR, Neelameggham NR, Pekguleryuz MO (Eds.). *Magnesium Technology 2009*, pp. 135-140.

[Yang et al. 2008(a)] Yang Z, Li JP, Zhang JX, Lorimer GW, Robson J (2008), 'Review on research and development of magnesium alloys'. *Acta Metallurgica Sinica (English Letters)*, 21(5) pp. 313-328.

[Yang et al. 2008(b)] Yang M, Pan F, Cheng R, Tang A (2008), 'Effect of Mg-10Sr master alloy on grain refinement of AZ31 magnesium alloy'. *Materials Science and Engineering Ai*, 491 pp. 440-445.

[Youssef et al. 2005] Youssef YM, Dashwood RJ, Lee PD (2005), 'Effect of clustering on particle pushing and solidification behaviour in TiB_2 reinforced aluminium PMMCs'. *Composites Part A,* 36 pp. 747–763.

[Zhang et al. 2005] Zhang MX, Kelly PM, Qian M, Taylor JA (2005), 'Crystallography of grain refinement in Mg-Al based alloys'. *Acta Materialia*, 53(11) pp. 3261-3270.

[Zhang et al. 2007(a)] Zhang Z, Chen XG, Charette A (2007), 'Particle distribution and interfacial reactions of Al–7%Si–10%B_4C die casting composite'. *Journal of Materials Science*, 42 pp. 7354-7362.

[Zhang et al. 2007(b)] Zhang ZQ, Le QC, Cui JZ (2007), 'Ultrasonic treatment of magnesium alloy melts and its effects on solidification microstructures'. *Materials Science Forum*, 546– 549 pp. 129–132.

[Zhao et al. 1991] Zhao Z, Zhijian S, Yingkun X (1991), 'Effect of microstructure on the mechanical properties of an A1 alloy 6061-SIC particle composite'. *Materials Science and Engineering A*, 132 pp. 83-88.